UNDERSTANDING OF EPOXY NANOCOMPOSITES FOR INSULATION STRUCTURES IN POWER APPARATUS AND FOR EMI SHIELDING

A Project Report

submitted by

ABHISHEK SHARMA

in partial fulfilment of the requirements
for the award of the degree of

MASTER OF TECHNOLOGY

DEPARTMENT OF ELECTRICAL ENGINEERING
INDIAN INSTITUTE OF TECHNOLOGY MADRAS
JUNE 2021

QUOTATIONS

Karmaṇyevādhikāraste mā phaleṣhu kadāchana,
Mā karmaphalaheturbhūrmā te saṅgo'stvakarmaṇi.

You have the right to perform your duty,
but you are not entitled to the fruits of action.
Let not the fruits of action be your motive,
and never be attached to not doing your duty.

BHAGAVAD GITA

DEDICATION

To my late Mother

CERTIFICATE

This is to certify that the project report titled **UNDERSTANDING OF EPOXY NANOCOMPOSITES FOR INSULATION STRUCTURES IN POWER APPARATUS AND FOR EMI SHIELDING**, submitted by **ABHISHEK SHARMA**, to the Indian Institute of Technology Madras, for the award of the degree of **Master of Technology**, is a bona fide record of the research work done by him under my supervision. The contents of this project report, in full or in parts, have not been submitted to any other Institute or University for the award of any degree or diploma.

Place: Chennai

Date: 29th June 2021

Dr R. Sarathi
Project Guide
Professor
Dept. of Electrical Engineering
IIT, Madras 600 036

ACKNOWLEDGEMENTS

Words are too frail to express my inward emotions of ineffable indebtedness and profound gratitude towards my esteemed guide Dr R Sarathi for his constant interest and expert guidance. His inspiring and adroit leadership, constructive criticism and invaluable advice infused in me the spirit of dedicated hard work. His relentless support and words of wisdom facilitated me in completing my project in the highest standards of this premier institution.

I offer my sincere gratitude to Dr. R. Velmurugan, Department of Aerospace Engineering and Dr V. Subramanian, Department of Physics for sharing their valuable knowledge and lending their precious time which helped me in understanding concepts better and implementing the same in this work.

I am extremely grateful to Mr Chandrasekaran for continuously extending his support in the laboratory for the entire duration of project work. I would also like to express my sincere thanks to my colleagues, Mr Amizhtan and Mr Myneni Sukesh Babu for sparing their valuable time and sharing their knowledge, which helped me immensely in the timely completion of my work. I would also like to thank Mr Balaji, Mr Chinnapandi and Mr Krishna Prasad of Composite Manufacturing Laboratory and Mr Vinaya Kumar of Microwave Laboratory for their forthcoming help in carrying out various crucial tasks associated with this project. I would like to express my deep gratitude to all my colleagues in High Voltage Laboratory for the cherished and treasured moments and constant motivation to work hard.

It is extremely difficult to express my deepest feelings of indebtedness towards my father who has been a constant source of inspiration in my life. His persistent support in all my endeavours is immeasurable. I take this opportunity to thank my wife who has been the motivational and emotional support in my life that keeps encouraging me to achieve my goal. I would also like to thank my grandmother for her blessings and my daughter for being the precious source of joy that keeps me going.

Last but not the least, I would like to thank God for showing me the path of knowledge and wisdom and keeping me in good mental and physical health during the tough phases thereby helping me to achieve my goal.

ABSTRACT

KEYWORDS: Nanocomposites, Corona Inception Voltage, Trap Distribution, Potential Decay, Digital Image Correlation, MWCNT, Relative Permittivity, EMI Shielding Efficiency, Conductivity, Unidirectional Carbon Fiber Fabric, MATLAB.

Nanoparticles are characterized as small particles that range between 1 and 100 nanometers in size. Nanoparticles exhibit considerably different physical and chemical properties as compared to their lager versions. At the atomic scale, the material properties changes that can be attributed to the increase in the surface area to volume ratio that results in the material's surface atoms dictating the behavior of the material. The small size of the nanoparticles as compared to the bulk material provide a very large surface area to volume ratio that determines their unique optical, physical and chemical properties.

The present study was carried out in two parts, firstly, to analyze the electrical and mechanical properties of epoxy based silica (SiO_2) nanocomposites and secondly, to study the electromagnetic shielding efficiency (EMI SE) of epoxy bases multi walled carbon nanotubes (MWCNT) and unidirectional carbon fiber fabric (UCFF) composites. In the first part the electrical and mechanical properties of epoxy-silica nanocomposites were studied to find out the efficacy of these nanocomposites as insulating materials and thereby also investigating the impact of shear mixing time on the electrical and mechanical properties in the process of preparation of the nanocomposite samples. Shear mixing is utilized to disperse the nanofillers in the epoxy matrix. It breaks down agglomerates into smaller particles. In low concentration of nano-fillers, shear mixing is essential for even distribution of the nanofillers in the epoxy matrix. In the present study 1% nano-silica was mixed with epoxy for different time spans at a constant speed of 2000 rpm. The effect of shear mixing times on the extent of dispersion and formation of bonds between the nanoparticles and the matrix resulting into direct influence on the water initiated corona discharge voltage, surface potential decay and contact angle as a part of electrical properties and tensile strength of the material as a part of mechanical properties were studied. The water droplet initiated corona inception voltage (CIV) increased with the shear mixing time under both AC and DC voltages. A marginal increase in contact angle as a function of shear mixing time was noticed. A direct correlation was observed between water

droplet initiated CIV and the contact angle. The epoxy-silica nanocomposite sample fabricated with 7 hr of shear mixing time led to 46.68% increment in CIV under AC voltage and 24.81% increment in contact angle compared to base epoxy resin. The Young's modulus and ultimate tensile strength (UTS) followed an increasing trend with shear mixing time and at 7 hr of shear mixing time an increase of 45.78% and 43.77% of UTS and Young's modulus respectively was observed as compared to base epoxy resin. In the digital image correlation (DIC) studies the strain versus time plot showed an increase in the time period before breakdown occurs up to 7 hr of shear mixing time. The time at which the maximum strain occurred increased to 91.49% before the breakdown of epoxy-silica nanocomposite sample which was prepared with 7 hr of shear mixing time as compared to base epoxy resin. The existing models on theoretical estimation of Young's modulus confirmed to the experimental results.

In the second part, the impact of reinforcing MWCNT in the epoxy polymer matrix on the EMI SE are studied in the X-band frequency range (8-12 GHz). The study is carried out at varying wt% of MWCNT, functionalization, thickness and impact of various inclusions on the EMI SE of epoxy-MWCNT nanocomposites. It was observed that the increase in wt% of pristine MWCNT increased the EMI SE of the nanocomposite while the defect functionalization of MWCNT reduced the average EMI SE of the nanocomposite. Also, a slight increment in average EMI SE was noticed with the increase in thickness of the sample. The comparative study on the effect of various inclusions viz. Molybdenum disulfide (MoS_2), Nickel (Ni), Copper (Cu) Nanoparticles indicated decrease in the EMI SE due to oxidized nanoparticles. Inclusion of UCFF, as a layer, enhances the EMI SE of the structure to a great extent giving an EMI SE of around 76 dB at 12 GHz for UCFF sandwiched 5wt% MWCNT-epoxy composite. The layered structure, epoxy-MWCNT:UCFF:epoxy-MWCNT introduces heterogeneity and this results in a SE much higher than the individual contributions of MWCNT and UCFF. The analysis suggests that the presence of thin layer of UCFF absorbs the radiation apart from inducing multiple scattering enhancing the absorption within the MWCNT-epoxy region. Its average EMI SE is noticed to be 53.3 dB which is 35.5 times as compared to pure epoxy and the maximum value is 76.2 dB which is almost 3.8 times more than the commercially accepted value of 20 dB. The study on the shielding efficiency due to reflection (SE_R) and absorption (SE_A) have reflected that the SE due to absorption is the major contributor towards the total SE. The permittivity and conductivity values calculated through existing theories agree to the reported values of the material.

TABLE OF CONTENTS

Table of Contents (Continued)

Table of Contents (Continued)

Table of Contents (Continued)

LIST OF TABLES

List of Tables (Continued)

LIST OF FIGURES

List of Figures (Continued)

List of Figures (Continued)

GLOSSARY

The following are some of the commonly used terms in this thesis:

Agglomeration	The term agglomeration in nanotechnology refers to nanoparticles that have associated into a cluster composed of two or more nanoparticles.
Electromagnetic Interference	Electromagnetic Interference (EMI) is a disturbance generated by an external source that affects an electrical circuit by electromagnetic induction, electrostatic coupling, or conduction.
Fracture Toughness	Fracture Toughness refers to the property which describes the ability of a material containing a crack to resist further fracture.
Functionalization	Functionalization is the process of adding new functions or properties to a material by changing the surface chemistry of the material.
Hydrophobicity	A surface is hydrophobic if it tends not to adsorb water or be wetted by water. Generally, if the water contact angle is larger than 90°, the solid surface is said to exhibit hydrophobicity.
Permittivity	A measure of the ability of a material to interact with an electric field and become polarized by the field, so that the field within the material is weaker than the field in the absence of the material.
Strain	Strain is defined as the amount of deformation experienced by the body in the direction of force applied with respect to the initial dimensions of the body.
Skin Depth	Skin Depth is a measure of the current density, and is defined as the distances from the outer edges of a conductor to the point at which the current density falls to 1/e of the value at the surface.
Skin effect	The non-uniform distribution of electric current over the surface or skin of the conductor carrying AC is called the skin effect. The concentration of charge is more near the surface as compared to the core of the conductor.

Glossary (Continued)

Poisson's Ratio	The Poisson's ratio is defined as the ratio of the transverse strain to that of the axial strain under the influence of the same force. It is a material property and remains constant.
Ultimate Tensile Strength	UTS is a material's maximum resistance to fracture. It is equivalent to the maximum load that can be carried by one square inch of cross-sectional area when the load is applied as simple tension.
Young's Modulus	Young's modulus or Elastic Modulus is a measure of the stiffness of an elastic material, and it is defined as the ratio of stress to strain.

ABBREVIATIONS

GIS	Gas Insulated Switchgear
UHF	Ultra High Frequency
DIC	Digital Image Correlation
EMI	Electromagnetic Interference
SE	Shielding Efficiency
MWCNT	Multi Walled Carbon Nano Tubes
SWCNT	Single Walled Carbon Nano Tubes
ITU	International Telecommunication Union
UCFF	Unidirectional Carbon Fiber Fabric
TEM	Transmission Electron Microscope
SEM	Scanning Electron Microscope
CIV	Corona Inception Voltage
VNA	Vector Network Analyzer

NOTATION

English Symbols

q	Electron Charge
k	Boltzmann Constant
$f_o(E)$	Occupancy Rate of Initial Electrons
E_C	Conduction Band Energy
E_M	Demarcation Energy
v	Escape Frequency of Electron
V_p	Volume Fraction
E_c	Young's Modulus of Composite Medium
E_m	Young's Modulus of Matrix Material
E_c^{Kerner}	Kerner Young's Modulus
$E_c^{Nielsen}$	Nielsen Young's Modulus
$V_{p\,max}$	Maximum Packing Fraction
P_{in}	Power of Incident EM Waves
P_{tr}	Power of Transmitted EM Waves
R	Reflectivity
T	Transmissivity
E^+	Electric Field Amplitude of the Forwarding Radiation
E^-	Electric Field Amplitude of the Returning Radiation

Notation (Continued)

Greek Symbols

λ	Decay Rate
$\Delta(E)$	Trap Depth
θ_y	Young Contact Angle
θ_m	Measured Contact Angle
ϕ_m	Mass Fraction
ρ_m	Matrix Density
ρ_p	Nanoparticle Density
ν_m	Matrix Poisson Ratio
σ_c	Ultimate Tensile Stress of Nanocomposite
σ_m	Ultimate Tensile Stress of Matrix
μ	Permeability
ε	Permittivity
α	Attenuation Constant
β	Phase Constant
γ	Complex Propagation Factor

CHAPTER 1

INTRODUCTION

1.1 General

Ordinary materials, when reduced to nanoscale, often exhibit novel and unpredictable characteristics such as extraordinary strength, chemical reactivity, electrical conductivity, superparamagnetic behaviour and other characteristics that the same material does not possess at the micro or macroscale. The agglomeration of the atoms and molecules in the range of 1-100nm forms the basis of nano particles and they exhibit an extensive range of properties. The nano particles essentially bridges the gap between small molecules and bulk materials in terms of energy states. Based on their chemical and electromagnetic properties, nano particles can exist as dispersed aerosols, suspensions/colloids or in an agglomerate state. Normally nano particles tend to adhere to each other and to form agglomerates because of Van der Waals forces that act over short distances, magnetic interactions, electrostatic forces present in the particles and adhesion forces related to the liquids adsorbed on their surfaces. Agglomeration due to Brownian motion is classified as 'coagulation'. To avoid agglomeration, several processes include a post-synthesis stage to modify the particle surface by coating it with another organic or inorganic substance. In an agglomerate state, nano particles may behave as larger particles, depending on the size of the agglomerate. Once nano particles are synthesized, it is important to fully characterize and understand their structure [1].

The high aspect ratio and specific surface area of nano structures improves the electrical, mechanical and thermal properties of the nanocomposites [2,3]. Fillers in low concentration in the base matrix results in uneven dispersion whereas high concentrations lead to agglomeration leading to decrease in the load bearing capacity of the material [4]. Another parameter that can affect the mechanical properties is the amount and shape of filler. For every filled polymer system, there is a maximum volume fraction of particles that can be incorporated into the polymer matrix. Otherwise, it results in stress concentration points giving rise to a more brittle material with a lower ultimate tensile strength [5]. It is known through various studies that the improvement in tensile behaviour of nanocomposite materials depends on the efficient filler

dispersion and the interfacial adhesion between filler and the matrix [6,7,8]. Therefore, it is an utmost concern for the researchers to identify the optimized mixing rate and time and the filler concentration which ensures the efficient filler dispersion in the polymer matrix for enhancing the overall properties of the material. Since the rate and time during the preparation of the nanocomposites determine the extent of dispersion and adhesion therefore it is relevant to reach some optimum values for attaining the best properties from the nanocomposites. Also, the charge transport through the material as a function of localized surface traps needs to be studied especially due to under or over processing during the synthesis of the nano materials. Under the normal operating condition, the inherent defective states in the insulating material accumulate the charge within the bulk volume initiated from the surface trap sites, causing the local electric field enhancement, leading to internal damage locally and over a period of time, a catastrophic failure can occur [9,10]. Therefore, the electrical and mechanical characterization of the nano composite material is essential for understanding the behaviour of the material and subsequently categorizing it for various applications.

Epoxy resin is a vital material, that is used as an insulating material in power system equipment such as dry type transformers and can also be used as spacers in GIS [2, 11]. Base epoxy resin can be reinforced with different weight percentages of nanoparticles by different methods to enhance electrical, mechanical and thermal properties [12-14]. The desired properties such as high breakdown strength, low dielectric loss, low surface charge accumulation and high mechanical strength can be achieved due to the high aspect ratio and specific surface area of filler particles [9,15-17]. In one of the studies Imai et al. have stated that the inclusion of SiO_2 particles reduces thermal expansion coefficient of epoxy nanocomposites [18]. Also another study indicates that the inclusion of the silica fillers improves the mechanical strength of the composites [19]. Filler-concentration plays a vital role in the preparation of composite material, as the low filler-concentration may result in uneven dispersion and high filler-concentration may lead to agglomerations if the composite materials are not properly prepared [4]. Also, the efficient filler dispersion in the polymer matrix depends upon the shear mixing rate and time during the sample preparation, for enhancing the properties of the material [5].

It has been established in various studies that shear mixing is an effective method of dispersing nanoparticles in epoxy, which can break the agglomerates of the nanoparticles apart. Pullicino et al. have studied the effect of variation in shear mixing rate and time in epoxy

nanocomposites and have indicated that the optimum combination of shear mixing time and rate results in better dispersion of nanoparticles [20]. While they have varied the shear mixing rates but they have limited the study to 1 hour and 2 hours of shear mixing times. Hence, in the present study, the shear mixing time during the preparation of the nanocomposites is varied by keeping shear mixing rate as constant, in order to identify the suitable shear mixing time for enhancing the overall properties of epoxy nanocomposites.

Water droplet presence on the insulating material because of fog, rain and humid environmental conditions can initiate micro discharges that occur at the triplet junction of a water droplet, air and the insulator surface. This results in conductive paths on the surface of the insulating material leading to surface flashover. Sarathi et al. have performed corona inception studies in water droplet present on the insulating material, and have stated that UHF signals are radiated due to water droplet-initiated discharges [21]. Hence, it is necessary to identify the voltage at the initiation of corona phenomenon due to these accumulated water droplets on the surface of the insulators. In addition to this, the study of surface potential decay measurement and trap distribution analysis are also important in electrical characterization of epoxy nanocomposites.

Recent studies have indicated that the superior tensile properties in case of polymeric nanocomposites can be obtained by good matrix-filler interfacial adhesion and proper filler dispersion [6-8,22]. Also, the bonding at the matrix-filler interface plays an important role in effective load transfer and also on the strain distribution of the composite material [23-24]. Digital Image Correlation (DIC) is an image-based technique which can be applied for strain field displacement calculation [25]. Hence, this technique is applied for tensile test, to study the influence of shear mixing time variation on mechanical behaviour of epoxy-silica nanocomposites.

Therefore, to study the electrical and mechanical properties of epoxy-silica nanocomposites and thereby also establish the impact of shear mixing time on epoxy-silica nanocomposites, the following methodical studies were performed; (i) Water droplet-initiated corona inception studies, (ii) Contact angle analysis (iii) Surface potential decay measurement and trap distribution analysis and (iv) Digital image correlation studies.

Electromagnetic Interference (EMI) is a major problem in the present world due to the enormous advancements and usage of electronics in every facet of life. EMI poses threat to the functioning of various electronic equipment to the tune of rendering it completely inoperative. Due to the serious effects of EMI, it has become imperative to protect the various instruments, appliances and other electronic goods from its detrimental effects [26].

Carbon nano tubes (CNT) are known to exhibit superior properties such as light weight, high mechanical strength, and corrosion resistance. With its high conductivity, CNT is one of the most sought contenders for EMI shielding applications as it also enhances the mechanical properties [27-29]. There have been many studies in the literature regarding the improvement of EMI shielding efficiency (SE) by adding MWCNT nanofillers in different polymers [28].

For any commercial application, it is desirable to have a SE more than 20 dB. A high value of EMI SE can be achieved either by increasing the concentration of CNT in the composite or by increasing the thickness of composite material [30]. The mechanical strength of a nanocomposite is equally important while preparing a material for high EMI SE. Though the absence of concentric walls makes SWCNTs less defected, however, MWCNTs are preferred over SWCNTs owing to its excellent mechanical properties [31]. Functionalization of CNT is another potential technique to improve the mechanical strength of the nanocomposites [32,33]. However, the impact of defect functionalization on the EMI SE of CNT has not been studied to a great extent in the past. Also, it is well known that an increase in the mechanical strength of CNT based materials can be achieved only for low loading level, after which the reduction in the mechanical properties have been noticed due to improper dispersion, agglomeration etc. [34]. Therefore, a better way to achieve high value of EMI SE is to include another material along with CNT to get a combined effect of the different particles resulting into a better EMI SE value at a desirable thickness of the composite.

Further, conductivity plays an important role in the EMI SE of a composite. It has been established in various works that more the conductivity of the filler, more is the EMI SE of the composite [35,36]. However, the combined effect of two or more different types of conductive fillers may give varied result due to the interaction between them and the matrix. The same has been attempted with various fillers in the present work. Another important property that affects the EMI SE of a composite is the skin effect. It has been found in various studies that a conductive filler of smaller unit size is more effective than a conductive filler with a large unit

size. It is due to the fact that for effective use of the entire cross-section of a filler unit for EMI shielding, the unit size of the filler should be comparable to or less than the skin depth [37,38].

Also, studies have been carried out with carbon fiber fabrics (CFF) for enhancing the mechanical strength of the composite materials [39]. However, only a limited study has been carried out on the effect of addition of CFF on the EMI SE. Hence, in the present work, effect of inclusion of a thin layer of unidirectional carbon fiber fabric (UCFF) in epoxy polymer matrix on EMI SE of nanocomposites is studied.

The X-Band as defined by IEEE is a frequency range from 8 to 12 GHz [40]. The X-Band has a short wavelength making it suitable for radar applications as higher resolution imaging for target identification is required. Also, it finds utility in satellite and ground communications. The International Telecommunication Union (ITU) has allocated 8.175 to 8.215 GHz for meteorological satellites for monitoring weather conditions, 8.75 to 8.85 for aeronautical radio navigation, 8.85 to 9.0 for maritime radio navigation, 9.3 to 9.9 GHz for active space research and 10.6 to 10.7 GHz for passive space research [41]. The present study is undertaken in the frequency range between 8 and 12 GHz as this range is mostly used in academic and research purposes.

There have been many studies with respect to the EMI SE of MWCNT nanocomposites in different polymer matrix [28]. The epoxy chosen for the present study is CY230-1 because of its low viscosity (which serves as a good matrix for MWCNT), high mechanical strength, high resistance to atmospheric and chemical degradation and good electrical properties.

With epoxy as the polymer base, present work investigates the EMI SE (in the X-band region) by the epoxy polymer matrix due to the (i) addition of pristine MWCNT (0, 1, 3, and 5 wt%) (ii) addition of functionalized MWCNT (0,1,3 and 5 wt%) (iii) Varying thickness of pristine MWCNT – epoxy nanocomposites (1,3 and 4mm) (iv) Addition of fillers (MoS_2, Ni and Cu nanoparticles) (v) Introduction of single thin layer of UCFF along with pristine MWCNT (0, 3 and 5 wt%).

1.2 Literature Review

Nano is the word used to describe 10^{-9}th part of any matter. In the lecture 'There is a plenty of room at the bottom' in December 1959 at the American Physical Society **Richard P Feynman** first introduced the concept of nano particles [42]. Further, in 1974 **Norio Taniguchi** invented the term 'Nanotechnology' and later it was popularized by **K Eric Drexler**. Silica is a widely found material on earth. Naturally occurring silica such as rocks, clays, and quarts sand are commonly used as raw materials in the industries. These raw materials are treated to produce direct silica sources like sodium silicate and silicon tetrachloride to be utilized in the production of industrial silica products such as silica gel, precipitated silica, silica sol and fumed silica. There have been studies carried out exploring the applications of silica in various fields like in microelectronics by **Salleo et al**. [43], in optical communications by **Che et al.** [44], in thin-film technology by **Suzuki et al**. [45] and medicine and Pest control by **Barik et al.** [46].

The review paper by **Rahman, I.A.** and **Padavettan** give the methods of synthesis of silica nanoparticles, characterization on size-dependent properties, and surface modification for the preparation of homogeneous nanocomposites. It also summarizes the effect of nano-silica on the properties of various types of silica-polymer composites [47]. **Veena et al.** in their work studied the properties of nanocomposites wherein they established that the electrical resistivity (ρ), ultimate tensile strength, and hardness of the composites increased with SiO_2 weight fraction up to 10 wt% and decreased thereafter [48].

A water droplet on the insulator surface due to wetting conditions like rain or condensation of fog can cause local electric field intensification on the insulator. Excessively high electric field intensity at any point causes corona discharge that leads to reduction in hydrophobicity of the material and arcing. **Reid et al.** found in their study that the corona discharge activity on insulators often precedes arcing causing extensive damage to insulation of the power equipment [49]. A study on the water droplet initiated discharges on silicone rubber carried out by **Lopes et al.** yielded that the corona discharge threshold electric field is between 3 to 3.5 kV/cm [50]. **El-Kishky et al.** in their study on corona discharges initiated due to water droplets concluded that electric field intensity is high near the triple point junction [51]. **Sarathi et al.** in their study on epoxy nanocomposite samples of different clay content subjected to water droplet initiated discharge tests using controlled harmonic content, high voltage supply found that the discharges caused damage near the high voltage electrode and that the surface

carbonization is related to the accumulated dissipated energy during the discharge process. Further analysis indicated that the discharges occur around the voltage peak and also when the rate of rise of voltage is high and the number of discharges is higher in the positive half cycle as compared to the negative half cycle [52].

Miao et al. studied the mechanical behaviour of nano-silica/epoxy under uniaxial compression and found that the presence of nano-silica only reinforces slightly the peak stress (compressive yield strength) of the composites under both quasi-static and dynamic loading conditions [53]. Further, the effect of nano-silica loading on mechanical property, thermo-mechanical properties, morphology, and dielectric properties was studied by **Guchhait et al.** in which they observed that the tensile properties decrease with the increase in nano-silica loading for all the nanocomposites system except for 3 wt% nano-silica loading. This has been attributed to the better dispersion of nano-silica particles in modified epoxy matrix at 3 wt% loading compared to other systems which were observed from transmission electron microscopy (TEM) images [54].

Since the first reporting of Carbon Nano Tubes by **Iijima** in 1991 [55], CNTs have been studied extensively for varied applications owing to its superior electrical and mechanical properties. **Dresselhaus M.S., Dresselhaus G.** and **Saito R.** have explained the structure of CNTs and the fundamental relations governing the geometry in their study [56]. **Popov V.N.** in his report has provided details of various work carried out in the field of the carbon nanotube research and its possible industrial applications [57]. **Yuen et al.** in their study have discussed in detail the thermal, electrical, and morphological properties of MWCNT-epoxy composites wherein they observed that the addition of MWCNTs to the epoxy resin enhanced the electrical properties, glass transition temperature and dielectric constant. However, there was an insignificant effect on the thermal conductivity and thermal expansion of MWCNT/epoxy composites [58]. **Lachman N.** and **Wagner H. D.** studied the correlation between CNT–epoxy interfacial molecular structure and overall composite mechanical properties in a number of carbon material based systems including pristine, carboxylated, and aminated CNTs and found that the composite toughness increased with enhanced interfacial adhesion [59].

In one of the studies by **Cha et al.**, CNTs were functionalized by attaching melamine to improve the dispersing ability and interfacial bonding between CNTs and matrix. The tensile tests performed at various weight fraction indicated improvement in Young's modulus,

ultimate tensile strength and fracture toughness in the functionalized CNT-Epoxy nanocomposites [60]. **Nam et al.** in their study suggested a novel procedure for preparation of electromagnetic wave shielding/absorbing composites made of carbon nanotube (CNT)-embedded epoxy. Multi-layered CNT–epoxy composites (CNT plates) were fabricated by stacking the CNT films layer-by-layer to improve the electrical properties of the composites. Electromagnetic interference (EMI) shielding effectiveness and sheet resistance of the composites were investigated with variation of thickness. Results showed improvement of shielding properties in a frequency band of interest from 1 to 5 GHz for epoxy based CNT nanocomposites [61]. **Singh et al.** suggested preparation of MWCNT/carbon fiber (CF) fabric materials reinforced in epoxy resin to make multi scale composites for microwave absorption in the X-band. It was observed that the incorporation of MWCNTs on the carbon fabric produced a significant enhancement in the electromagnetic interference shielding efficiency to approximately 51 dB for composites of 2 mm thickness. Also, it was observed that the inter-laminar shear strength doubled for multiscale composites thereby making them an efficient microwave shield in terms of mechanical strength [62].

1.3 Objectives

The proposed project is aimed at studying the properties of nanofiller reinforced epoxy materials. Two types of nanofillers have been selected in the project to study the electrical, mechanical and EMI shielding efficiency of the nanocomposites. The objectives of the first study comprising of epoxy reinforced with nano-silica particles are: -

- Establishing an optimum weight percentage of the nanoparticles in the epoxy matrix in a low loading scenario.
- Establishing an optimum shear mixing time for the nanoparticles in the epoxy matrix to obtain a homogeneous mixture exhibiting good electrical and mechanical characteristics.
- Theoretical modelling of the experimental results based on existing theories to confirm the mechanical properties of the nanocomposite.

The objectives of the second study comprising of epoxy reinforced with MWCNT for EMI SE studies are: -

- Studying the effect of weight percentage, functionalization, thickness and inclusion of various fillers in the EMI SE of the nanocomposites.
- Obtaining a high value of EMI SE of the nanocomposites under study.
- Theoretical modelling of the experimental results based on existing theories to evaluate various parameters of the nanocomposites.

1.4 Organisation of Thesis

Chapter 2 gives the physical details and the source of procurement of the various materials used in the study. It also gives in detail the methods used in the preparation of the various nanocomposites in both the studies. Also, the chapter provides the list of samples studied in the present work and their respective sample codes.

Chapter 3 gives the detailed study of electrical characterization of the epoxy based silica nanocomposite. It provides the details of laboratory tests and experiments carried out for ascertaining the electrical properties of the nanocomposites. The various tests discussed in the chapter are the water initiated corona inception voltage test, contact angle test and the surface potential decay measurement and trap distribution analysis test.

Chapter 4 provides the detailed study of mechanical characterization of the epoxy based silica nanoparticle. It gives the details of tensile test and digital image correlation test carried out for establishing the mechanical properties of the nanocomposites. The chapter also illustrates the methodology for theoretical modelling of the mechanical characteristics of nanocomposites based on existing theories.

Chapter 5 gives the methodology opted for carrying out the EMI shielding efficiency measurement of the various epoxy based MWCNT/Inclusion nanocomposites. It also gives out the plane wave theory for three layer and multi-layer systems based on which the theoretical modelling of the system is carried out to obtain the various parameters of the nanocomposites.

Chapter 6 provides the results obtained from the various laboratory tests and experiments and gives the detailed justification of the various observations. It also gives out the details of the results obtained from theoretical modelling and their comparison with the experimental results.

Chapter 7 discusses the various conclusions deduced from the study and gives out the future scope of work that can be carried out based on the results of the present work.

CHAPTER 2

MATERIAL AND SAMPLE PREPARATION

2.1 General

Material preparation is the most crucial part of the present work. It is important to follow all the steps in the preparation of the nanocomposites diligently so that that there is a homogeneous mix, accurate size and no undue foreign particles or air bubble in the prepared samples.

2.2 Materials: Epoxy-Silica Nanocomposite

The materials used in the preparation of the nano composite are Bisphenol-A epoxy resin (CY205) as a base polymer matrix, Tri-ethylene tetra-amine (TETA) hardener as a curing agent and nano-silica particles of the size 15nm APS, 99.5% purity supplied by Nanostructured & Amorphous Materials, Inc. Houston, Texas, USA.

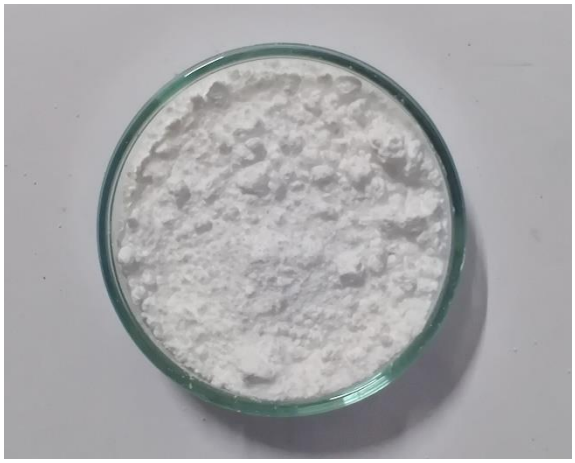

Fig. 2.1: Nano Silica Powder

2.3 Sample Preparation: Epoxy-Silica Nanocomposite

The nano composite material was prepared at varying weight percentages of 0, 1, 3, 5 and 10 wt% and later at only 1 wt% by exposing the mixture to different shear mixing timings varying at regular intervals of 2 hours, 5 hours, 7 hour and 10 hours at constant speed of 2000 rpm and

one pure sample of the epoxy without nanofiller. At the outset, the required quantity of nano silica powder was heated at 110 °C for 24 hours to remove the traces of moisture in it, if any. Thereafter heated nano filler was mixed with ethanol and was kept in sonic water bath for 45 min. Subsequently, the nanoparticle dispersed ethanol was mixed with epoxy resin and sonicated at high frequency sonication process (20 kHz) for one hour. The mixture was then subjected to shear mixing of 2 hours, 5 hours, 7 hours and 10 hours respectively for preparation of different samples. Thereafter, again the mixture was subjected to high frequency sonication process (20 kHz) for one hour while maintaining the sample temperature at 40 °C in ice filled water bath. The mixture was then kept in an oven for allowing the excess ethanol to evaporate. At the last stage, the required quantity of hardener was added to the nanoparticle dispersed epoxy mixture and mixed thoroughly till uniform dispersion was achieved. On degassing, the mixture was poured into moulds in required dimensions for various tests.

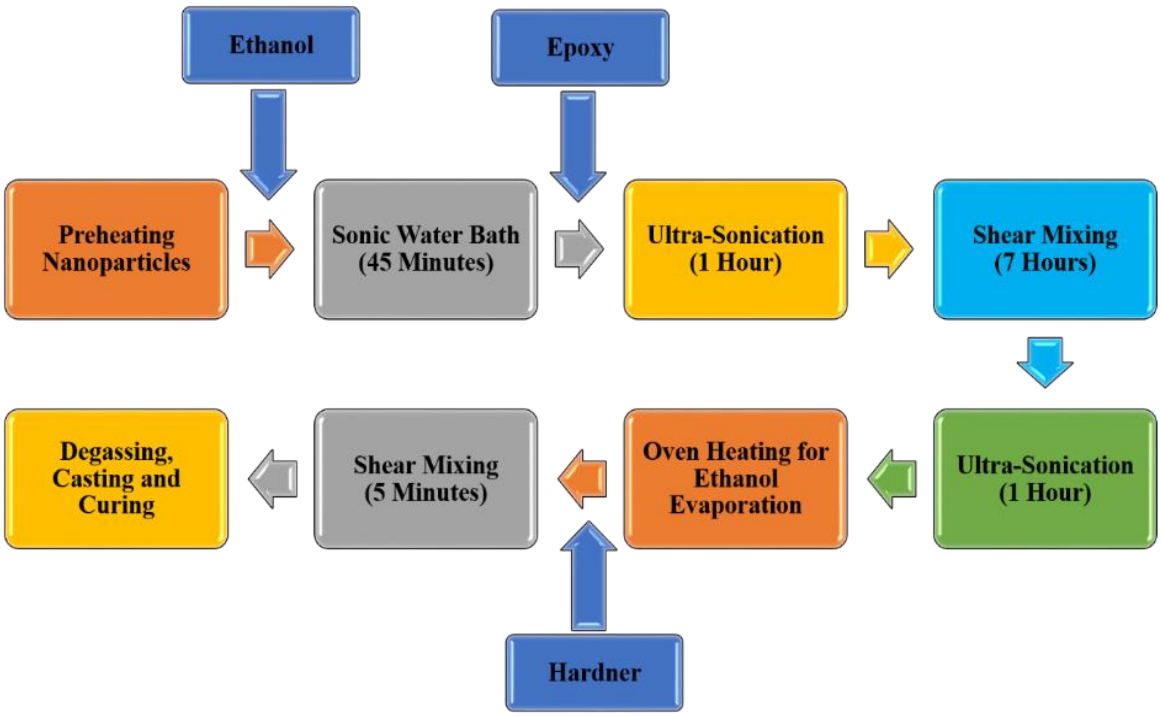

Fig. 2.2: Schematic Diagram of Sample Preparation

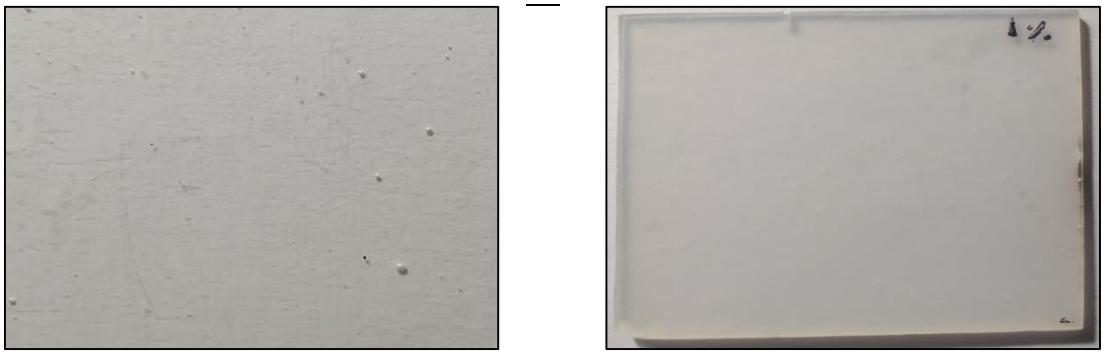

(a) Pure Epoxy Sample (b) Epoxy-Silica Sample

Fig. 2.3: Samples for Electrical Characterization Tests

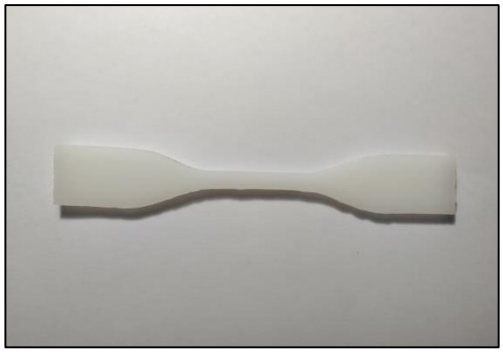

Fig. 2.4: Dumb Bell Shaped Sample for Mechanical Characterization Test

Table 2.1 Epoxy-Silica Sample Details

Sample Code	**Sample Details**	
	Silica Wt%	**Shear Mixing Time**
Pure	- (Base epoxy resin)	-
1 wt%	1	7
2 wt%	2	7
3 wt%	3	7
5 wt%	5	7
10 wt%	10	7
2 hr	1	2
5 hr	1	5
7 hr	1	7
10 hr	1	10

2.4 Materials: Epoxy-MWCNT-Inclusion Nanocomposites

The materials used in the preparation of the epoxy nanocomposite samples are Bisphenol-A epoxy resin (CY230-1) as base matrix, MWCNT, Purity 95%, OD 5-20nm, length 1-10um (imported and marketed by Reinste Nano Ventures Private Limited, New Delhi), Nano Copper, 20nm, 99% dry powder with bta coating and Nano Nickel, 20nm (supplied by Hongwu International Group Ltd, Hong Kong), MoS_2 nano powder 20nm, 99% purity (supplied by Loba Chemie, Mumbai), UCFF 0.111mm and Tri-ethylene tetra-amine hardener as curing agent. Various materials are shown in Fig. 2.5.

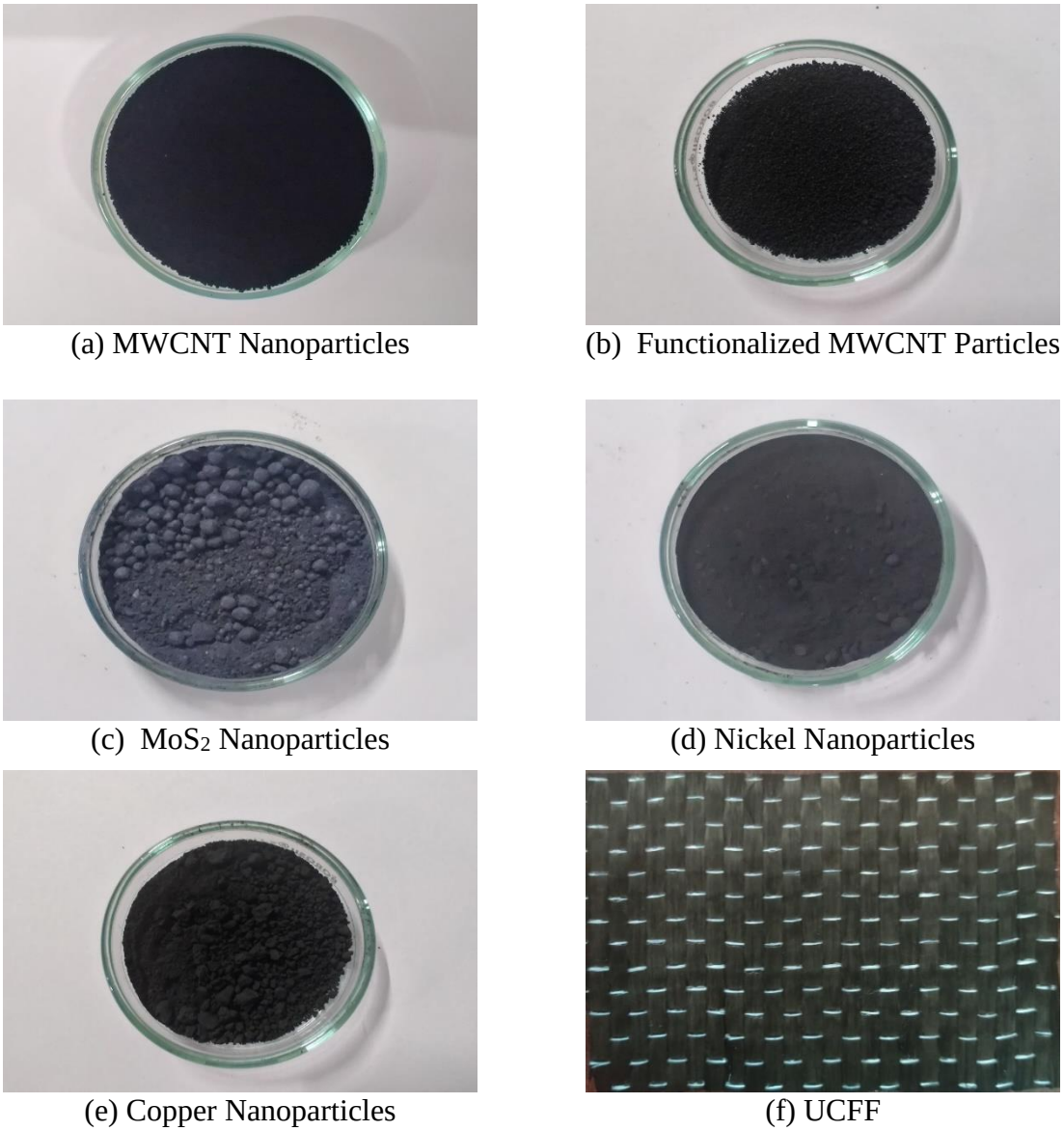

(a) MWCNT Nanoparticles (b) Functionalized MWCNT Particles

(c) MoS_2 Nanoparticles (d) Nickel Nanoparticles

(e) Copper Nanoparticles (f) UCFF

Fig. 2.5: Various Nanoparticles and Carbon Fiber Fabric

2.5 Defect Functionalization of MWCNT

Functionalization of MWCNT was carried out by placing MWCNTs in a 3:1 H_2SO_4/HNO_3 solution. The MWCNT in solution was sonicated in an ultrasonic bath for 3h at ambient temperature. Thereafter, the solution was diluted with distilled water and then filtered with large amount of distilled water. The concentration of acidity was measured periodically with pH strips and continued to wash with distilled water until the pH of MWCNTs in solution was equal to the pH of the distilled water. The MWCNTs were then dried overnight to obtain functionalized MWCNTs.

2.6 Sample Preparation: Epoxy-MWCNT-Inclusion Nanocomposites

Nanocomposites of various wt% of pristine/functionalized MWCNT (0,1,3 and 5wt%) and thickness (1,3 and 4mm) along with the inclusions (MoS_2, Ni and Cu) or UCFF were prepared. The various nano powders were heated at a temperature of 110 °C for 24 hours to remove the traces of moisture in it. Thereafter the nano fillers were dispersed in ethanol and were kept in sonic water bath for 45 min. Then, the above mixture was mixed with epoxy resin and sonicated at high frequency sonication process (20 kHz) for one hour. The mixture was then subjected to shear mixing of 7 hours for thorough mixing and dispersion. Thereafter, the mixture was again subjected to high frequency sonication process (20 kHz) for one hour. Then, this mixture was transferred to an oven to evaporate the excess ethanol. Thereafter, the hardener was mixed thoroughly and degassed, the final mixture was poured in various moulds and kept under compress moulding for 18 hrs and later kept for curing for another 6 hrs. For UCFF samples, a single layer of UCFF was placed in the moulds with pure epoxy/MWCNT mixture equally layered on both sides of the fiber fabric to form a sandwich structure as shown in Fig. 2.6.

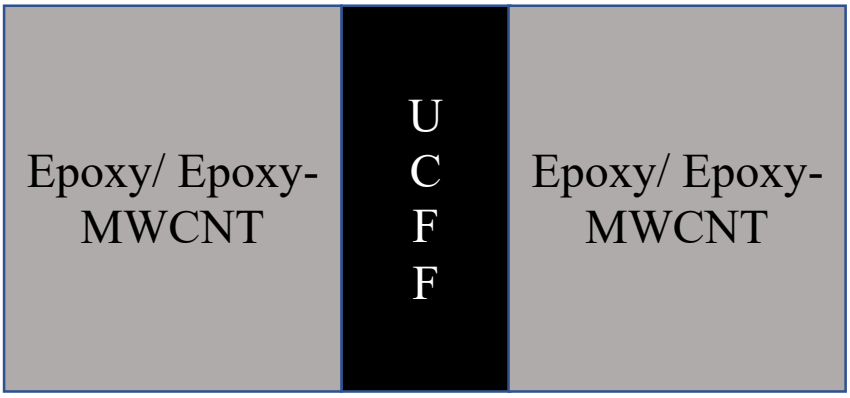

Fig. 2.6: Schematic of Sandwich Structure

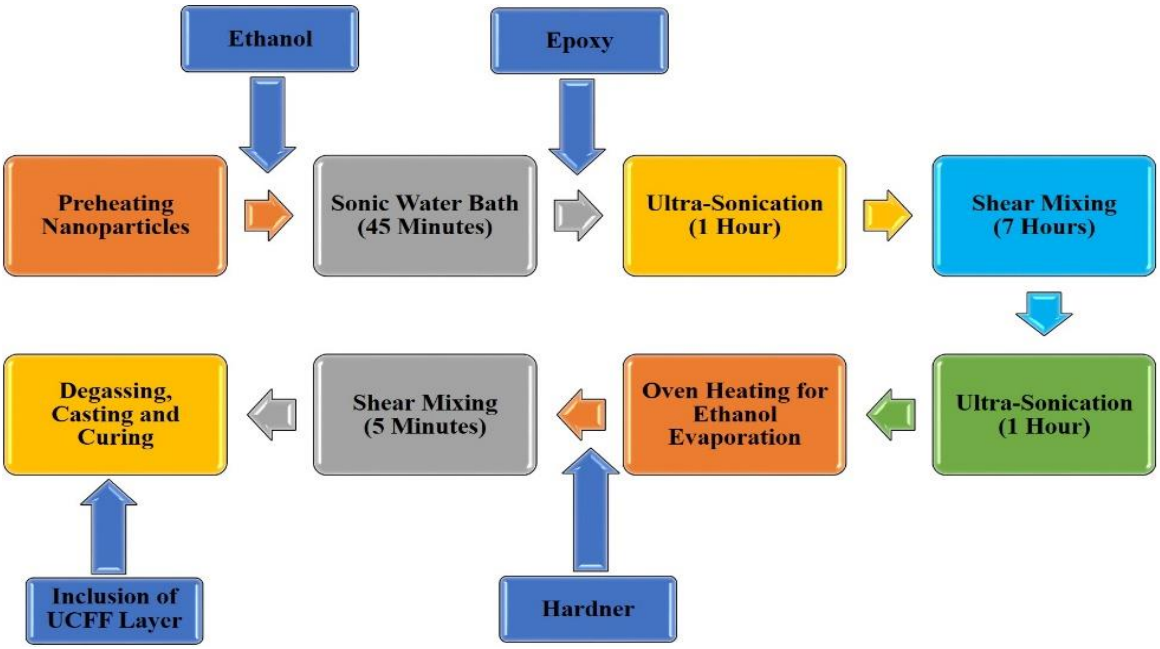

Fig. 2.7: Schematic Diagram of Sample Preparation

(a) Epoxy-Pristine MWCNT Sample

(b) Epoxy-Functionalized MWCNT Sample

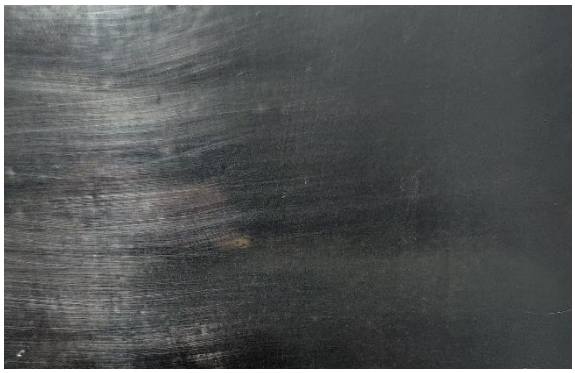

(c) Epoxy-MWCNT/Inclusion Sample

(d) Epoxy-UCFF Sample

Fig. 2.8: Epoxy/MWCNT/Inclusion/UCFF Samples

Table 2.2 Epoxy-MWCNT Sample Details

Sample Code	Sample Details		
	MWCNT Type and Wt%	**Inclusion and Wt%/Layer**	**Thickness (mm)**
Pure Epoxy	-	-	1
P MWCNT 1 wt% 1mm	Pristine, 1 wt%	-	1
P MWCNT 3 wt% 1mm	Pristine, 3 wt%	-	1
P MWCNT 5 wt% 1mm	Pristine, 3 wt%	-	1
F MWCNT 1 wt% 1mm	Functionalized, 1 wt%	-	1
F MWCNT 3 wt% 1mm	Functionalized, 3 wt%	-	1
F MWCNT 5 wt% 1mm	Functionalized, 5 wt%	-	1
P MWCNT 5 wt% 3mm	Pristine, 5 wt%	-	3
P MWCNT 5 wt% 4mm	Pristine, 5 wt%	-	4
MWCNT/MoS_2 1mm	Pristine, 3 wt%	MoS_2, 2 wt%	1
MWCNT/Ni 1mm	Pristine, 3 wt%	Ni, 2 wt%	1
MWCNT/Cu 1mm	Pristine, 3 wt%	Cu, 2 wt%	1
UCFF SL 1mm	-	UCFF Single Layer	1
MWCNT 3 wt%/UCFF 1mm	Pristine, 3 wt%	UCFF Single Layer	1
MWCNT 5 wt%/UCFF 1mm	Pristine, 5 wt%	UCFF Single Layer	1

2.7 Summary

The chapter gave out the materials used and the method of preparation of samples under study. Sample preparation is a vital step in the entire study and the samples were prepared in sufficient quantity to be able to cater for any damages during the various tests. The sample codes given to the various samples shall be used throughout the project work while discussing the particular material. The samples were prepared in the High Voltage Laboratory, Department of Electrical Engineering and Composite Manufacturing Laboratory, department of Aerospace Engineering, IIT Madras.

CHAPTER 3

ELECTRICAL CHARACTERIZATION OF EPOXY - SILICA NANOCOMPOSITES

3.1 General

In this chapter, various tests that were conducted to investigate the electrical properties of the silica epoxy nanocomposite have been discussed in detail. Tests were also conducted to verify the behaviour of the composites which were shear mixed at various lengths of time. Initially a CIV test was conducted to ascertain the weight percent of nano-silica to be used for the studies. Following the CIV test, various tests were conducted that includes water droplet initiated corona inception voltage test, contact angle analysis and surface potential decay measurement and trap distribution analysis.

3.2 Water Droplet Initiated Corona Inception Voltage Test

The usage of insulators exposed to the environmental conditions demand the studies of corona activity on the surface of an insulator due to the presence of water droplet on the surface. Increase in conductivity of water droplet reduces CIV. The CIV is high under negative DC as compared to positive DC/AC voltages. Surface charge accumulation studies indicate that the charge retention capability of the insulating material gets reduced drastically with the damage caused due to corona resulting into the degradation of surface. An under or over preparation of a composite leads to variation in water droplet induced CIV therefore an optimum mixing time of a mixture is important to reach an acceptable range of CIV of a material. It was observed in previous studies that the water droplet initiated discharges under AC and DC voltages radiate UHF signal in the bandwidth 0.3-1.2 GHz.

The experimental setup used for understanding the corona discharge activity, due to a water droplet on the nanocomposite under AC and DC voltages is shown in Fig. 3.1. The experimental setup consists of a high voltage source, the test electrode, a UHF sensor connected to the high bandwidth digital storage oscilloscope and the partial discharge measurement unit.

The test electrodes used in the present study consisted of two angular stainless steel electrode tips cut at 45° (as per IEC 60112), and placed on the sample. The electrodes were separated by a distance of 20 mm. One electrode was connected to the high voltage source through a resistance of 10 MΩ (R_s), and the other electrode was connected to the ground. To understand the characteristics of the UHF signal generated due to water droplet, a broadband UHF sensor is used. The output of the UHF sensor was measured using a high bandwidth digital storage oscilloscope (LeCroy Wavepro 7300A, 3 GHz bandwidth, operated at 20 GSa/s). Fig. 3.2 shows the electrode position and Fig. 3.3 shows the frequency response of the sensor as measured using a UHF calibration system.

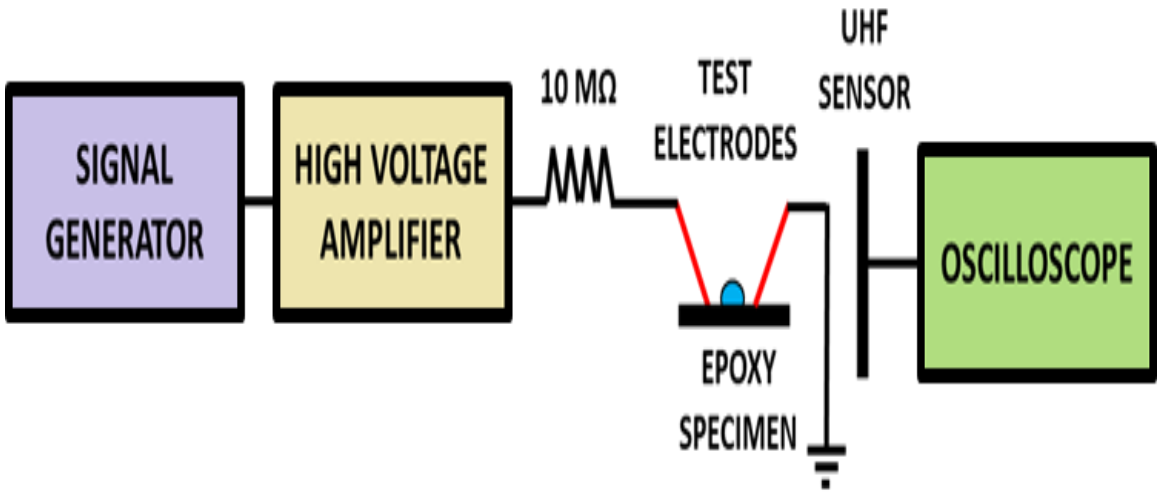

Fig. 3.1: Experimental Setup for Water Droplet Initiated Corona Inception Voltage Test

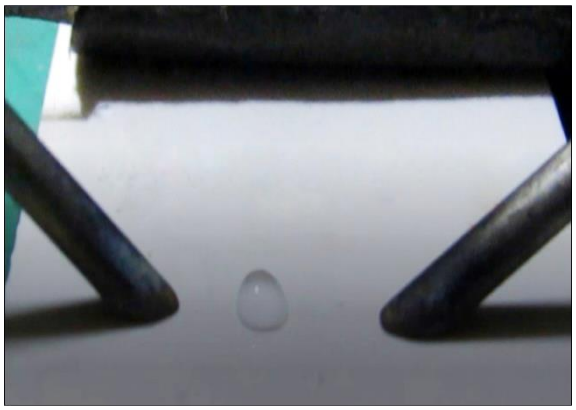

Fig 3.2: Electrode Position

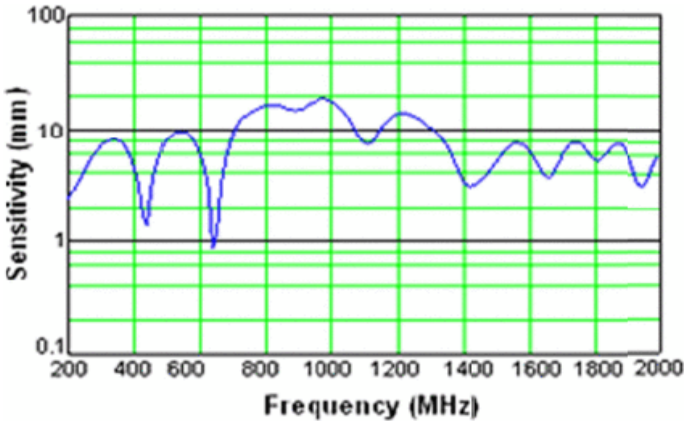

Fig 3.3: Frequency Response of UHF Sensor

3.3 Surface Potential Decay Measurement and Trap Distribution Analysis

Fig. 3.4 depicts the arrangement for measuring surface potential decay of the nanocomposite. The surface potential decay characteristics of the charge deposited on the nano silica composites by corona discharge process was analyzed using an electrostatic voltmeter. The gap between the sensor and the surface of the specimen was maintained at 1.5mm. In the system, the needle electrode was used to generate a corona discharge over the sample. The sample was first charged for 3 min at 10 kV with both +ve and –ve DC. After being charged, the sample was quickly moved to the measurement system via a sliding platform for measuring the surface potential characteristics. The measurement system consisted of a sensor, a noncontact electrostatic voltmeter and a computer. Electrostatic voltmeter, Trek model 341B was used for the measurement. The surface potential discharge measurement for each specimen was performed for three times for confirming the repeatability of the characteristics. The charge (Q) on the surface of the nanocomposite was calculated as:

$$Q = V\varepsilon_0\varepsilon_r \frac{A}{d} \tag{3.1}$$

Where, ε_0 and ε_r are the relative permittivity of vacuum and of the medium, respectively.

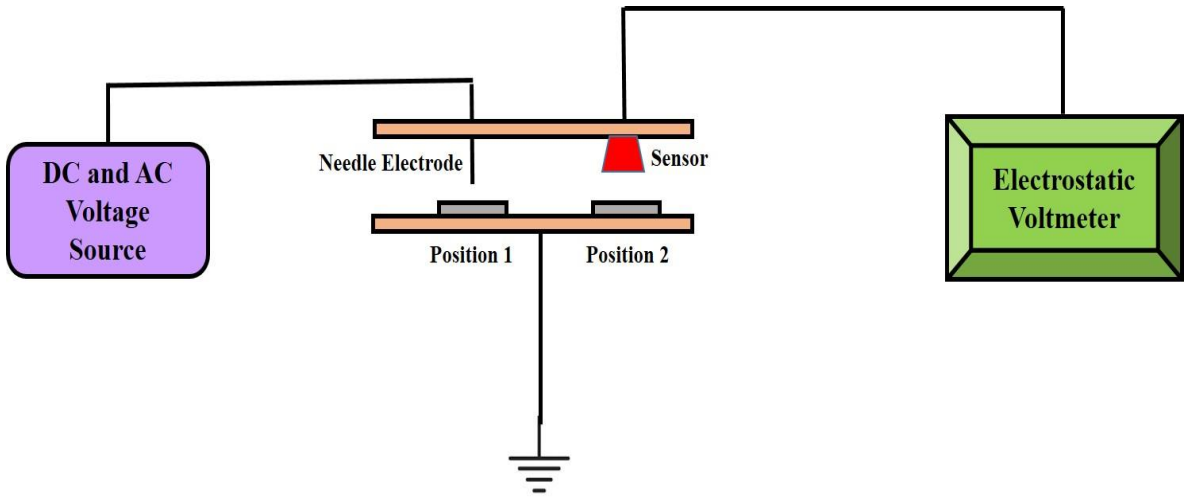

Fig 3.4: Setup for Surface Potential Decay Measurement and Trap Distribution Analysis

The variation in the surface potential decay characteristics exhibited the exponential decay and can be quantified as: -

$$V = V_o e^{-\lambda t} \tag{3.2}$$

where V_o is the initial potential and λ is the decay rate.

The charge transport characteristics of a material is affected by the impurities present in the material [63]. For the present experiment specifications, the applied electric field is not high enough for the charge carriers to transport through the volume of the material. Thermal agitation due to collision of charges allows the injected charge carriers to accumulate on the surface trap sites during the corona charge injection. The accumulated charge at the surface of the specimen decays by recombining with the ions of opposite sign in the surrounding, rather than transporting through the bulk, under the absence of applied voltage. Thus, the decay in surface potential measured through electrostatic voltmeter is directly related to decay of surface charge under the present experimental conditions.

The trap distribution in all the samples can be estimated using the surface potential decay characteristics as [64]: -

$$N(E) = \frac{2\,\varepsilon_o \varepsilon_r}{qL^2 kTf_o(E)} t \frac{dV}{dt} \tag{3.3}$$

where q is the electron charge, L is sample thickness, k is the Boltzmann constant, T is the absolute temperature, t is time, and f_o (E) is occupancy rate of initial electrons.

The trap depth Δ(E) can be represented as;

$$\Delta E = E_C - E_M = kT \ln(vt) \tag{3.4}$$

where E_C is conduction band energy and E_M demarcation energy, k is the Boltzmann constant, v is the escape frequency of electron (10^{12} Hz) and T is the absolute temperature.

3.4 Contact Angle Analysis

Contact angle is a quantitative measure of wetting of a solid by a liquid. It is the angle formed by a liquid at the three phase boundary where a liquid, gas and solid intersect. Fig. 3.5 gives the diagrammatic representation of the contact angle. The well-known Young equation describes the balance at the three phase contact of solid-liquid and gas [65,66].

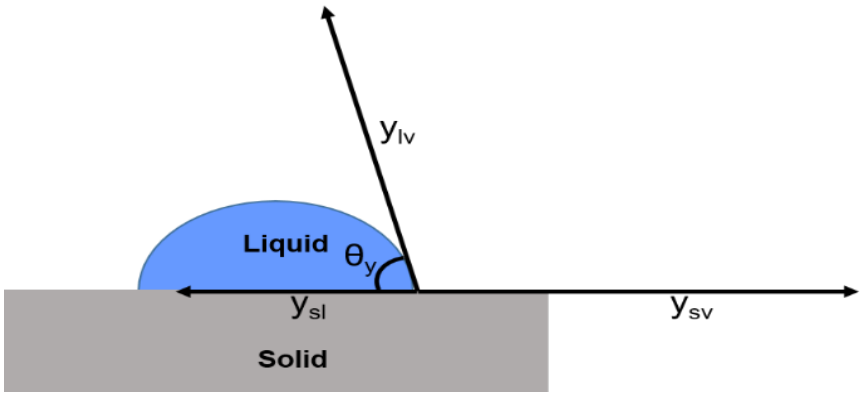

Fig. 3.5: Contact Angle.

$$y_{lv}\cos\theta_y = y_{sv} - y_{sl} \tag{3.5}$$

where y_{sv}, y_{sl} and $y_{lv,}$ called the interfacial tensions, form the equilibrium contact angle of wetting or the Young contact angle θ_y. Liquids with low contact angle values are expected to spread on the surface while liquids with high contact angle values exhibit poor spreading. Liquids with contact angle less than 90° is said to wet the surface with zero contact angle

representing complete wetting. While the liquids with contact angle greater than 90° are considered as not wetting the surface. In the present study we investigate the static contact angle on the surface of the nanocomposite. Static contact angles are measured when droplet is standing on the surface and the three phase boundary is not moving [67,68]. The static contact angle was measured using the following equation [69].

$$\theta = 2\tan^{-1}\frac{2h}{d} \tag{3.6}$$

Where h is the height while d is the diameter of liquid drop. Fig. 3.6 shows the arrangement for measuring contact angle of the water droplet on the nanoparticle using a sessile drop goniometer while Fig. 3.7 shows the experimental images of contact angle measurement [70].

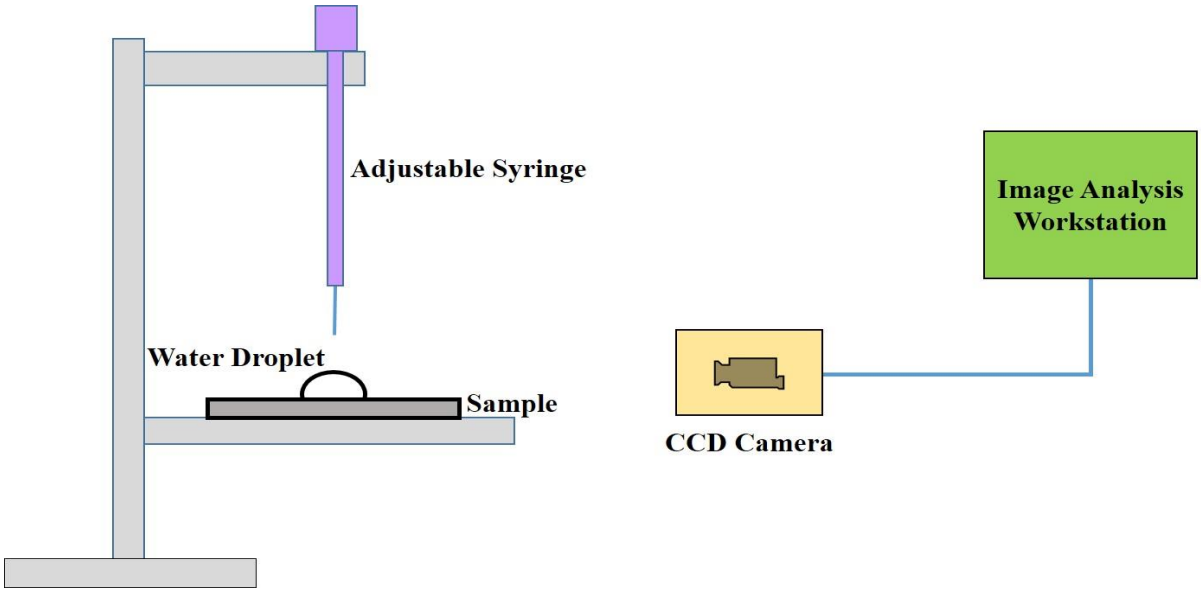

Fig. 3.6: Experimental Setup for Contact Angle Measurement.

Young's equation assumes that the surface is chemically homogenous and smooth. This may not be the case in real surfaces which can exhibit a range of contact angles between the advancing and receding values. On the ideal surface, Young's equation applies however on a real surface, the actual contact angle is the angle between the tangent to the liquid-fluid interface and the local surface of the solid. However, the measured (apparent) contact angle is the angle between line that represents the apparent solid surface and the tangent to the liquid-fluid

interface. Wenzel defined the relationship between roughness and wettability in 1936 wherein he stated that adding surface roughness enhances the wettability. For example, a chemically hydrophobic surface will become more hydrophobic when surface roughness is applied. Wenzel's statement can be described by [71]: -

$$\mathrm{Cos}\theta_m = r\mathrm{Cos}\theta_y \tag{3.7}$$

where the measured contact angle is represented by θ_m, Young's contact angle by θ_y and the roughness ratio by r. Here the roughness ratio is the ratio between the actual and projected solid surface area. The value of r is1 for a smooth surface while it is greater than 1 for a rough surface. The equation given by Wenzel is based on the assumption that the liquid completely penetrates the roughness grooves.

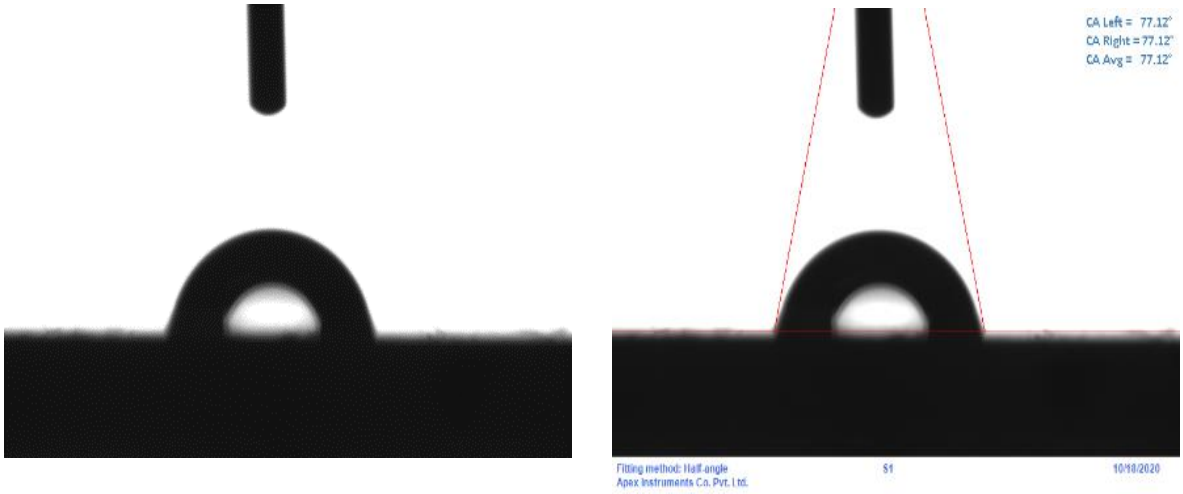

Fig. 3.7: Experimental Images of Contact Angle Measurement

3.5 Summary

The chapter discussed the various tests conducted for electrical characterization of epoxy-silica nanocomposites and the theory associated with the same. All the experiments and tests were conducted in High Voltage Laboratory, Department of Electrical Engineering, IIT Madras.

CHAPTER 4

MECHANICAL CHARACTERIZATION OF EPOXY-SILICA NANOCOMPOSITES

4.1 General

In this chapter, Digital Image Correlation test to investigate the mechanical properties of the silica epoxy nanocomposites has been discussed in detail. The experimental results were then compared with the existing Theoretical models to confirm the mechanical properties of the nanocomposites and its efficacy in insulation applications.

4.2 Tensile Test and Digital Image Correlation

It has been widely established that the amount of information gathered about the fine details of deformation during mechanical tests is increased in digital image correlation and tracking due to the ability to provide both local and average data as compared to the strain gauges and extensometers.

The Digital Image Correlation (DIC) method is an optical–numerical method developed for estimating full-field displacement. The DIC method matches the maximum correlation between small zones of the specimen, coated by a random pattern, in the un-deformed and deformed states. The image correlation is performed by comparing subsets from a reference image with subsets from each of the deformed images. In order to determine the displacement of each point, a square reference subset of (2M + 1) x (2M + 1) pixels from un-deformed image is chosen, where M is a positive integer. This subset is used to find the corresponding target subset on the deformed image. From a given image-matching procedure, the displacement fields, or displacement at different positions, in the analysis region can be computed. For this purpose, the minimization of the correlation coefficient is taken into account, which provides the in-plane displacement fields designated by u(x,y) and v(x,y) associated with x and y coordinates [72]

To investigate the effect of shear mixing time in a silica nanocomposite on its resistance to breakage under applied stress, the prepared samples are conventionally tested with Universal Testing Machine with a displacement rate of 2 mm/min at the room temperature. The specimens were prepared according to ASTM D-638 (Type IV) standard procedure in the dumbbell shape with the dimensions 115 X 6 X 3 mm^3 and 25 mm gauge length. For reliability and repeatability of results, tests were conducted on 3 samples of same shear mixing time and averaged. The experimental setup illustrating the schematic of DIC method is shown in Fig 4.1. Initially, the specimen is coated with thin white paint and speckled with black dots. Under the tensile loading, the displacement in the speckle pattern is recorded continuously by a camera placed in front of the universal testing machine. The VIC 2D software was employed to acquire the digital images of objects for digital image correlation.

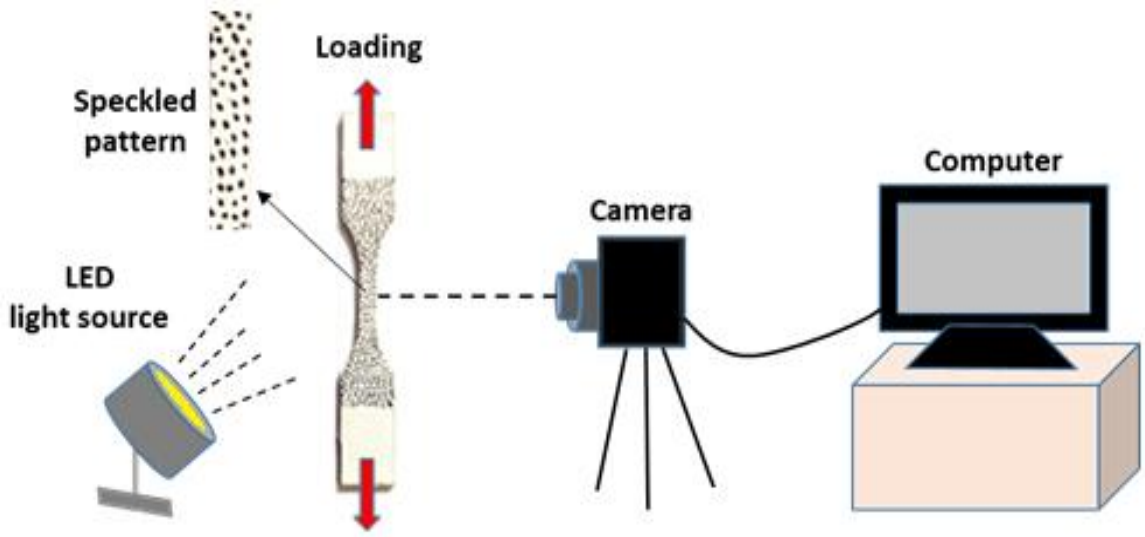

Fig. 4.1: Experimental Setup Illustrating the Schematic of DIC Method.

4.3 Theoretical Modelling

The various Theoretical models were studied to establish the conformity of experimental results with the Theoretical values. The models that define the Young's modulus of the composites, especially in low loading scenario and that analyses the strength of adhesion between the nanofillers and the base matrix were studied to confirm the results obtained experimentally.

4.3.1 Young's Modulus

Einstein, Kerner and Nielsen models are three well known Theoretical models for characterizing mechanical behaviour of nano composites [73]. However, the theories associate the volume fractions of the particles rather than the weight fraction. In order to apply these models for confirmation, the volume fraction of the particles was calculated. The nanoparticle volume fractions were calculated based on the rule of mixtures;

$$\mathrm{Vp} = \frac{\phi \mathrm{m}}{\phi \mathrm{m} + (1 - \phi \mathrm{m}) \frac{\rho \mathrm{p}}{\rho \mathrm{m}}} \tag{4.1}$$

where ϕ_m, ρ_m and ρ_p represent the mass fraction, matrix density and nano-particle density, respectively.

As per Einstein theory [74,75] the Young's modulus of binary composite systems containing a dispersed phase in a continuous matrix at low concentration of spherical particle, considering perfect adhesion between particle and matrix and assuming perfect dispersion of particle into matrix is defined by the following equation: -

$$\mathrm{E_c} = \mathrm{E_m}[1 + 2.5\mathrm{V_p}] \tag{4.2}$$

where E_c and E_m are Young's moduli of the composite medium and the matrix material, respectively, and V_p is the particle volume fraction.

In the Kerner's model [76,77], the particles are assumed to be perfectly bonded to the suspending medium, and are taken to be spheres in the mean. Therefore, Young's modulus for a composite that contains spherical particles with greater Young's modulus than the matrix is given by;

$$\mathrm{E_c^{Kerner}} = \mathrm{E_m}\left[1 + \frac{\mathrm{V_p}}{1 - \mathrm{V_p}} \frac{15(1 - \nu_\mathrm{m})}{(8 - 10\nu_\mathrm{m})}\right] \tag{4.3}$$

where ν_m is the matrix Poisson ratio.

A third model by Nielsen [78] based on Einstein and Kerner models was proposed which depends on Einstein's coefficient and a function that considers the maximum volumetric packing fraction of the filler phase. The expression for Young's modulus of composite materials is given by;

$$E_c^{Nielsen} = E_m[\frac{(1+A_1B_1V_p)}{(1-\Psi B_1V_p)}] \quad (4.4)$$

where Ψ is a factor which depends on the maximum packing fraction ($V_{p\,max}$) of the particle.

$$\Psi = 1 + V_p[\frac{(1-V_{p\,max})}{V_{p\,max}^2}] \quad (4.5)$$

the coefficients A_1 and B_1 are defined for spherical particle by;

$$A_1 = \frac{7-5V_m}{8-10V_m} \quad (4.6)$$

$$B_1 = \frac{\frac{E_p}{E_m}-1}{\frac{E_p}{E_m}+A_1} \quad (4.7)$$

In the present study, following values have been used for calculations: -

ρ_m = 1.15 g/cm^3
ρ_p = 2.30 g/cm^3
V_m = 0.30
Vp_{max} = 0.629
E_p = 74.8 GPa
E_m = Experimentally calculated value

4.3.2 Compressive or Tensile Strength

A number of models have been proposed to investigate the strength of adhesion between the filler and matrix [79]. One of the models that considers poor adhesion of particle with the matrix

proposes the following relation to define a relationship between ultimate tensile stress (σ_c) and volume fraction (V_f) of nanocomposites [80, 81].

$$\sigma_c = \sigma_m \ (1 - aV_f^b) \tag{4.8}$$

where σ_c is the ultimate tensile stress of the nanocomposite, σ_m is ultimate tensile stress of the matrix and a & b are constants that depend on the shape and arrangement of the nanoparticles. The values of 'a' and 'b' are equal to 1.21 and 0.66 when there is no adhesion between the nanofillers and the matrix [82]. In the present study σ_m is taken as the experimentally calculated value.

4.4 Summary

The chapter discussed in detail the process of Tensile Test and Digital Image Correlation Analysis conducted for mechanical characterization of epoxy-silica nanocomposites and the theory associated with the same. The experiments and tests were conducted in the Composite Manufacturing Laboratory, Department of Aerospace Engineering, IIT Madras.

CHAPTER 5

EMI SHELDING EFFICIENCY STUDIES OF EPOXY-MWCNT-INCLUSION NANOCOMPOSITES

5.1 General

In this chapter, the EMI SE measurement technique and the methodology of theoretical calculations of various parameters of the material is discussed in detail. Permittivity and conductivity of a material plays an important role in the EMI SE of any material. The same has been discussed here for the materials under study by using the SE values acquired experimentally to obtain the parameters theoretically using MATLAB.

5.2 EMI Shielding Efficiency Measurement

The SE of the test samples were measured in the frequency range of 8-12 GHz, using an Agilent N5230A vector network analyzer (VNA) and a waveguide test bench. Both reflection and transmission spectra were recorded. The block diagram of VNA setup is given in Fig. 5.1. The total EMI SE of a material consists of three mechanisms; absorption, reflection from the front surface and multiple internal reflections. The absorption mechanism is associated with the dielectric/magnetic polarization or energy dissipation. The reflection, involves the interactions between the electromagnetic fields and the mobile charge carriers. It can also be related with the impedance mismatch between the air and an absorber. Internal multiple reflections are due to the scattering at the bulk and reflections between the opposite faces of a material. The internal multiple reflections enhance the absorption and reflection with proper phase matching. Combining the multiple reflections with both reflection and absorption, the shielding effectiveness for the nanocomposites is calculated by the following equation [83-85].

$$SE_T = 10 \log \frac{P_{in}}{P_{tr}} = SE_A + SE_R \quad (5.1)$$

where P_{in} and P_{tr} are power of incident and transmitted EM waves, respectively.

Also, the absorption and reflection losses can be expressed as: -

$$SE_R = 10 \log[\frac{1}{(1-R)}] \quad (5.2)$$

$$SE_A = 10 \log[\frac{(1-R)}{T}] \quad (5.3)$$

where R and T represent the reflectivity and transmissivity respectively.

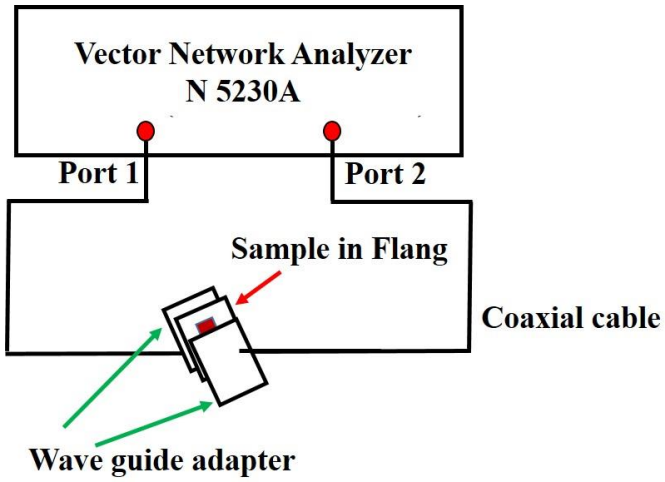

Fig. 5.1: Block Diagram of Vector Network Analyzer

5.3 Effective Material Properties

Based on plane wave theory for air-medium-air (S1-S2-S3) combination as shown in Fig. 5.2 and considering the sample as a homogeneous material with finite thickness (d), the relations between sample property and reflectivity, R, and transmissivity, T, are given by Equations 5.4 and 5.5.

$$R = \left|\frac{R_S(1-\exp(-2\gamma d))}{1-{R_S}^2\exp(-2\gamma d)}\right|^2 \quad (5.4)$$

$$T = \left|\frac{{T_S}^2\exp(-2\gamma d)}{1-{R_S}^2\exp(-2\gamma d)}\right|^2 \quad (5.5)$$

where R_s refers to the reflection coefficient at air-sample interface, T_s is the transmission coefficient across the air-sample interface, and γ refers to the complex propagation factor.

$$R_s = \frac{\frac{\mu}{\varepsilon}-1}{\frac{\mu}{\varepsilon}+1} \quad \text{and} \quad T_s = \frac{2\frac{\mu}{\varepsilon}}{\frac{\mu}{\varepsilon}+1} \tag{5.6}$$

Here μ and ε are the relative values of the complex magnetic permeability $(\mu' - j\mu'')$ and complex dielectric permittivity $(\varepsilon' - j\varepsilon'')$ respectively.

The complex propagation factor (γ) of a medium is expressed as, $\gamma = \alpha + j\beta$ where α is the attenuation constant and β is the phase constant given by (7) and (8).

$$\alpha = \sqrt{\frac{\mu_r'\varepsilon_r'\omega^2}{2c^2}}\sqrt{1+\left(\frac{\sigma}{\omega\varepsilon_r'}\right)^2 - 1} \tag{5.7}$$

$$\beta = \sqrt{\frac{\mu_r'\varepsilon_r'\omega^2}{2c^2}}\sqrt{1+\left(\frac{\sigma}{\omega\varepsilon_r'}\right)^2 + 1} \tag{5.8}$$

where, μ_r' is the real part of the relative magnetic permeability, ε_r' is the real part of the relative dielectric permittivity, σ is the conductivity and $\omega = 2\pi f$ is the angular frequency. A simple MATLAB code can give the values of dielectric constant and conductivity.

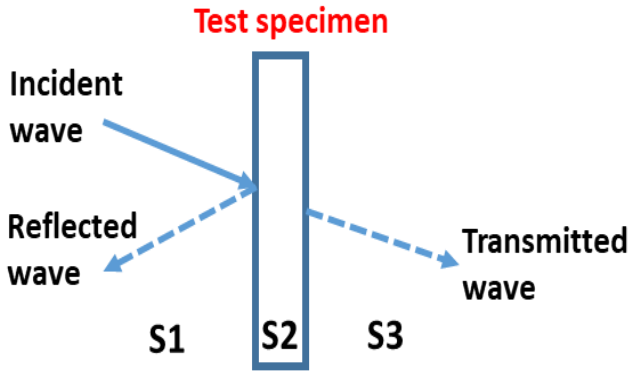

Fig. 5.2: Wave Propagation Schematic Diagram

5.4 Multi-Layer Model

To understand the propagation of EMI waves in a multi-layer system, the reflectivity and transmissivity of the electromagnetic radiation for the layered system is employed. In the matrix form, the electric field of the radiation in the $(n+1)^{th}$ medium entering from $(n)^{th}$ medium is given by: -

$$\begin{bmatrix} E_{n+1}^{+} \\ E_{n+1}^{-} \end{bmatrix} = \frac{1}{T_{n,n+1}} \begin{bmatrix} 1 & R_{n,n+1} \\ R_{n,n+1} & 1 \end{bmatrix} \begin{bmatrix} e^{-\gamma_n d_n} & 0 \\ 0 & e^{+\gamma_n d_n} \end{bmatrix} \begin{bmatrix} E_n^{+} \\ E_n^{-} \end{bmatrix} \tag{5.9}$$

where E_j^{+} and E_j^{-} refer to the electric field amplitude of the forwarding and returning radiation in the j^{th} medium respectively and γ_j is the complex propagation factor of the j^{th} medium. The coefficients, $R_{i,j}$ and $T_{i,j}$ refer to;

$$R_{i,j} = \frac{\frac{\mu_i}{\varepsilon_i} - \frac{\mu_j}{\varepsilon_j}}{\frac{\mu_i}{\varepsilon_i} + \frac{\mu_j}{\varepsilon_j}} \qquad \text{and} \qquad T_{i,j} = \frac{2\frac{\mu_i}{\varepsilon_i}}{\frac{\mu_i}{\varepsilon_i} + \frac{\mu_j}{\varepsilon_j}} \tag{5.10}$$

The reflectivity, R, and transmissivity, T, are now given by: -

$$R = \left|\frac{E_1^{-}}{E_1^{+}}\right|^2 \qquad \text{and} \qquad T = \left|\frac{E_n^{+}}{E_1^{+}}\right|^2 \tag{5.11}$$

From the R and T obtained experimentally, one can obtain the individual properties of the layer with an assumption that the layers are lossy dielectrics using another set of MATLAB codes. It may be noted that the real part of the dielectric permittivity of the epoxy and MWCNT loaded epoxy are considered from the air/medium/air layered system as discussed in Section 5.3.

5.5 Summary

This chapter explained the EMI SE measurement technique and the methodology of theoretical calculations of various parameters of the material in detail. The experiment discussed in this chapter was carried out in Microwave Laboratory, Department of Physics, IIT Madras.

CHAPTER 6

RESULTS AND DISCUSSION

6.1 General

In this chapter an in-depth study of the results of various experiments conducted have been carried out. The results of the tests establish the electrical and mechanical properties of epoxy based silica nanocomposites and electromagnetic shielding efficiency of the epoxy based CNT nanocomposites. The reason for the behaviour of the different samples in the presence of these nanoparticles have been discussed in detail that can be helpful for exploring its utilization in various other applications.

6.2 Epoxy-Silica Nanocomposites

The various test carried out to establish electrical and mechanical properties of Epoxy-Silica Nanocomposites were the water droplet initiated corona inception voltage test, contact angle analysis, surface potential decay measurement and trap distribution analysis and tensile and digital image correlation test. A theoretical modelling was also carried out to compare the experimental results with the theoretical values.

6.2.1 Water Droplet Initiated Corona Inception Voltage Test

The initial test was carried out for establishing the wt% of silica to be used for further studies. Studies were carried out by placing the droplet at the middle of the electrode gap. Table 6.1 and Fig. 6.1 show the CIV values of epoxy-silica nanocomposite samples with different weight percentages of the nanofillers, under AC, +DC and -DC voltages. Katada et al. studied the water droplet-initiated discharges on polymer insulating surface under different voltage profiles and have reported that the tips of the water droplet under applied voltage have induced charges, which are subjected to tensile forces that are proportional to magnitude of applied voltage [86]. In the present study it is observed that the CIV due to water droplet on the sample is low for the pure epoxy and significantly increases with inclusion of 1 wt% nanofillers. Sarathi et al. have

performed the water droplet-initiated corona inception studies on epoxy-clay nanocomposites under +DC and -DC voltages and have reported an enhancement in the CIV value of nanocomposites when compared to base epoxy resin up to a certain filler wt%. Thereafter, it was observed that the further increment in filler wt.% shows no further enhancement of CIV [87]. In the present study, a similar trend is observed wherein with increment in filler wt% beyond 1 only a marginal variation in CIV is noticed in case of both AC and DC voltages. Hence, considering the CIV values under AC, +DC and -DC voltages, epoxy nanocomposite with 1 wt% of silica fillers was selected for further analysis.

Table 6.1 Readings: Water Droplet Initiated CIV under AC and DC Voltages with Nanofiller Wt% Variation

Voltage Profile	0 Wt%	1 Wt%	2 Wt%	3 Wt%	5 Wt%	10 Wt%
AC (kV)	5.70	7.92	8.88	8.94	9.00	8.94
	5.88	8.34	8.46	8.64	8.64	9.00
	5.64	8.46	8.46	8.70	8.88	8.94
Average	**5.74**	**8.24**	**8.60**	**8.76**	**8.84**	**8.96**
Standard Deviation	0.12	0.28	0.24	0.15	0.18	0.03
Positive DC (kV)	7.38	9.06	9.66	10.20	10.20	10.74
	7.50	9.36	9.90	10.02	9.84	10.86
	7.50	9.18	10.02	9.72	9.84	10.92
Average	**7.46**	**9.20**	**9.86**	**9.98**	**9.96**	**10.84**
Standard Deviation	0.06	0.15	0.18	0.24	0.20	0.09
Negative DC (kV)	8.64	10.38	10.50	10.50	10.70	11.04
	8.88	10.44	10.62	10.68	10.78	11.34
	8.46	10.44	10.26	10.74	10.74	11.34
Average	**8.66**	**10.42**	**10.46**	**10.64**	**10.74**	**11.24**
Standard Deviation	0.21	0.03	0.18	0.12	0.04	0.17

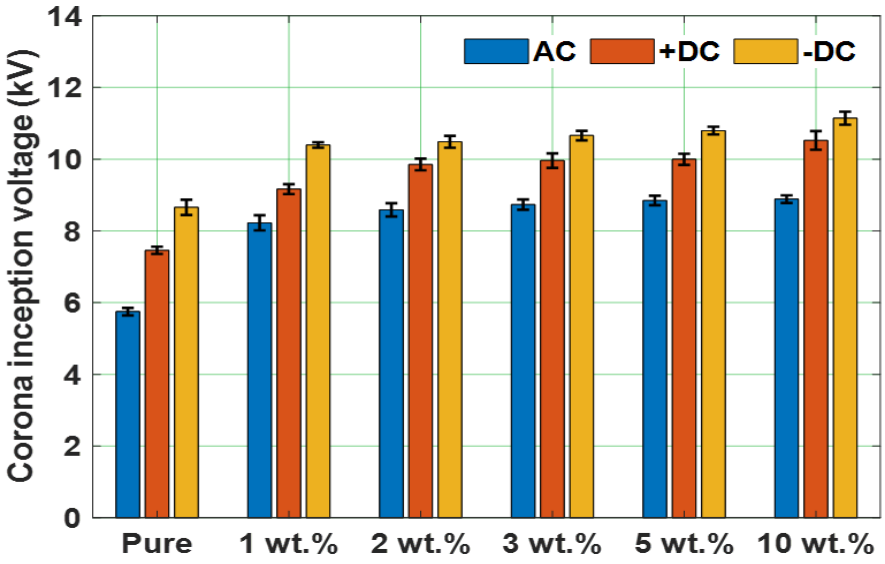

Fig. 6.1: Water Droplet Initiated CIV Under AC and DC Voltages with Nanofiller Wt% Variation

Further analysis was carried out to establish the optimal shear mixing time of the nanofiller. Table 6.2 and Fig 6.2 depict the water droplet-initiated CIV values of 1 wt% epoxy-silica nanocomposites with variation in shear mixing times, under different voltage profiles. It is observed that as the shear mixing time increases, the CIV values tend to increase and eventually saturates and becomes almost constant. The reason for this behaviour can be attributed to the interfacial bonding between nanoparticles and the polymer. The properties of polymer nanocomposites enhance with better interfacial bonding between the nanoparticles and the base matrix. This can be achieved by uniform dispersion of nanoparticles in polymer matrix [5]. Therefore, in the present study, better dispersion of nanofillers in the base epoxy matrix results in the improvement of the CIV values compared to pure epoxy sample. While the increment in the shear mixing time up to a certain time ensures better dispersion of nanofillers in the epoxy matrix thereby increasing the CIV values, but, after certain extent of shear mixing time i.e. above 7 hr in the present study, no significant improvement in the CIV values is noticed. It is known from various studies that the lack of adhesion between the nanoparticles and polymer may lead to agglomeration of nano particles which results in deteriorating the properties of polymer nanocomposite [5]. It was observed in the present study that with respect to the CIV test the 7 hr of shear mixing time is optimum.

The trend is similar for both AC and DC voltages, however, CIV is higher for –DC than +DC and AC voltages. Due to the polarization of the water droplet because of the AC voltage, the local electric field is formed quickly near the triplet junction of nanocomposite, water droplet and air. When the local electric field exceeds the local ionization potential, discharge inception occurs. Therefore, the CIV under AC voltage is lower as the rate of voltage change is high compared to DC [88]. Also, the CIV values under +DC voltage are lesser than that of CIV under -DC voltage as the high energy electrons accessible for discharge phenomenon near the electrode, in high field region are more in number under +DC voltage than -DC [89]. The other factor that affects the CIV value is the hydrophobicity of the nanocomposites. The hydrophobicity of the nanocomposite in the present study is observed to increase with the shear mixing time as discussed in the next segment. It is observed that the spreading of water droplet decreases with the increasing contact angle for a given volume and hence the CIV because of water droplet is lower.

Table 6.2 Readings: Water Droplet Initiated CIV under AC and DC Voltages with Shear Mixing Time Variation

Voltage Profile	Pure	2 hr	5 hr	7 hr	10 hr
AC (kV)	4.66	6.30	6.44	7.01	7.44
	4.98	5.94	6.65	7.22	7.15
	4.74	5.89	6.89	6.87	7.24
Average	**4.79**	**6.04**	**6.66**	**7.03**	**7.27**
Standard Deviation	0.16	0.22	0.22	0.17	0.14
Positive DC (kV)	6.56	7.02	7.81	8.22	7.94
	6.98	7.24	7.49	8.1	7.99
	6.82	7.12	7.61	8.1	7.87
Average	**6.78**	**7.12**	**7.63**	**8.14**	**7.93**
Standard Deviation	0.21	0.11	0.16	0.06	0.06
Negative DC (kV)	7.88	8.62	9.02	9.67	9.64
	8.23	8.44	9.16	9.43	9.12
	7.54	8.44	8.98	9.12	9.21
Average	**7.88**	**8.50**	**9.05**	**9.40**	**9.32**
Standard Deviation	0.34	0.10	0.09	0.27	0.27

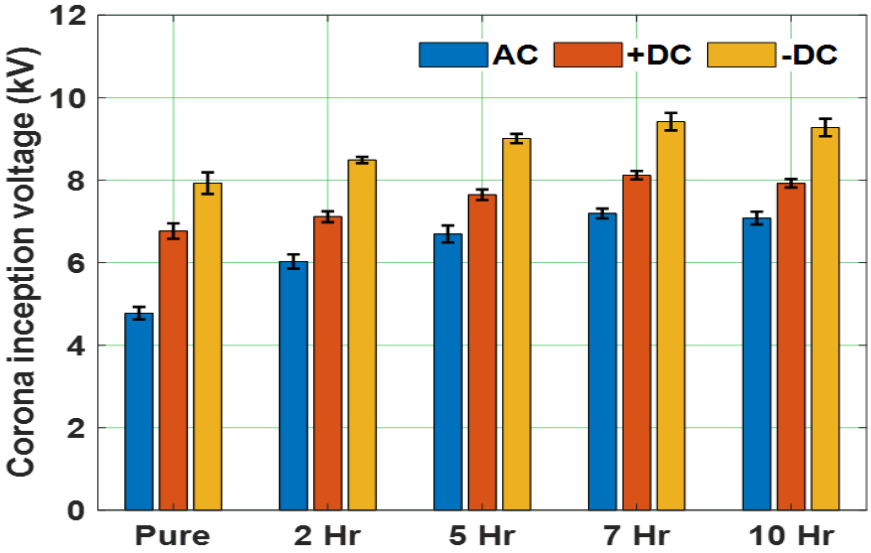

Fig. 6.2: Water Droplet Initiated CIV Under AC and DC Voltages with Shear Mixing Time Variation

6.2.2 Contact Angle Analysis

Table 6.3 and Fig. 6.3 show the variation of contact angle of the nano composite with respect to the shear mixing times. It is observed that the contact angle with 1% nano filler at 2 hr shear mixing time jumps 17.3% from the pure sample and thereafter 6.8% at 5 hr shear mixing time. Subsequently a minor drop is seen in the contact angle of the nano composite. It can be safely inferred that the contact angle remains approximately constant after 5 hours of shear mixing time.

Table 6.3 Readings: Contact Angle Measurement

Readings	**Pure**	**2 Hr**	**5 Hr**	**7 Hr**	**10 Hr**
	CA Avg (Deg)	**CA Avg (Deg)**	**CA Avg (Deg)**	**CA Avg (Deg)**	**CA Avg (Deg)**
Reading 1	68.02	84.37	86.12	83.98	80.27
Reading 2	68.11	79.95	86.53	83.79	81.06
Reading 3	69.66	78.23	85.28	84.46	82.12
Reading 4	67.54	80.53	83.3	90.06	79.88
Reading 5	67.77	77.12	86.11	83.46	82.22
Mean Value	68.22	80.04	85.468	85.15	81.11
Standard Deviation	0.74	2.48	1.15	2.47	0.94

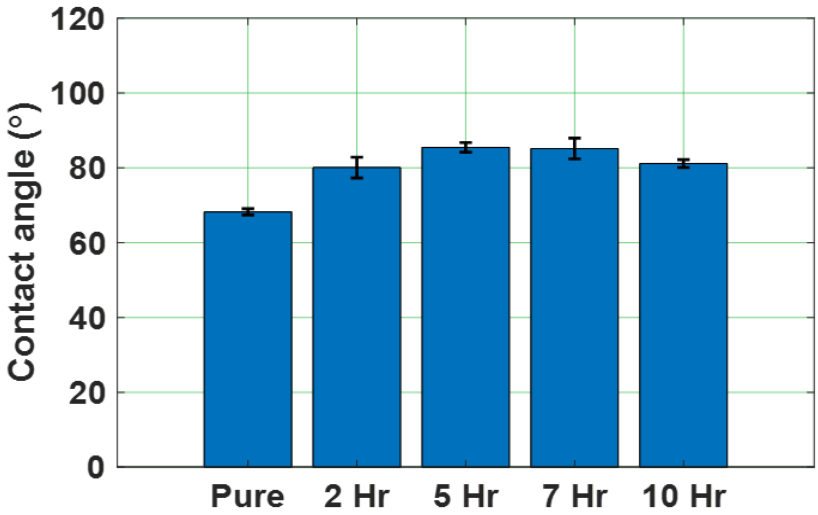

Fig. 6.3: Experimental Values of CA Measurement

The wetting behaviour of the surface has been related to the surface roughness and the surface energy of the material [90]. Since the pure epoxy resin is hydrophilic in nature, the contact angle is noticed to be less. The water contact angle of the nano composite should reduce with the increased surface roughness according to the Wenzel model. However, the contact angle is observed to be higher. This can be due to less percentage of filler added in the matrix and that the hydrophobic groups in the composite may have been exposed at the surface minimizing the free energy of the system. Also, with increment in shear mixing time, the contact angle has improved. It is because of the better dispersion of the nanofillers in to the base matrix. Proper dispersion of the nanofillers have aided for the improvement of the hydrophobicity of the composite. In Fig. 6.4 (stacked chart) the curve in the figure runs parallel to each other depicting the interdependence of contact angle and CIV.

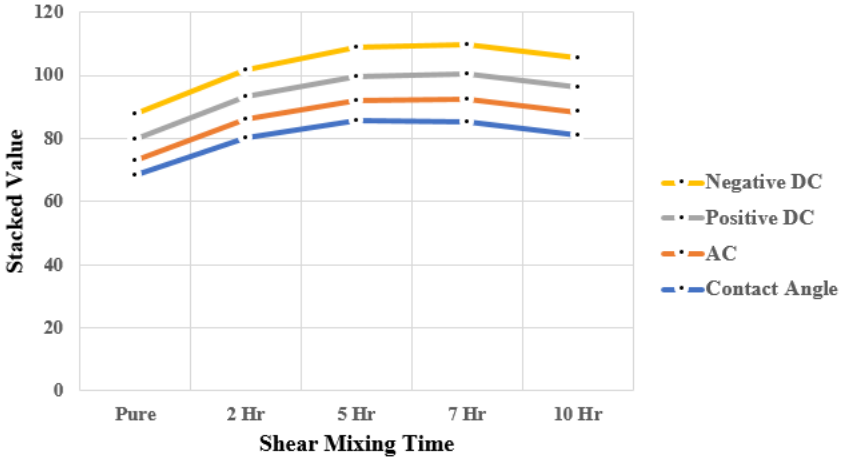

Fig 6.4: Stacked Values of CA and CIV Showing Interdependence

6.2.3 Surface Potential Decay Measurement and Trap Distribution Analysis

Fig. 6.5 shows the surface potential decay characteristics of silica epoxy nanocomposites prepared at different duration of shear mixing. Decay rate for all the samples are shown in the Table 6.4 and it clearly shows that shear mixing time duration has strong influence on the surface potential decay rate. Increment in the mixing time duration, decreased the decay rate under positive DC voltage but in case of negative DC voltage till 2 hr of mixing time, decay rate increased and on further increment of the mixing time lead to the decrement in the decay rate and again for 7 hr of shear mixing time, decay rate enhanced. Also, decay rate was observed to be higher under negative DC corona as compared with positive DC corona, for all time duration of shear mixing. It was described that interface binding force affects the different chemical and physical trap energy levels [91]. Different hours of shear mixing affected the dispersing ability of SiO_2 nanoparticles in the base epoxy matrix and hence altered the binding force between the base epoxy resins and silica nanoparticles at its molecular level, which can be reason for the change in decay rate. Du et al. indicated that fast potential decay can be attributed to the de-trapping of charge carriers from shallower traps and slow potential decay was due to the de-trapping phenomenon from deeper traps [92].

Fig. 6.6 shows the trap distribution characteristics of silica epoxy nanocomposites prepared at different hours of shear mixing. It was observed that trap energy level varies in the range of 0.72-0.92 eV. The trap energy level corresponds to the maximum energy density is observed as trap depth [93], and corresponding trap depth under both DC voltage profile is shown in Table 6.4. It was observed that trap depth increased for the samples under positive DC corona but under negative DC voltage, trap depth was lowest for the 2 hr shear mixed sample and further increment in the mixing time increased the trap depth of the nanocomposites. Increment in the trap depth symbolizes the increment in deep trap levels which reduced the probability of de-trapping phenomenon to occur. Hence relating the trap depth and decay rate, it shows the inverse relation.

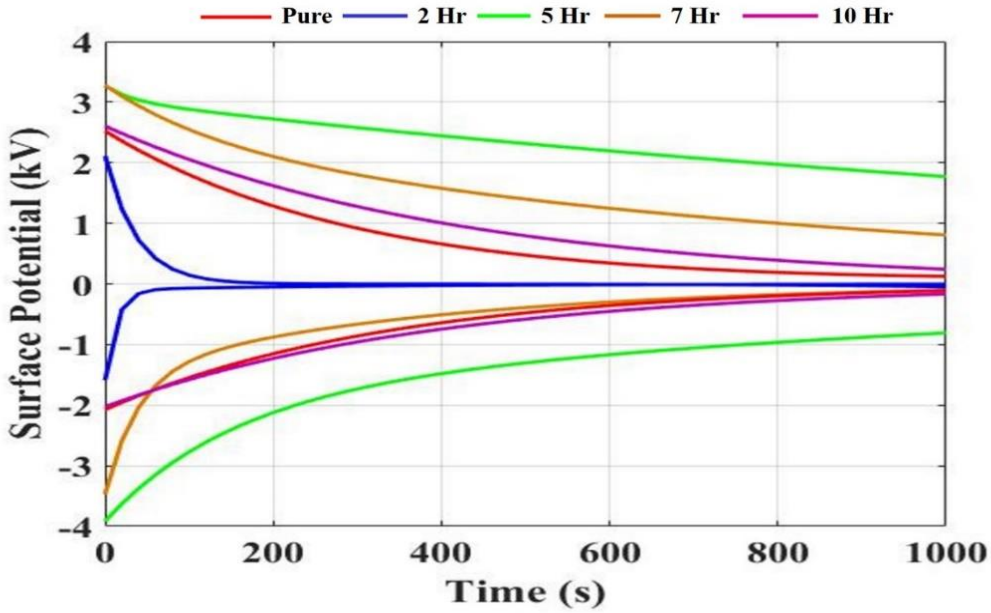

Fig. 6.5: Surface Potential Decay Characteristics.

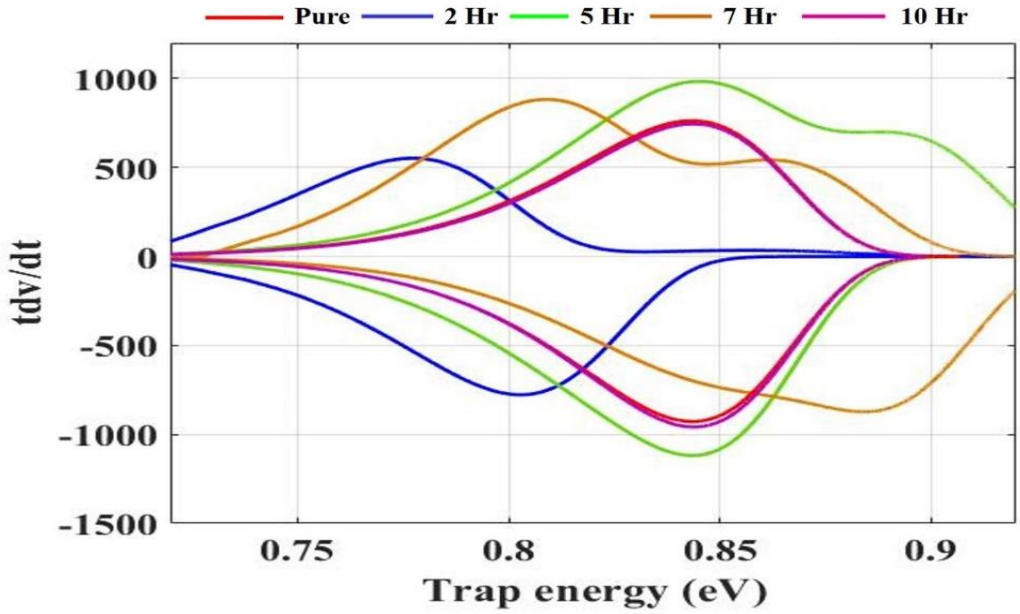

Fig. 6.6: Trap Distribution Characteristics.

Table 6.4 Variation of Decay Rate and Trap Depth of Nanocomposites under DC Voltage

Shear mixing duration	+DC		-DC	
	Decay rate (λ)	**Trap depth (eV)**	**Decay rate (λ)**	**Trap depth (eV)**
0 hours (Pure epoxy)	0.003381	0.8436	0.0034	0.8435
2 hours	0.02693	0.8023	0.07475	0.7774
5 hours	0.002268	0.8456	0.002364	0.8441
7 hours	0.001072	0.8842	0.02575	0.8090
10 hours	0.002375	0.8439	0.002498	0.8437

6.2.4 Tensile Properties Analysis

To confirm the repeatability of the test, the tensile test was conducted three times per sample. The three stress-strain characteristics of Pure epoxy and 7 Hr samples are depicted in Fig. 6.7 as Set 1-3. Table 6.5 gives the average and standard deviation of the tensile parameters calculated from three set of readings of each sample. The stress-strain characteristics with extreme set of values (Set-1 and Set-3) are neglected and the middle set of values (Set-2) are considered for further analysis. The stress-strain characteristics plotted with the middle set of values of all the test samples are shown in Fig. 6.8 and the corresponding tensile parameters are tabulated in Table 6.6. An instant drop in the stress-strain curves, as soon as the material underwent the maximum load point indicates intrinsic brittle nature of the nano composites. Also, the reduction in the strain at fracture point of samples and enhancement in tensile properties of nanocomposites are observed over the pure epoxy material. It is because of the inclusion of silica nanoparticles into the epoxy matrix, which improves the mechanical strength of the composite [79].

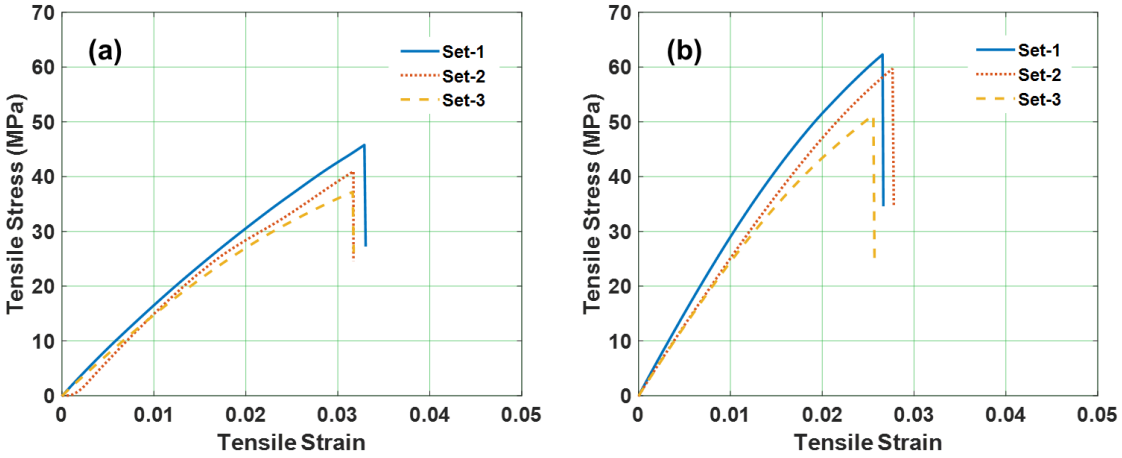

Fig. 6.7: Tensile Stress-Strain Curves of (a) Pure Epoxy (b) 7 Hr Samples

It is observed from Table 6.6, that the Young's modulus increased with the time of shear mixing. Also, the ultimate tensile strength and the load at breakpoint of the nanocomposites is higher than the pure epoxy sample. However, the ultimate tensile strength and the corresponding load decreases slightly below the pure epoxy at 10 hours of shear mixing time. The static toughness values of the samples are given in Table 6.6. Toughness indicates the ability of the sample to absorb energy by undergoing plastic deformation without fracturing, under applied tensile stress. The toughness value is dependent on the tensile strength and strain of the specimens. Addition of nanofillers to base epoxy matrix has successfully improved the static toughness of the nanocomposites, up to 7 Hr sample compared to base epoxy sample. This could be due to efficient load transfer between matrix and filler up to 7 Hr sample. However, 10 hours of shear mixing time has resulted in lower static toughness compared to that of base epoxy resin.

After the addition of the filler to the pure epoxy and shear mixed for 2 hours, the nano particles start dispersing and tend to make stronger bonds with the base epoxy matrix. As the time of the shear mixing is increased it is observed that the Young's modulus of nanocomposites improved up to 7 hours of shear mixing time. This could be due to efficient load transfer between matrix and filler in 7 Hr sample. The interfacial bonding between nanoparticles and polymer is a key factor in enhancing the properties of polymer nanocomposites, which can be achieved by uniform dispersion of nanoparticles in polymer matrix [5]. Hence, better dispersion of nanofillers in the base epoxy matrix results in the improvement of the material properties

compared to base epoxy resin. Increment in the shear mixing time up to a certain time, has ensured the better dispersion of nanofillers in the epoxy matrix and it led to the increment in the tensile properties. But, after certain extent of shear mixing time (above 7 hours in the present study), no significant improvement in the material properties have been noticed. Lack of adhesion between the nanoparticles and polymer can possibly form strongly bonded nanoparticle-aggregates during the nanocomposite preparation, which results in an early failure at the interface of the nanocomposite or can lower the properties of polymer nanocomposite compared to that of base polymer [5]. It is noticed from Figure 2 that the agglomeration count is reducing with increment in shear mixing time up to 7 hours and the agglomeration count is noticed to increase in 10 Hr sample compared to 7 Hr sample. Pullicino et al. have studied the effect of variation in shear mixing rate and time in epoxy nanocomposites and have indicated that the reduced tensile strength in epoxy nanocomposites is due to the larger sizes of agglomerates which act as stress raisers and result in premature failure [20]. Kim et al. have indicated that the tensile strength and the ductility show inverse relationship [94]. The highest shear mixing time in the present study i.e., 10 hours of shear mixing time have reflected least tensile strength compared to other nanocomposites, providing the highest ductility. Hence, in the present study, the reduction in tensile parameters of nanocomposites with above 7 hours of shear mixing time could be due to the presence of higher agglomerates, which might possibly lead to poor interfacial bonding between epoxy matrix and nanoparticles.

Table 6.5 Average Value and Standard Deviation of Tensile Properties of Epoxy-Silica Nanocomposites

Shear Mixing Time	**Load at Maximum Tensile Stress (N)**	**Young's Modulus, E (MPa)**	**Ultimate Tensile Strength (MPa)**	**Static Toughness (kJ/m^3)**
Pure Epoxy	753.93 ± 78.52	1602.52 ± 119.29	41.31 ± 4.31	663.47 ± 83.25
2 Hr	1208.69 ± 50.46	1737.48 ± 74.43	67.28 ± 2.79	1521.87 ± 105.28
5 Hr	1150.76 ± 58.17	1814.66 ± 76.99	63.93 ± 3.23	1265.46 ± 70.15
7 Hr	1044.51 ± 103.63	25000.95 ± 231.86	57.60 ± 5.71	769.13 ± 98.75
10 Hr	649.94 ± 62.77	2176.17 ± 180.28	38.06 ± 3.68	355.55 ± 98.42

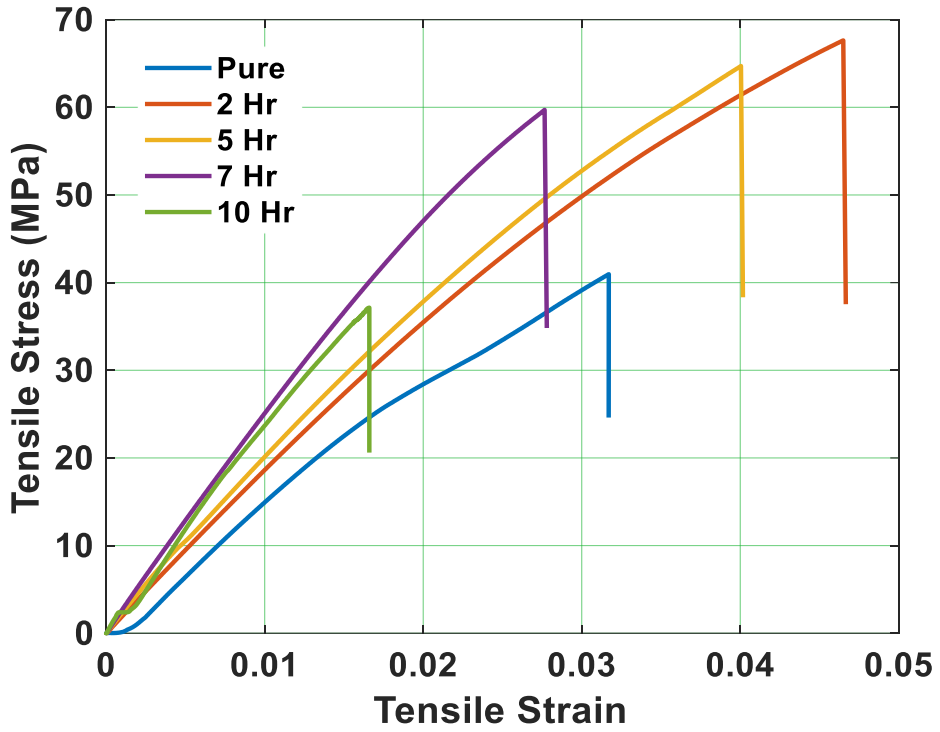

Fig. 6.8: Tensile Stress-Strain Curve for Epoxy-Silica Nanocomposites at Different Shear Mixing Time

Table 6.6 Tensile Properties of Epoxy-Silica Nanocomposites

Shear Mixing Time	**Load at Maximum Tensile Stress (N)**	**Young's Modulus, E (MPa)**	**Ultimate Tensile Strength (MPa)**	**Static Toughness (kJ/m^3)**
Pure epoxy	747.46	1653.86	40.96	649.42
2 Hr	1217.38	1758.86	67.63	1572.39
5 Hr	1164.83	1825.46	64.71	1295.49
7 Hr	1074.73	2377.71	59.71	825.78
10 Hr	634.36	2159.51	37.15	308.34

6.2.5 Theoretical Modelling

Table 6.7 represents the values of Young's modulus calculated based on experimental results and theoretical models. The Young's modulus calculated from theoretical models, tends to increase with the increment in shear mixing time and is within acceptable range till the 5 hours of shear mixing time after which it is giving a high deviation. Since, the deviation between experimental values and theoretical values of Young's modulus is very less up to 5 hours of shear mixing time, it is observed that the theoretical models have successfully estimated the Young's modules of the epoxy nanocomposites. Again, with shear mixing time greater than 7 hours, the deviation is noticed to be high. From Fig 6.9, the Scanning Electron Microscope (SEM) images of the epoxy nanocomposite samples, it is noticed that the agglomeration count is reducing with increment in shear mixing time up to 7 hours and the agglomeration count is noticed to increase in 10 Hr sample compared to 7 Hr sample. Hence, in the present study, the reduction in tensile parameters of nanocomposites prepared with above 7 hours of shear mixing time could be due to the higher agglomerates which might possibly lead to poor interfacial bonding between epoxy matrix and nanoparticles. Also, the experimental values could have been deviated from the expected theoretical values due to this poor interfacial bonding between epoxy matrix and nanoparticles. Hence, according to Young's modulus calculation from theoretical models, it is considered that the nano particles would have dispersed perfectly in the range of 5 to 7 hours of shear mixing.

Table 6.7 Young's Modulus as per Various Models and Experimental Values

Model	**Young's Modulus for 1 wt% of SiO_2 (GPa)**	**Experimental Value**	
		Shear Mix Time	**Young's Modulus Calculated Experimentally (GPa)**
		Pure	1.65
Einstein Model	1.67	2 Hr	1.76
Kerner Model	1.73	5 Hr	1.82
Nielsen Model	1.67	7 Hr	2.37
		10 Hr	2.16

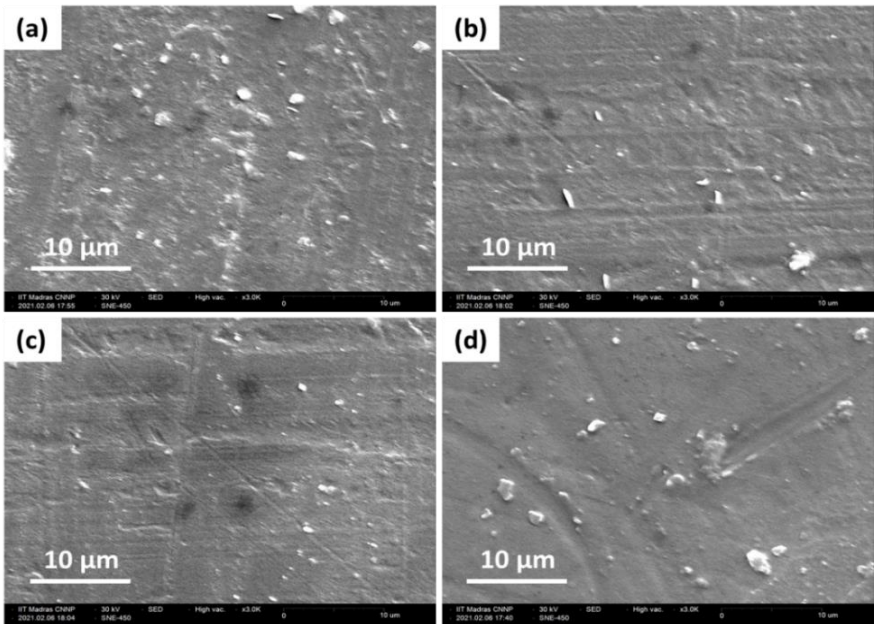

Fig. 6.9: SEM Images of Samples Prepared by (a) 2, (b) 5, (c) 7 (d) 10 Hrs of Shear Mixing

Table 6.8 shows the calculated value of the ultimate tensile stress of the nanocomposite (σ_c) when calculated by keeping the values of a and b as 1.21 and 0.66 and when there is no matrix-filler adhesion. With 2, 5 and 7 hours of shear mixing, the percentage deviation between theoretical and experimental value of ultimate tensile stress where there is no matrix-filler adhesion, is very high. Whereas, the theoretical value of ultimate tensile strength when there is minimum to no matrix-filler adhesion, is approximately equal to the experimental value of ultimate tensile strength of the nano composite prepared with 10 hours of shear mixing time, justifying the poor matrix-filler interfacial bond due to excessive shear mixing.

Table 6.8 Ultimate Tensile Stress as per the Theoretical Model and Experimental Values

Ultimate Tensile Stress Calculated as per the Theoretical Model, (MPa)	**Sample**	**Experimental values of Ultimate Tensile Stress (MPa)**	**Percentage Deviation**
39.68	2 Hr	67.63	70.43%
	5 Hr	64.71	63.08%
	7 Hr	59.71	50.48%
	10 Hr	37.15	6.37%

6.2.6 Digital Image Correlation Analysis

It is important to understand the overall average strain experienced by the sample as well as the strain experienced by the sample at the breaking point. To understand the same, DIC analysis was carried out for the average strain and the strain at the particular point of breakage. Fig. 6.10 depicts the strain distribution of the sample during the entire process of elongation at the starting point, at 10s and at the breaking point of the test samples. The strain field distribution can be used in identifying the highly-stressed areas, just before the occurrence of fracture. Thus, the DIC method is advantageous than the normal tensile test, by representing the strain field corresponding to deformations [72,95]. Also, the strain magnitude at any point on the surface of the specimen can be deciphered by the colour scheme for each sample and at each instant of time. It is observed that the average strain on the sample increases with time and suddenly drops around the occurrence of breakage. Also, the variation of average e_{yy} along with the time is depicted in Fig. 6.11 It is observed that the elongation progresses linearly with time for all the samples. It is noticed that the nanocomposite specimen with 2 hours of shear mixing time has higher strain magnitude and it is noticed that the strain magnitude at any time instant before breaking reduces with increment in shear mixing time up to 7 hours of shear mixing time. Even though the 5 Hr sample has reached breakpoint in less time, it is noticed from Fig. 6.11 that the 5 Hr sample has recorded higher tensile strength and lesser strain magnitude compared to 2 Hr sample. The 7 Hr sample has reflected lesser strain magnitude and is also able to withstand stress for more time. But, the 10 hours of shear mixed sample recorded higher strain magnitude than 7 Hr samples and withstood less time, indicating poor load transfer between matrix and filler interfaces. Also it can be observed from Fig. 6.11 and 6.12 that the pattern of average strain in the entire sample is similar to the pattern of strain at the breakpoint depicting that the strain is equally spread across the sample.

Sample	At 0 Sec	At 10 Sec	At Break Point	eyy [1] - Lagrange
Pure	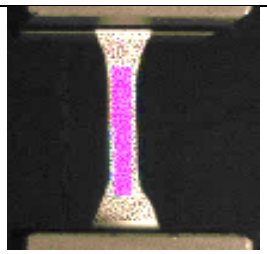	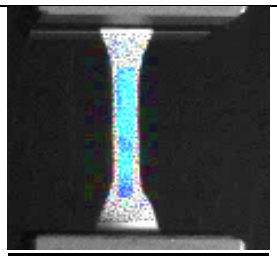	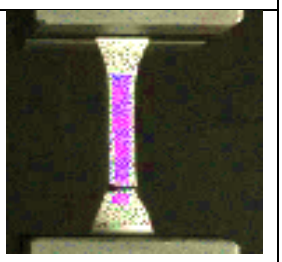	0.03 0.028125 0.02625 0.024375 0.0225 0.020625 0.01875 0.016875 0.015 0.013125 0.01125 0.009375 0.0075 0.005625 0.00375 0.001875 0
2 Hr	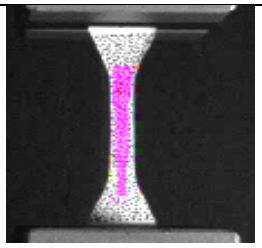	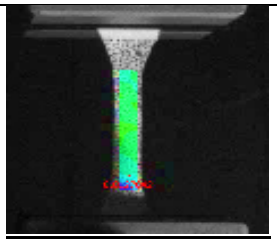	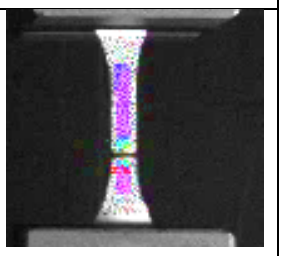	
5 Hr	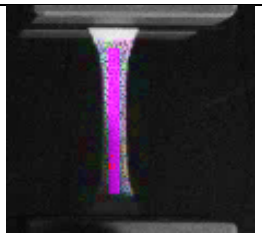	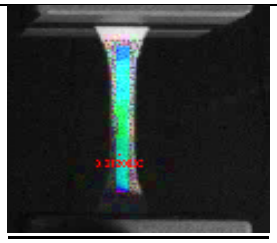	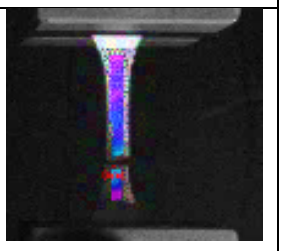	
7 Hr	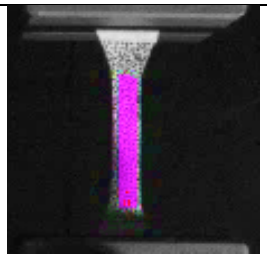	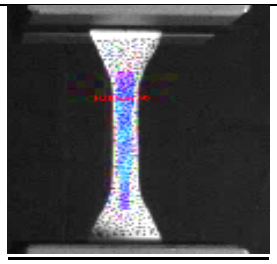	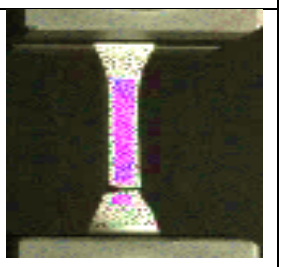	
10 Hr	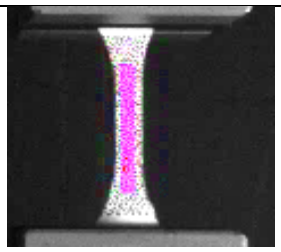	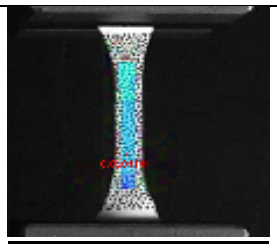	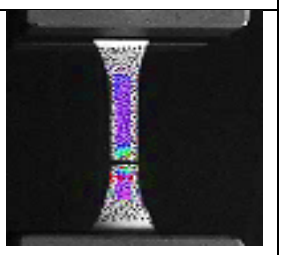	

Fig 6.10: Strain Distribution of the Sample During the Process of Elongation at the Starting Point, at 10s and at Breaking Point

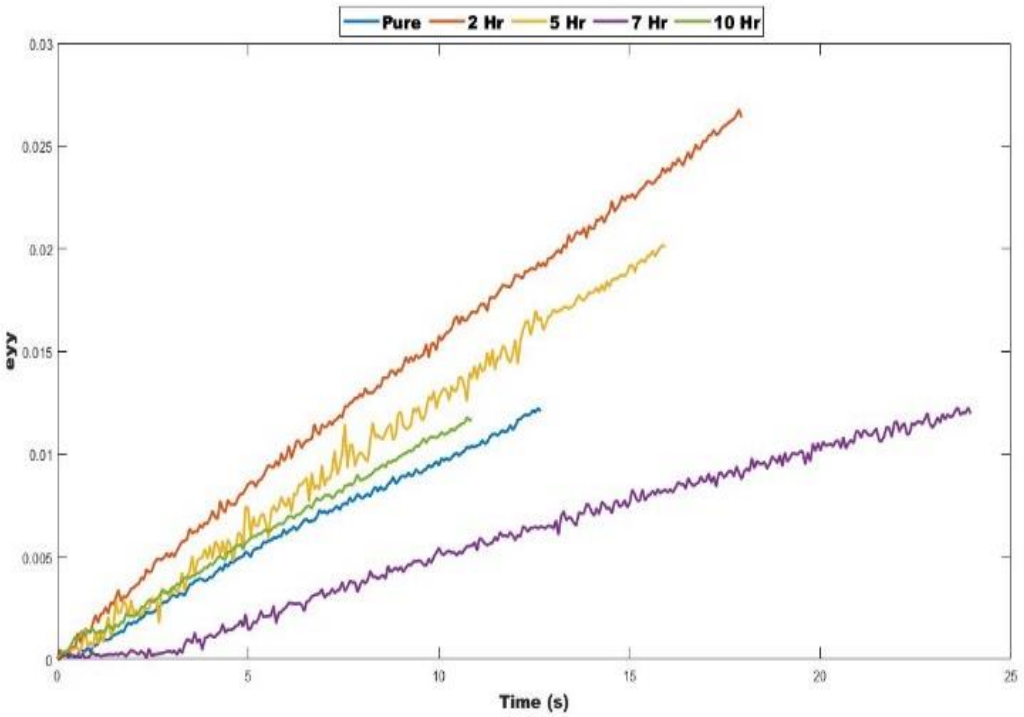

Fig. 6.11: Variation of Average Strain as a Function of Time

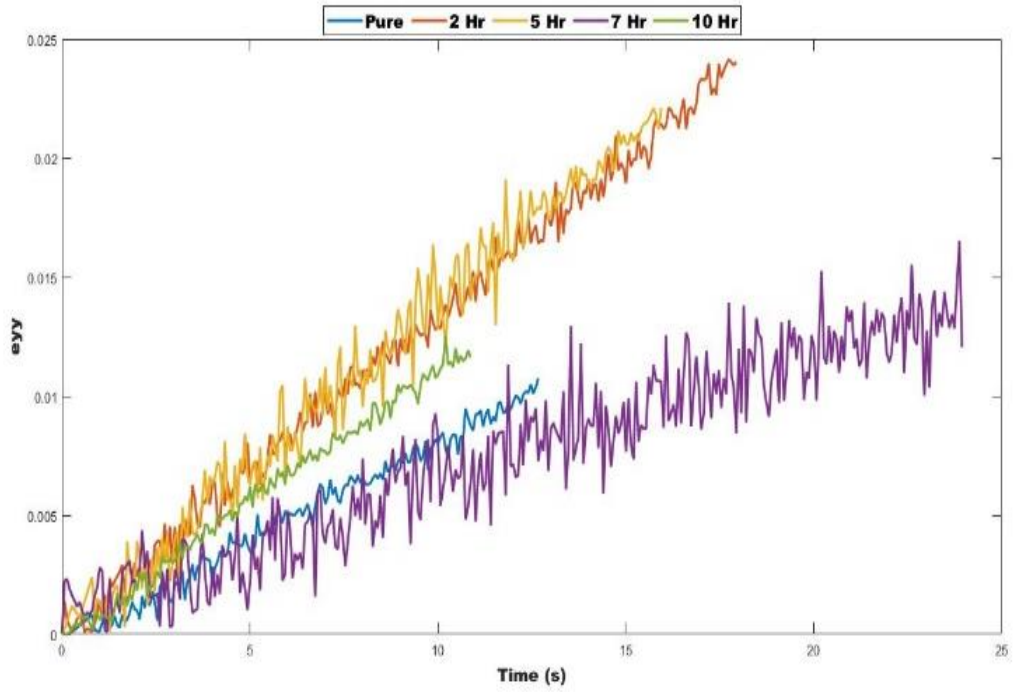

Fig. 6.12: Variation of Strain at Break Point as a Function of Time

6.3 Epoxy-MWCNT Nanocomposites

A systematic study of the EMI SE of the various samples prepared was carried out aiming to obtain a high value of shielding efficiency. The experimental values were utilised to obtain parameters like permittivity and conductivity of the samples and the layers in the multilayer samples.

6.3.1 Impact of Variation in Wt% and Functionalization of MWCNT on EMI SE

Fig. 6.13 and 6.14 represents the SE due to reflection (SE_R), shielding efficiency due to absorption (SE_A) and total shielding efficiency (SE_T) of pure epoxy, epoxy reinforced with pristine and functionalized MWCNT. It is observed that the total average SE of the nanocomposite increases by 2.8 times with 1 wt% MWCNT content as compared to the pure epoxy sample. Further increasing the MWCNT content by 3 wt% and 5 wt% increases the total average SE by 3.7 times and 5.7 times respectively as compared to the pure epoxy sample. However, the functionalized MWCNT as a nanofiller decreases the SE of nanocomposites decreases by 3.2 times, 3.7 times and 5.1 times for 1, 3 and 5 wt% samples as compared to pristine MWCNT of same wt% and the values are approximately equal to the EMI SE of pure epoxy. The decrease in the SE can be attributed to the fact that the walls of the MWCNT nanoparticles are damaged due to prolonged exposure to the acid solution during functionalization process. Also, by altering the CNT structure by functionalizing them disrupts the conductivity of isolated nanotubes. Similar results have been reported in a studies wherein it was observed that the mild functionalization of CNT increases the EMI SE of the material while it essentially decreases the EMI SE owing to the damage of the CNT walls [96]. Therefore, whereas the functionalization process increases the mechanical strength of the nanocomposite but it can have a reverse effect in the EMI SE capabilities of the material.

It may also be noted that the absorption is the main contributor towards the total SE. The increase in overall SE as compared to pure epoxy can be attributed to the increase in overall conductivity of the composite due to the presence of MWCNT. The absorption due to the conduction loss is enhanced due to the multiple scattering within the bulk. The increase in SE_R and SE_A indicates the increase in conductivity of the sample. The marginal fluctuations

throughout the frequency range might be due to the wave-current interaction and microstructure defects [97]. Fig. 6.15 shows the comparative EMI SE of the nanocomposites. The highest average value of EMI SE reached in this phase is 8.6 dB with peak value of 9.1 dB for 5 wt% of pristine MWCNT. The results are tabulated in Table 6.9.

Table 6.9 Average and Peak EMI SE of Pristine and Functionalized Epoxy-MWCNT Nanocomposites with Variation in Filler Wt%

Sample	Peak SE Frequency (GHz)	Average SE (dB)	Peak SE (dB)
Pure Epoxy	9.1	1.5	3.4
P MWCNT 1 wt% 1mm	8.4	4.2	5.2
P MWCNT 3 wt% 1mm	8.7	5.5	6.2
P MWCNT 5 wt% 1mm	8.5	8.6	9.1
F MWCNT 1 wt% 1mm	10.8	1.3	2.6
F MWCNT 3 wt% 1mm	9.2	1.5	2.9
F MWCNT 5 wt% 1mm	8.8	1.7	3.0

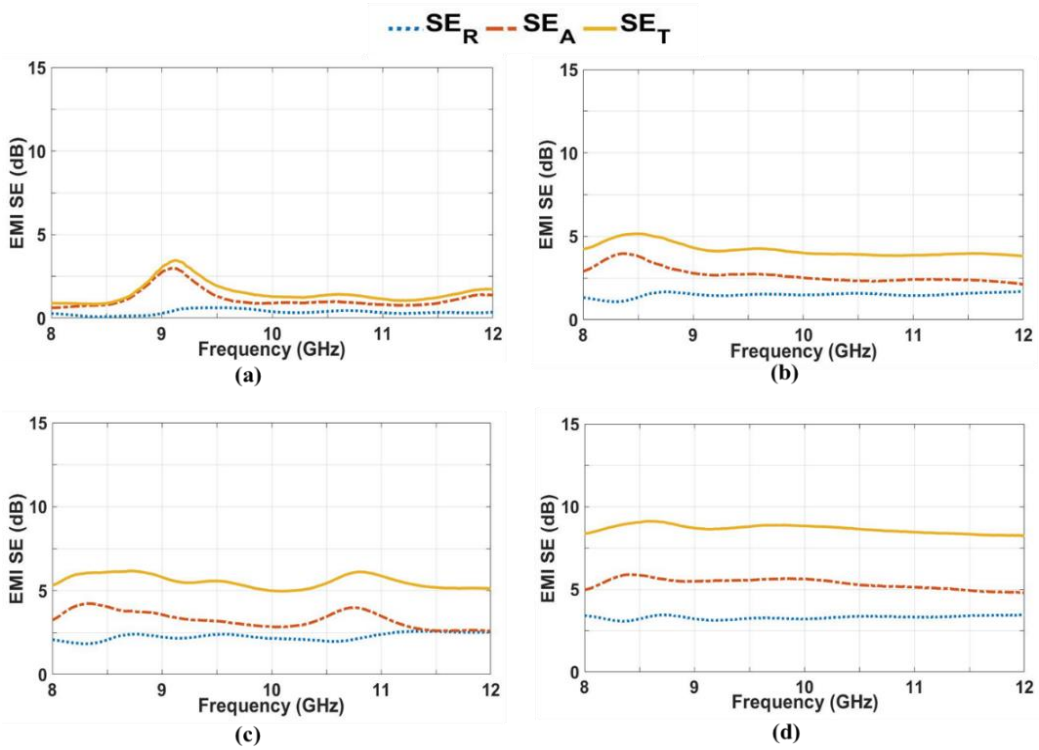

Fig. 6.13: SE_R, SE_A and SE_T of (a) Pure Epoxy (b) P MWCNT 1wt% 1mm (c) P MWCNT 3wt% 1mm (d) P MWCNT 5wt% 1mm

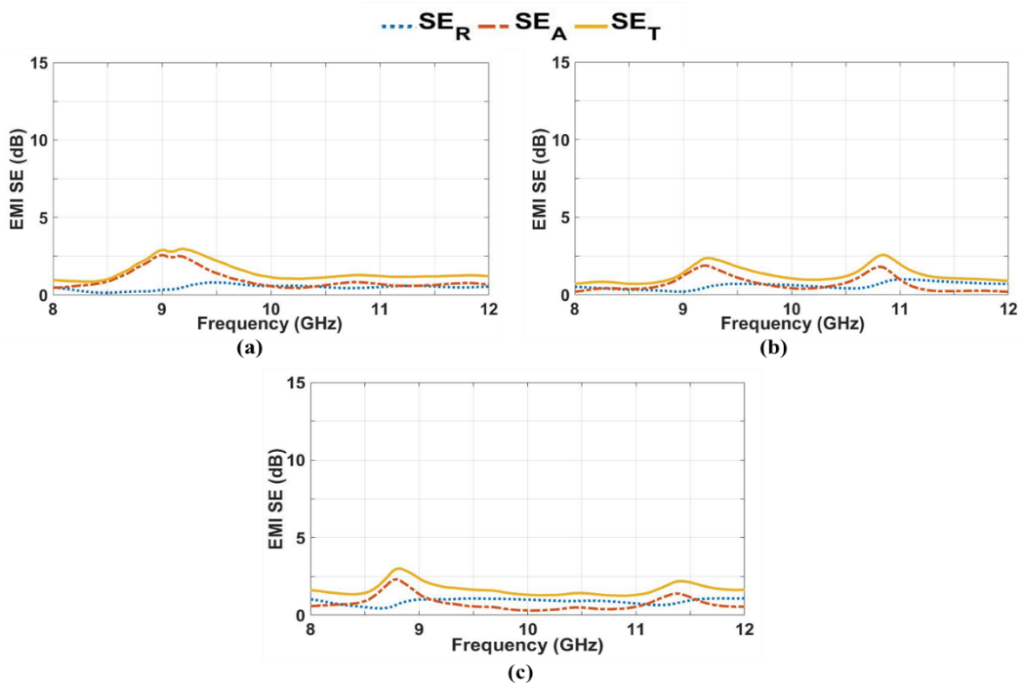

Fig. 6.14: SE_R, SE_A and SE_T of (a) F MWCNT 1wt% 1mm (b) F MWCNT 3wt% 1mm (c) F MWCNT 5wt% 1mm

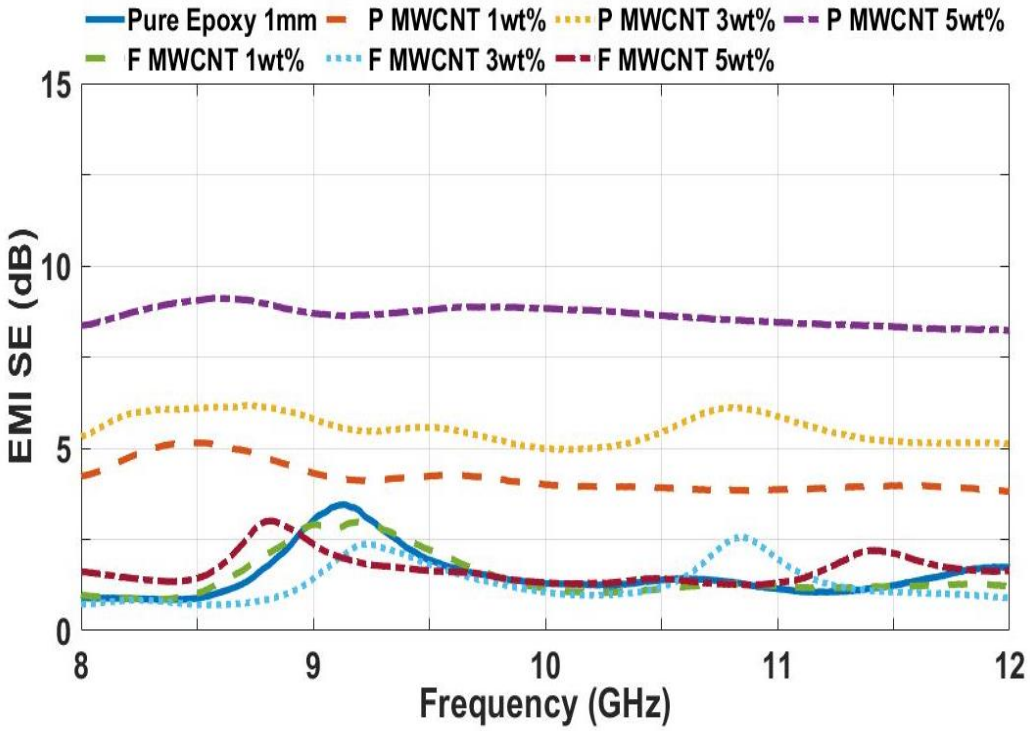

Fig. 6.15: Comparison of SE_T of Pristine and Functionalized MWCNT-Epoxy Nanocomposites

6.3.2 Impact of Variation in Thickness of Sample on EMI SE

As the highest SE was obtained at 5 wt% of pristine MWCNT in the previous measurement, further study was carried out by varying the thickness of 5 wt% samples to understand the effect of thickness on the EMI SE. It has been established from various studies that the EMI SE increases with the thickness of a material [98]. However, the increase in the present study is not substantial and going beyond the thickness of 4mm to get a higher value of EMI SE is not a viable solution commercially and economically. Table 6.10 shows the average and peak values of SE for 5 wt% pristine MWCNT samples with varying thickness. Fig. 6.16 represents the SE due to reflection (SE_R), shielding efficiency due to absorption (SE_A) and total shielding efficiency (SE_T) of epoxy reinforced with 5 wt% pristine MWCNT at 1mm, 3mm and 4mm sample thickness. The average SE of 3mm and 4mm thickness samples increase by 1.26 and 1.3 times as compared to 1mm thickness sample. It is observed that while the SE of the nanocomposites increase with the increase in thickness, the increase is not considerably large which may be due to the agglomeration of nanoparticles that form clusters in the sample decreasing the homogenity of the mixture which in turn decreases the conductivity as well as the mechanical strength of the material. It is also observed that the SE due to absorption is the main contributor towards the total SE. Fig 6.17 shows the comparison of the total SE of the samples. The highest average value of EMI SE reached in this phase is 11.1 dB with peak value of 14.0 dB for 5 wt% of pristine MWCNT of 4mm thickness.

Table 6.10 Average and Peak EMI SE of Pristine Epoxy-MWCNT Nanocomposites of Varying Thickness

Sample	Peak SE Frequency (GHz)	Average SE (dB)	Peak SE (dB)
P MWCNT 5 wt% 1mm	8.5	8.6	9.1
P MWCNT 5 wt% 3mm	8.0	10.9	12.6
P MWCNT 5 wt% 4mm	8.0	11.1	14.0

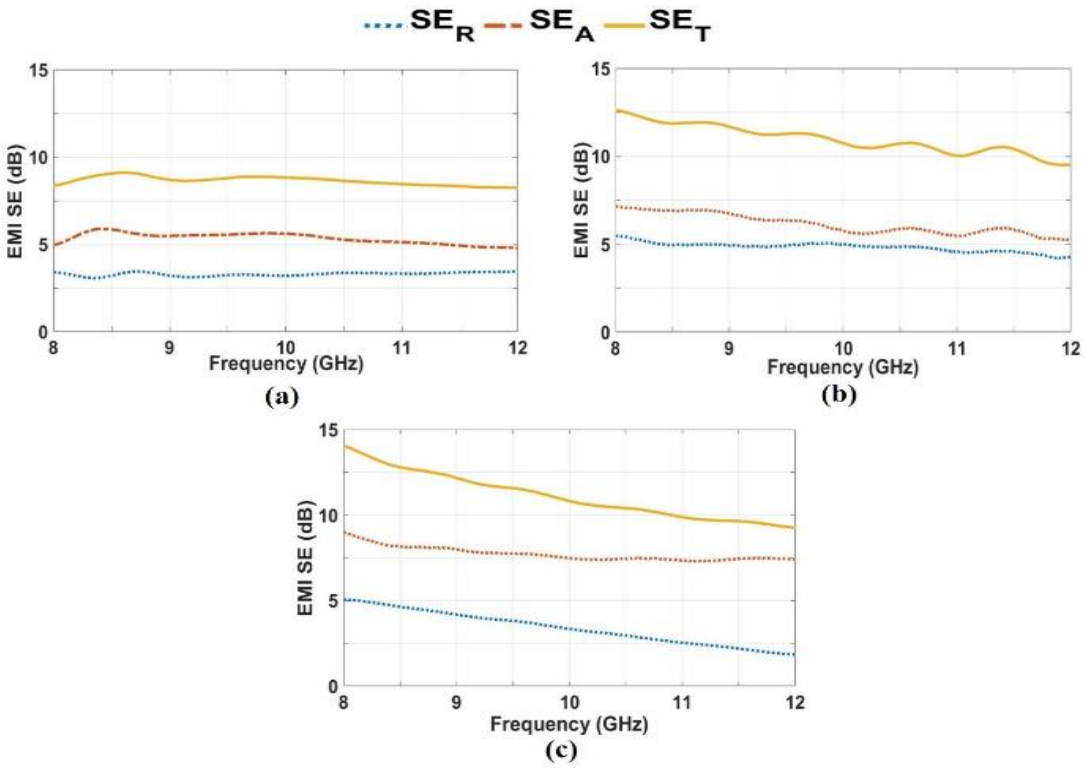

Fig. 6.16: SE_R, SE_A and SE_T of (a) P MWCNT 5 wt% 1mm (b) P MWCNT 5 wt% 3mm (c) P MWCNT 5 wt% 4mm

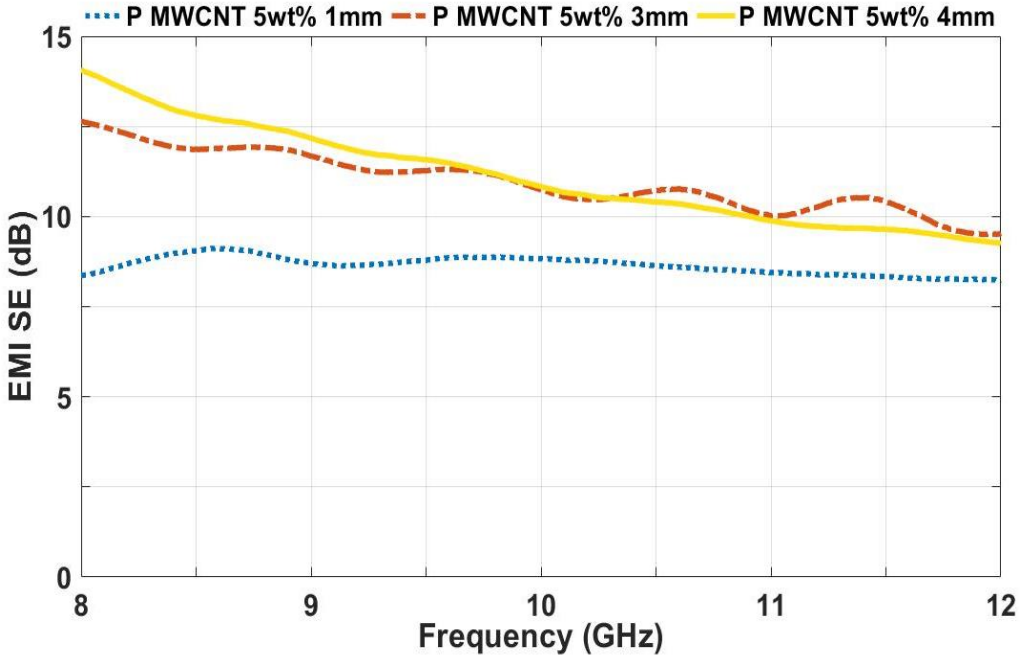

Fig. 6.17: Comparative Graph of Total EMI SE of Varying Thickness Samples

6.3.3 Impact of Addition of Inclusions in Epoxy-MWCNT Nanocomposites on EMI SE

As the increase in thickness of the sample up to 4mm did not have a substantial effect on the EMI SE of the nanocomposite therefore various inclusions in the proportion 3 wt% MWCNT and 2 wt% inclusion (to maintain total 5 wt%) were added in epoxy matrix of 1mm thickness to study their effect on the EMI SE. From Table 6.11 it is observed that the average EMI SE increased by 1.3 times, 2.7 times, and 3.6 times for MoS_2, Ni and Cu nanoparticles respectively as compared to pure epoxy. The result can be attributed to the fact that the conductivity of MoS_2 < Ni < Cu therefore the values of EMI SE increases in the same sequence. However, since the nanoparticles used for the sample preparation were pre-prepared therefore the oxidation of the particles has considerably reduced the shielding efficiency. Fig. 6.18 shows that absorption as well as reflection contribute almost equally towards the total SE of nanocomposite with MoS_2, Cu and Ni nanofillers. From Fig. 6.19 it can be observed that the EMI SE values are more or less constant throughout the range of the frequency under study with peaking around 8-9.5 GHz. The highest average value of EMI SE reached in this phase is 5.4 dB with peak value of 6.3 dB for 3 wt% of pristine MWCNT – 2 wt% Cu nanocomposite of 1 mm thickness.

Table 6.11 Average and Peak EMI SE of Epoxy-MWCNT Nanocomposites with Inclusions

Sample	Peak SE Frequency (GHz)	Average SE (dB)	Peak SE (dB)
MWCNT/MoS_2 1mm	8.0	2.0	2.5
MWCNT/Ni 1mm	8.6	4.1	4.6
MWCNT/Cu 1mm	8.8	5.4	6.3

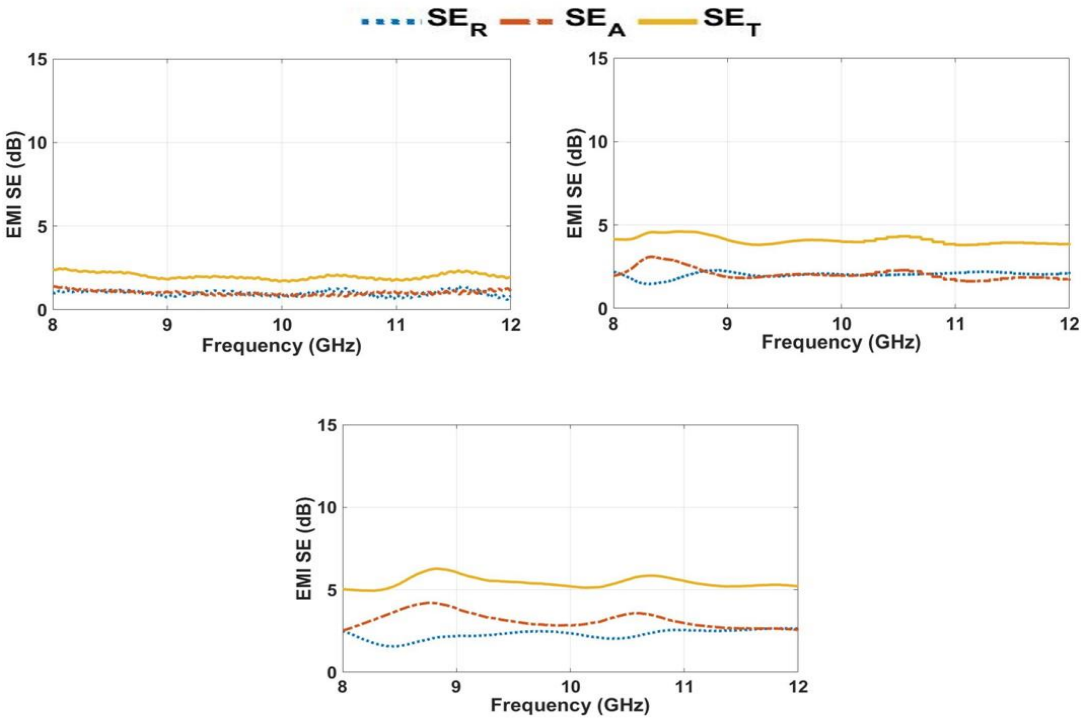

Fig. 6.18: SE_R, SE_A and SE_T of (a) MWCNT/MoS_2 1mm (b) MWCNT/Ni 1mm (c) MWCNT/Cu 1mm

Fig.

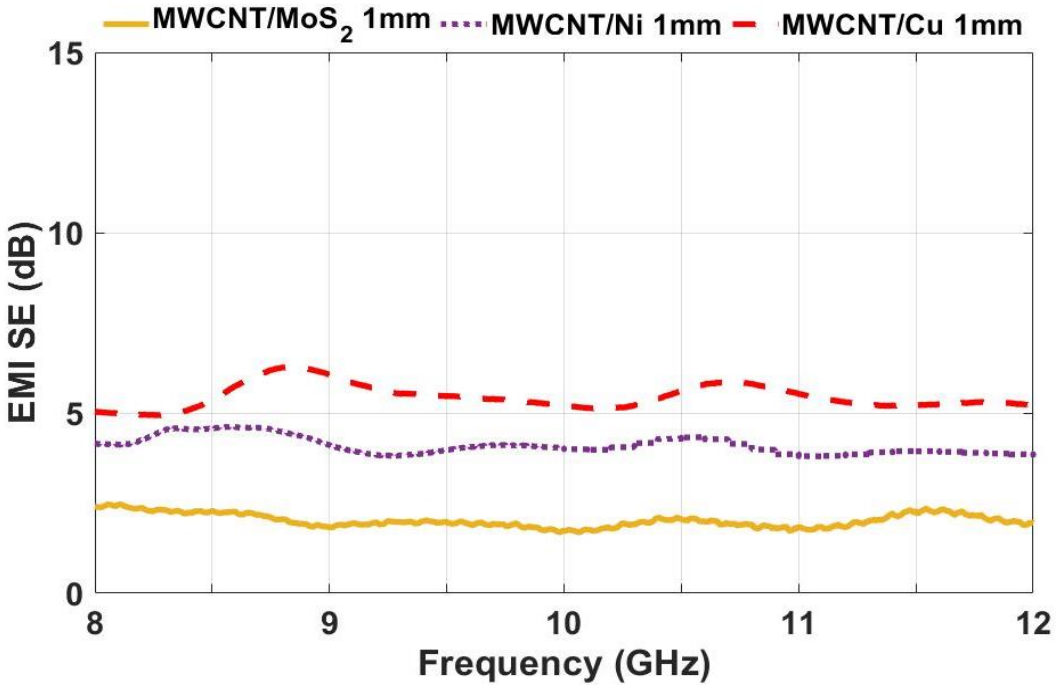

6.19: Comparison of SE_T of Epoxy-MWCNT-Inclusion Nanocomposites

6.3.4 Impact of Addition of UCFF Single Layer in Epoxy-MWCNT Nanocomposites on EMI SE

A single layer of UCFF is sandwiched between two layers of pure epoxy, 3 wt% and 5 wt% MWCNT-epoxy nanocomposites to study its effect on EMI SE. Since the total thickness of the structure is 1 mm, the epoxy/ epoxy-MWCNT with thickness around 0.445 mm are kept on either side of the UCFF. This structure is heterogeneous along the propagation direction. Table 6.11 shows that the average EMI SE increased by 35.5 times as compared to pure epoxy, while it increased by 6.2 times and 5.2 times as compared to only MWCNT 5 wt% and only UCFF SL respectively for 1mm thickness. Increasing the number of layers of UCFF could possibly increase the EMI SE however it is not economically and commercially suitable therefore the present study was limited to a single layer of UCFF. It is observed that the EMI SE of MWCNT 5 wt% - UCFF nanocomposites of 1mm thickness increases with the increase in frequency. Fig. 6.20 shows the shielding efficiency due to reflection (SE_R), shielding efficiency due to absorption (SE_A) and total shielding efficiency (SE_T). The contribution of absorption in the total SE is significantly greater than the reflection, though there is a definite increase in the reflection due to the introduction of UCFF. Similar results were reported with the epoxy composites sandwiched with bidirectional woven carbon fibers which are electro-deposited with nickel [99]. This can be attributed to the hybrid structure formation comprising MWCNT- and UCFF. Fig 6.21 shows the comparative graph of Total EMI SE of Epoxy-Pristine MWCNT-UCFF Nanocomposites. The results are tabulated in Table 6.12.

Table 6.12 Average and Peak EMI SE of Epoxy-MWCNT-UCFF Nanocomposites

Sample	Peak SE Frequency (GHz)	Average SE (dB)	Peak SE (dB)
UCFF SL 1mm	9.3	10.3	12.0
MWCNT 3 wt%/UCFF 1mm	10.6	31.0	38.7
MWCNT 5 wt%/UCFF 1mm	11.9	53.3	76.2

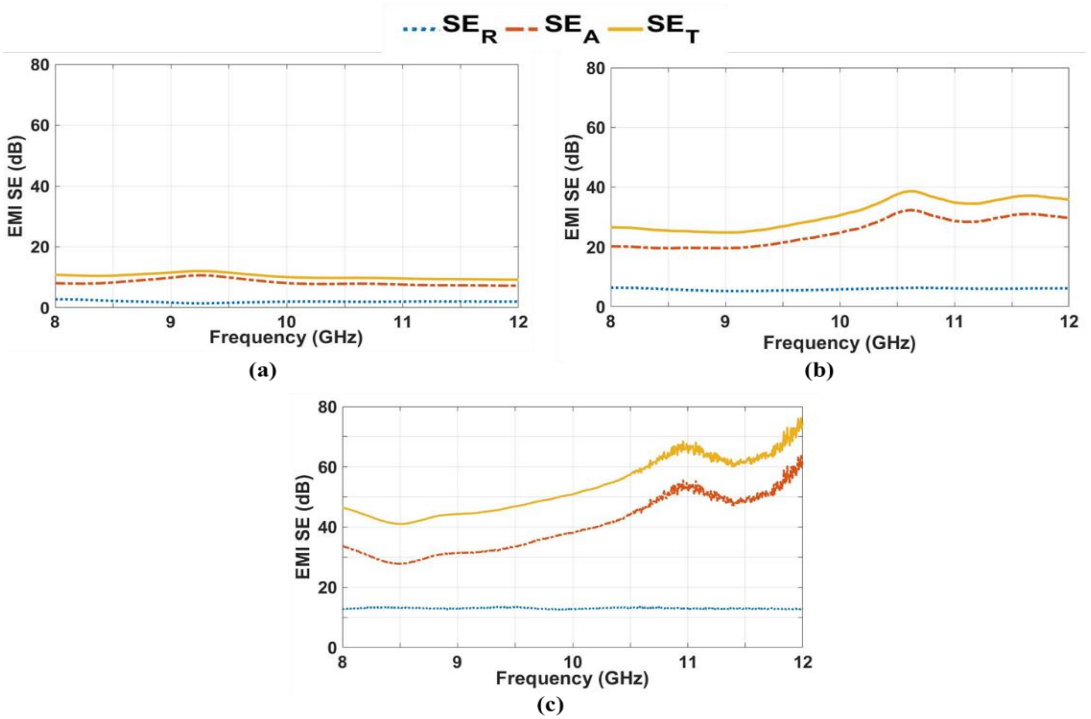

Fig. 6.20: SE_R, SE_A and SE_T of (a) UCFF SL 1mm (b) MWCNT 3 wt%/UCFF 1mm (c) MWCNT 5 wt%/UCFF 1mm

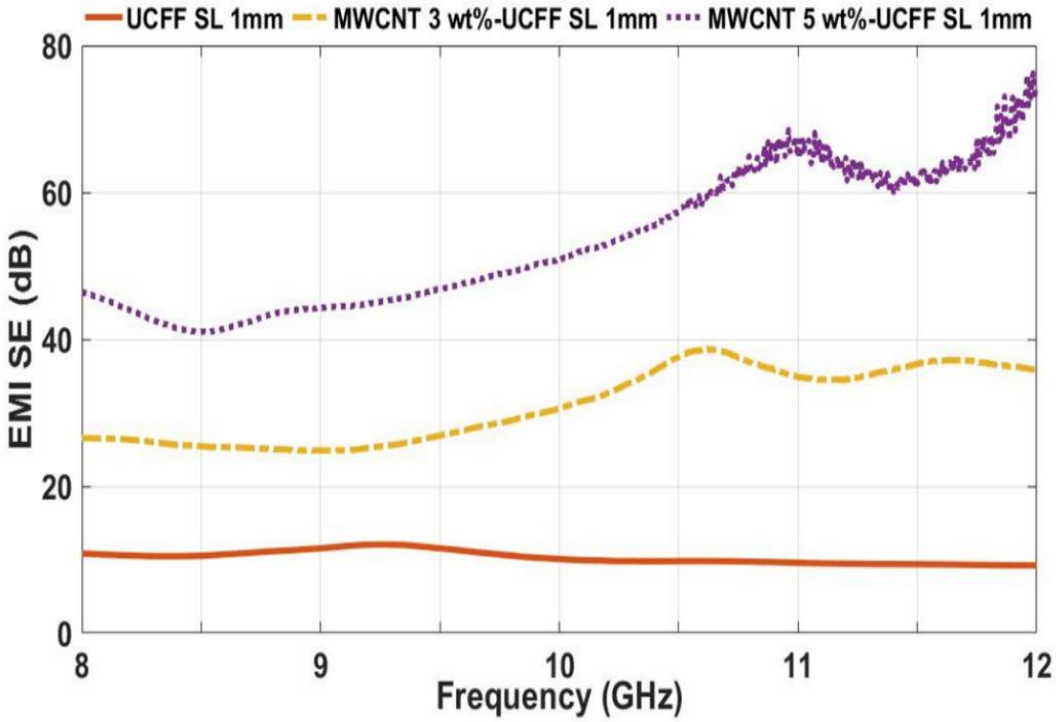

Fig. 6.21: Comparison of SE_T of Epoxy-MWCNT-UCFF Nanocomposites

6.3.5 Theoretical Evaluation of Relative Permittivity and Conductivity Values of Pristine MWCNT Samples

Table 6.13 provides the evaluated values of relative permittivity and conductivity of pure epoxy and pristine MWCNT samples extracted at 8,9,10,11 and 12 GHz frequencies using MATLAB codes. Fig. 6.22 and 6.23 depicts the same in graphical form. The relative permittivity or dielectric constant enhances (from approximately 4 to 21 at 8 GHz) with increase in the addition of MWCNT since the MWCNT increases the dipolar nature of the composites. The enhancement in the effective conductivity is expected since the conducting MWCNT is added as a scattering agent, though the amount of conductivity (around 2.5 S/m for 0 wt% to 6.5 S/m for 5 wt%) is not very significant to have the structure as an efficient EMI shielding structure.

Table 6.13 Evaluated Values of Relative Permittivity and Conductivity of Pure Epoxy and Pristine MWCNT Samples

Frequency (GHz)	**Frequency**							
	Pure Epoxy		**MWCNT 1 wt%**		**MWCNT 3 wt%**		**MWCNT 5 wt%**	
	ε_r	**σ (S/m)**	**ε_r**	**σ (S/m)**	**ε_r**	**σ (S/m)**	**ε_r**	**σ (S/m)**
8	4.2	0.42	9.5	2.71	13.4	3.28	21.6	6.69
9	2.0	1.70	9.6	2.62	12.9	3.84	18.0	7.94
10	4.2	0.63	8.6	2.29	11.4	2.80	16.4	8.37
11	3.6	0.57	7.8	2.20	11.6	3.85	16.2	7.39
12	3.4	1.02	8.1	1.91	11.0	2.61	15.9	6.82

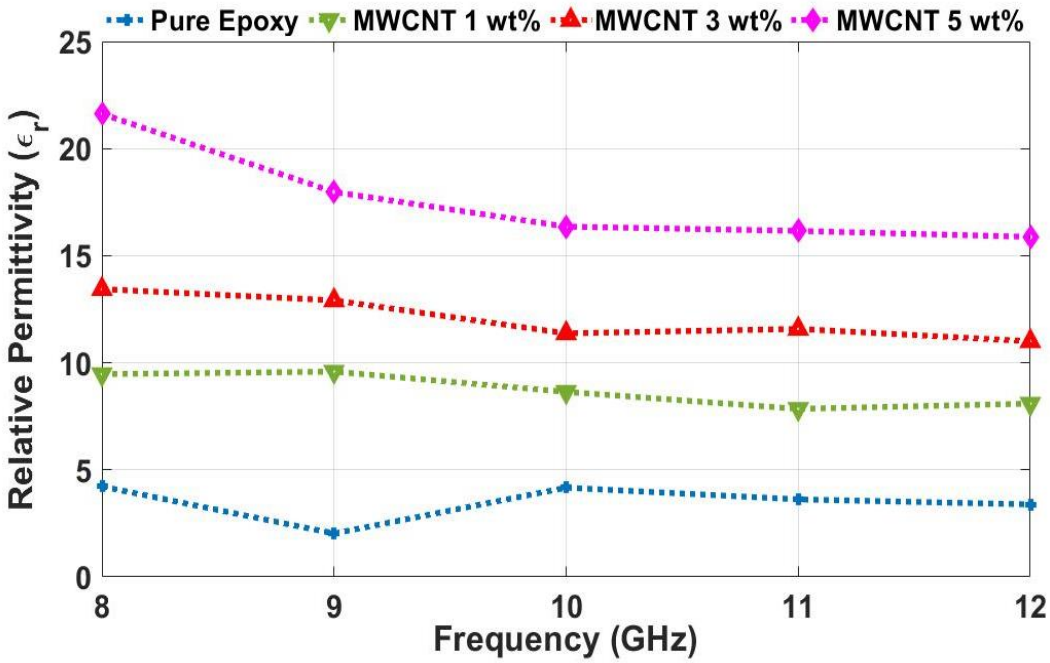

Fig. 6.22: Relative Permittivity of Epoxy-MWCNT Nanocomposites as a Function of Frequency

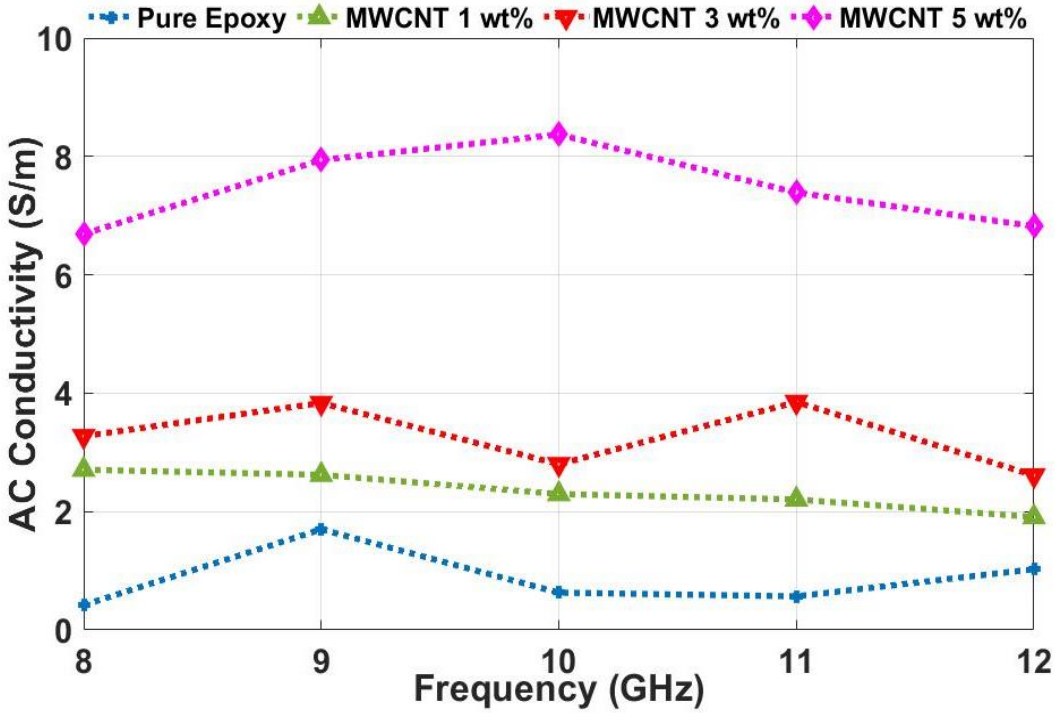

Fig. 6.23: Conductivity of Epoxy-MWCNT Nanocomposites as a Function of Frequency

6.3.6 Theoretical Evaluation of Conductivity Values in the Multi Layered System

Table 6.14 provides the evaluated values of conductivity of the layers extracted at 8,9,10,11 and 12 GHz frequencies using MATLAB codes by importing the relative permittivity values from the previous section. Considering the air/epoxy/UCFF/epoxy/air layered structure, assuming the dielectric constant of UCFF as unity, the conductivity is found to vary between 135 and 94 S/m when the frequency is increased from 8 to 12 GHz. The obtained value of UCFF agrees with the reported values of 106 S/m [100]. Fig. 6.24 provides the conductivity of the individual layer obtained from the extraction of parameters.

Table 6.14 Evaluated Values of Conductivity of Multi-Layer System

Freq (GHz)	**System**	**Epoxy**		**MWCNT-Epoxy**		**UCFF**	
		ε_r'	**σ (S/m)**	ε_r'	**σ (S/m)**	ε_r'	**σ (S/m)**
8	Epoxy/UCFF/Epoxy	4.2	0	--	--	1	122
	3wt%MWCNT-Epoxy/UCFF/3wt%MWCNT-Epoxy	--	--	13.4	88.7	1	122
	5wt%MWCNT-Epoxy/UCFF/5wt%MWCNT-Epoxy	--	--	21.6	380.8	1	122
9	Epoxy/UCFF/Epoxy	2.0	0	--	--	1	134.7
	3wt%MWCNT-Epoxy/UCFF/3wt%MWCNT-Epoxy	--	--	12.9	71.1	1	134.7
	5wt%MWCNT-Epoxy/UCFF/5wt%MWCNT-Epoxy	--	--	17.8	315.7	1	134.7
10	Epoxy/UCFF/Epoxy	4.2	0	--	--	1	108.8
	3wt%MWCNT-Epoxy/UCFF/3wt%MWCNT-Epoxy	--	--	11.4	120.8	1	108.8
	5wt%MWCNT-Epoxy/UCFF/5wt%MWCNT-Epoxy	--	--	16.4	421.8	1	108.8

11	Epoxy/UCFF/Epoxy	3.6	0	--	--	1	99.7
	3wt%MWCNT-Epoxy/UCFF/3wt%MWCNT-Epoxy	--	--	11.6	160	1	99.7
	5wt%MWCNT-Epoxy/UCFF/5wt%MWCNT-Epoxy	--	--	16.2	759.6	1	99.7
12	Epoxy/UCFF/Epoxy	3.4	0	--	--	1	93.9
	3wt%MWCNT-Epoxy/UCFF/3wt%MWCNT-Epoxy	--	--	11	163.8	1	93.9
	5wt%MWCNT-Epoxy/UCFF/5wt%MWCNT-Epoxy	--	--	15.9	942.8	1	93.9

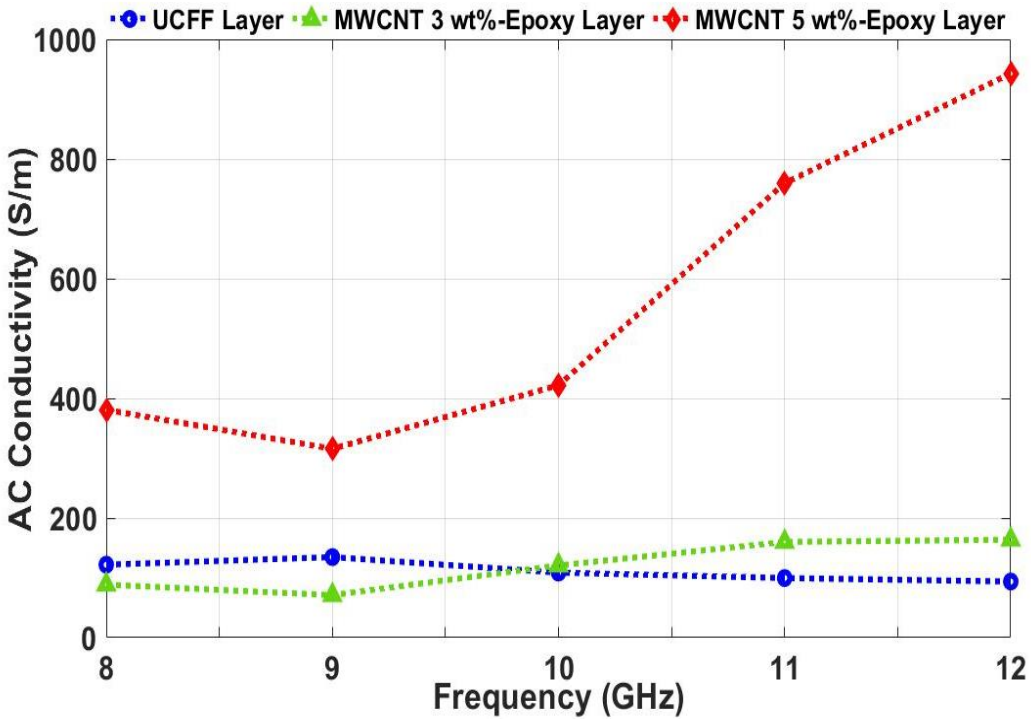

Fig. 6.24: Conductivity of Various Layers as a Function of Frequency

From Fig. 6.24, it is interesting to note that the obtained conductivity values for the epoxy-MWCNT composite for the layered system is much higher than the values evaluated for the homogenous system without UCFF. This indicates that the layered system enhances the probability of multiple scattering mechanism due to the presence of MWCNT in epoxy. Though

MWCNT does scatter the microwave, the overall increase in the effective loss mechanism is not appreciable. This is mainly due to the presence of only two interfaces (viz. air-material and material-air) that aid the scattering mechanism by the MWCNT to retain the radiation within the bulk. But when a thin, moderately conducting UCFF sheet with the skin depth higher than the thickness of the layer is inserted, MWCNT region gets two pairs of interfaces viz. air-MWCNT and MWCNT-UCFF. Therefore, every MWCNT has at least two times more probability of scattering the radiation in both the regions sandwiching UCFF. This dramatically increases the reflection and absorption of microwave through an effective conduction mechanism. This also proves that the Theoretical prediction of multi-layer formulation underestimates the effective conduction mechanism responsible for reflection and absorption. Fig. 6.25 provides the schematic of the possible mechanism that indicates the enhancement of the effective conductivity that improves the overall absorption coefficient in the layered structure.

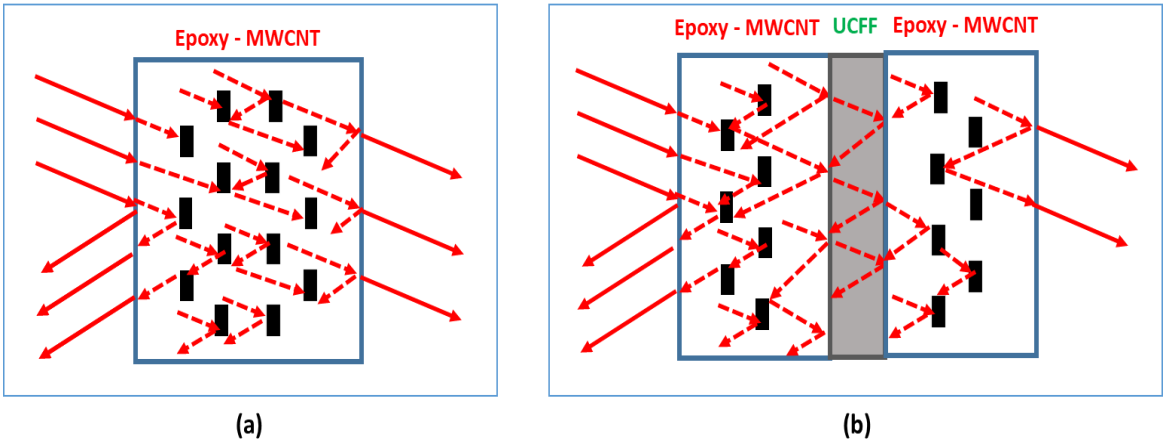

Fig. 6.25: Schematic Indicating the Possibility of Multiple Scattering (a) without UCFF (b) with UCFF.

6.3.7 Comparative Analysis of All Samples under Study

Fig. 6.26 shows the summary of average and peak EMI SE of all the nanocomposites under present study. It can be observed that the functionalized MWCNT gives the lowest values of EMI SE while MWCNT-UCFF nanocomposites gives the highest values. The EMI SE in X-band range as reported by Marta González et al. from various sources ranges from 17 dB to 58 dB and up to 80 dB in some cases however the same is achieved at higher wt% and higher

thickness of the nanocomposites [98]. The average EMI SE of 53.3 dB and peak value of 76.2 dB for 5 wt% pristine MWCNT loaded UCFF sandwiched epoxy nanocomposite specimen at 1mm thickness, in the present study is a promising result that is 2.67 times and 3.8 times better than the universally accepted value of 20 dB for industrial and commercial purposes as it attenuates 99% of impinging EM signals [101]. Therefore, the 5 wt% pristine MWCNT loaded UCFF sandwiched epoxy nanocomposite specimen is noticed to be a suitable material for EMI shielding purposes, especially in the X-band frequency range and can be further explored for utilization in aerospace and space research applications.

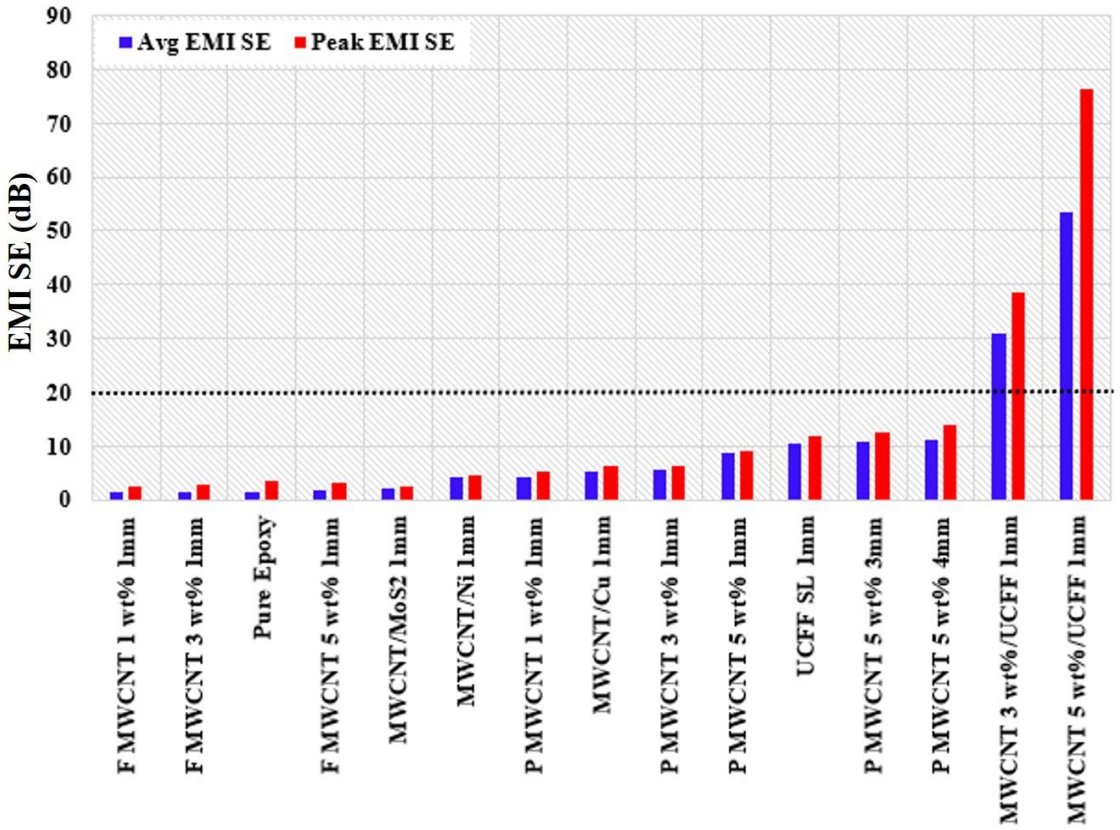

Fig. 6.26: Summary of Average and Peak EMI SE of all Nanocomposites under Present Study

6.4 Summary

The chapter discussed in detail the results of various experiments and tests conducted in the present work. The discussion in the chapter led to establishing the various characteristics of the nanocomposites and has been able to achieve all the objectives of the project work with the help of various observations, results and their justifications.

CHAPTER 7

CONCLUSION

7.1 Epoxy-Silica Nanocomposites

The electrical and mechanical characteristics of Epoxy-Silica nanocomposites were investigated in the present project work. The nanocomposites were studied for water droplet initiated discharge, contact angle and surface potential decay measurement and trap distribution analysis for electrical characterization and tensile test and digital image correlation for mechanical characterization. Following important conclusions are drawn from the present study: -

- CIV due to water droplet on the sample is low for the pure epoxy and significantly increases with inclusion of 1 wt% nanofillers and does not vary much up to 10 wt%.
- CIV is higher for –DC than +DC and AC voltages.
- CIV for 7 Hr shear mixed sample is highest among the samples under study.
- CIV increases with the increase in shear mixing time.
- Contact angle increases with shear mixing time up to 5 hours and thereafter remains approximately remains constant.
- Increment in the shear mixing duration, decreased the decay rate from 2hr to 5 hr and further increased at 7 hr.
- Decay rate was observed to be higher under negative DC corona as compared with positive DC corona, for all time duration of shear mixing.
- It was observed that trap energy level varies in the range of 0.72-0.92 eV.
- Trap depth was lowest for the 2 hours shear mixed sample and the trap depth and decay rate showed the inverse relation.

- Tensile properties of the nano composites increases with the increase in shear mixing time up to 7 hours beyond which it reduces.
- Einstein, Kerner and Neilson models confirm to the experimental values more closely between 5-7 hours shear mixing time.
- The studied model for effect on compressive or tensile strength confirms the weak bonds at 10 hours shear mixing time.
- From DIC studies it is observed that the elongation progresses linearly with time for all the samples.
- The nanocomposite specimen with 2 hours of shear mixing time has higher strain magnitude and it is noticed that the strain magnitude at any time instant before breaking reduces with increment in shear mixing time up to 7 hours of shear mixing time.
- Samples between 5-7 hours shear mixing time have recorded higher tensile strength and lesser strain magnitude.
- The 10 hours of shear mixed sample recorded higher strain magnitude than 7 Hr samples and withstood less time, indicating poor load transfer between matrix and filler interfaces.
- The pattern of average strain in the entire sample is similar to the pattern of strain at the breakpoint depicting that the strain is equally spread across the sample.

7.2 Epoxy-MWCNT Nanocomposites

A systematic study of the effect of MWCNT, UCFF and other inclusions in Epoxy based nanoparticles was carried out in order to obtain a high value of shielding efficiency. The experimental values were utilized to obtain parameters like permittivity and conductivity of the samples and the layers in the multilayer samples using theoretical approach. Following important conclusions are drawn from the present study: -

- Wt% of MWCNT has a direct impact on the EMI SE of the nanocomposite.

- Defect Functionalization of MWCNT has a negative impact on the EMI SE of the nanocomposite.
- Thickness of the nanocomposite has a direct impact on the EMI SE of the nanocomposite.
- Conductivity of the filler has direct impact on the EMI SE of the nanocomposites.
- SE due to absorption is the main contributor towards the total SE.
- Theoretical values of relative permittivity and conductivity agrees with the reported values.
- The relative permittivity or dielectric constant enhances with increase in the addition of MWCNT.
- Relative permittivity decreases with the increase in frequency.
- MWCNT-UCFF nanocomposite is a highly efficient EMI shielding material with EMI SE value of 76.2 dB, that is 3.8 times better than commercially accepted value of 20 dB.

7.3 Future Scope

There is an immense scope of advancing the present work in the field of insulation and EMI shielding. The first part of the work can be further studied to establish the characteristics of low loaded silica by carrying out additional tests that may include space charge and corona aging characteristics. In DIC analysis, the effect of variation in loading rate can be studied to further study the mechanical properties of the nanocomposites. Moreover, the present work can be taken as a reference for selecting the shear mixing time for homogeneous mixing of the material in preparation stage. Impact of shear mixing time in high loading of nanoparticles may also be studied in future.

The second part of the project work can be explored for effective utilization of the EMI shielding capabilities of unidirectional carbon fiber fabric. The high value of EMI shielding achieved in the present work is an exciting result that can be modified as per the requirement of shielding applications in the field of aerospace, radar or electronics engineering. The utility of carbon fibers in EMI shielding applications must be further researched with other nanofillers in addition to carbon nano tubes and maximum efficiency must be extracted for even better results for wide application.

REFERENCES

[1] Benelmekki, Maria. *Designing hybrid nanoparticles*. Morgan & Claypool Publishers, 2015: 1-9.

[2] Tanaka, Toshikatsu, and Takahiro Imai, eds. *Advanced nanodielectrics: fundamentals and applications*. CRC press, 2017.

[3] Tanaka, Toshikatsu. "Dielectric nanocomposites with insulating properties." *IEEE Transactions on Dielectrics and Electrical Insulation* 12, no. 5 (2005): 914-928.

[4] Paul, Siny, and T. K. Sindhu. "Effect of filler particle size on electric energy density of epoxy-aluminum nanocomposites." *IEEE Transactions on Dielectrics and Electrical Insulation* 23, no. 5 (2016): 2786-2794.

[5] Šupová, Monika, Gražyna Simha Martynková, and Karla Barabaszová. "Effect of nanofillers dispersion in polymer matrices: a review." *Science of advanced materials* 3, no. 1 (2011): 1-25.

[6] Olowojoba, Ganiu B., Sotirios Kopsidas, Salvador Eslava, Eduardo S. Gutierrez, Anthony J. Kinloch, Cecilia Mattevi, Victoria G. Rocha, and Ambrose C. Taylor. "A facile way to produce epoxy nanocomposites having excellent thermal conductivity with low contents of reduced graphene oxide." *Journal of materials science* 52, no. 12 (2017): 7323-7344.

[7] Sarojini, S., S. R. Avatar, B. Subhendu, and C. Lokesh. "Effects of nano-silica/nano-alumina on mechanical and physical properties of polyurethane composites and coatings." *Transact Electric Electron Mater* 14 (2013): 1-8.

[8] Lim, S. H., K. Y. Zeng, and C. B. He. "Morphology, tensile and fracture characteristics of epoxy-alumina nanocomposites." *Materials Science and Engineering: A* 527, no. 21-22 (2010): 5670-5676.

[9] Saha, D., A. G. Anisimov, R. M. Groves, I. A. Tsekmes, P. H. F. Morshuis, and R. Kochetov. "Epoxy-hBN nanocomposites: A study on space charge behavior and effects upon material." *IEEE Transactions on Dielectrics and Electrical Insulation* 24, no. 3 (2017): 1718-1725.

[10] Matsui, Kohei, Yasuhiro Tanaka, Tatsuo Takada, Tadashi Fukao, Kaori Fukunaga, Takashi Maeno, and John M. Alison. "Space charge behavior in low density polyethylene at pre-breakdown." *IEEE transactions on dielectrics and electrical insulation* 12, no. 3 (2005): 406-415.

[11] Du, B. X., and Y. G. Guo. "Tracking resistance of epoxy/Al 2 O 3 nanocomposites under DC voltage." *IEEE Transactions on Dielectrics and Electrical Insulation* 22, no. 1 (2015): 109-116.

[12] Qiang, Dayuan, Yan Wang, George Chen, and Thomas Andritsch. "Dielectric properties of epoxy silica and boron nitride nanocomposites and moisture/temperature influences." *IET Nanodielectrics 1*, no. 1 (2018): 48-59.

[13] Sun, Weixing, and Nicola Bowler. "Dielectric properties of silanized-silicon/epoxy nanocomposites." *IEEE Transactions on Dielectrics and Electrical Insulation* 23, no. 4 (2016): 2095-2101.

[14] Dai, Shaotao, Teng Zhang, Siming Mo, Yuan Cai, Wen Yuan, Tao Ma, Lei Hu, and Bangzhu Wang. "Study on preparation, thermal conductivity, and electrical insulation properties of epoxy/AlN." *IEEE Transactions on Applied Superconductivity* 29, no. 2 (2019): 1-6.

[15] Heid, Thomas, Michel Fréchette, and Eric David. "Epoxy/BN micro-and submicro-composites: dielectric and thermal properties of enhanced materials for high voltage insulation systems." *IEEE Transactions on Dielectrics and Electrical Insulation* 22, no. 2 (2015): 1176-1185.

[16] Tsekmes, I. A., P. H. F. Morshuis, J. J. Smit, and R. Kochetov. "Enhancing the thermal and electrical performance of epoxy microcomposites with the addition of nanofillers." *IEEE Electrical Insulation Magazine* 31, no. 3 (2015): 32-42.

[17] Luo, Pan, Man Xu, Shaohui Wang, and Yang Xu. "Structural, dynamic mechanical and dielectric properties of mesoporous silica/epoxy resin nanocomposites." *IEEE Transactions on Dielectrics and Electrical Insulation* 24, no. 3 (2017): 1685-1697.

[18] Imai, Takahiro, Fumio Sawa, Toshiyuki Nakano, Tamon Ozaki, Toshio Shimizu, Masahiro Kozako, and Toshikatsu Tanaka. "Effects of nano-and micro-filler mixture on electrical insulation properties of epoxy based composites." *IEEE Transactions on Dielectrics and Electrical Insulation* 13, no. 2 (2006): 319-326.

[19] Goyanes, S. N., P. G. König, and J. D. Marconi. "Dynamic mechanical analysis of particulate-filled epoxy resin." *Journal of Applied Polymer Science* 88, no. 4 (2003): 883-892.

[20] Pullicino, Edward, Wentao Zou, Matthieu Gresil, and Costas Soutis. "The effect of shear mixing speed and time on the mechanical properties of GNP/epoxy composites." *Applied Composite Materials* 24, no. 2 (2017): 301-311.

[21] Sarathi, R., and G. Nagesh. "UHF technique for identification of discharges initiated by liquid droplet in epoxy nanocomposite insulation material under ac voltages." *Journal of Physics D: Applied Physics* 41, no. 15 (2008): 155407.

[22] Gemi, L., S. Yazman, M. Uludağ, D. Dispinar, and M. Tiryakioğlu. "The effect of 0.5 wt% additions of carbon nanotubes & ceramic nanoparticles on tensile properties of epoxy-matrix composites: a comparative study." *Mater. Sci Nanotechnol* (2017): 15-22.

[23] Uslu, Emin, Mehmet Gavgali, Mehmet Okan Erdal, Şakir Yazman, and Lokman Gemi. "Determination of mechanical properties of polymer matrix composites reinforced with electrospinning N66, PAN, PVA and PVC nanofibers: A comparative study." *Materials Today Communications* 26 (2021): 101939.

[24] Yapici, A., V. Özkan, M. Yıldız, M. Erdal, L. Gemi, and Ş. Yazman. "The effect of nylon 6.6 nanofiber layers on mechanical properties of epoxy." *The International Journal of Engineering and Science* 5, no. 11 (2016): 86-89.

[25] Pan, Bing. "Digital image correlation for surface deformation measurement: historical developments, recent advances and future goals." *Measurement Science and Technology* 29, no. 8 (2018): 082001.

[26] Hanada, Eisuke, Yasuaki Antoku, Shigeki Tani, Michio Kimura, Akira Hasegawa, Shigeo Urano, Kazuhiko Ohe, Michiyasu Yamaki, and Yoshiaki Nose. "Electromagnetic interference on medical equipment by low-power mobile telecommunication systems." *IEEE Transactions on Electromagnetic Compatibility* 42, no. 4 (2000): 470-476.

[27] Puglia, D., L. Valentini, and J. M. Kenny. "Analysis of the cure reaction of carbon nanotubes/epoxy resin composites through thermal analysis and Raman spectroscopy." *Journal of Applied Polymer Science* 88, no. 2 (2003): 452-458.

[28] Dassan, Emayaruba G. Barathi, Aslina Anjang Ab Rahman, Mohd Shukur Zainol Abidin, and Hazizan Md Akil. "Carbon nanotube–reinforced polymer composite for electromagnetic interference application: A review." *Nanotechnology Reviews* 9, no. 1 (2020): 768-788.

[29] Bisht, Ankita, Kinshuk Dasgupta, and Debrupa Lahiri. "Effect of graphene and CNT reinforcement on mechanical and thermomechanical behavior of epoxy—A comparative study." *Journal of Applied Polymer Science* 135, no. 14 (2018): 46101.

[30] Al-Saleh, Mohammed H., and Uttandaraman Sundararaj. "Electromagnetic interference shielding mechanisms of CNT/polymer composites." *Carbon* 47, no. 7 (2009): 1738-1746.

[31] Bai, J. B., and Aïssa Allaoui. "Effect of the length and the aggregate size of MWNTs on the improvement efficiency of the mechanical and electrical properties of nanocomposites—experimental investigation." *Composites Part A: Applied Science and Manufacturing* 34, no. 8 (2003): 689-694.

[32] Theodore, Merlin, Mahesh Hosur, Jonathan Thomas, and Shaik Jeelani. "Influence of functionalization on properties of MWCNT–epoxy nanocomposites." *Materials Science and Engineering: A* 528, no. 3 (2011): 1192-1200.

[33] Koval'chuk, Anton A., Vitaliy G. Shevchenko, Alexander N. Shchegolikhin, Polina M. Nedorezova, Alla N. Klyamkina, and Alexander M. Aladyshev. "Effect of carbon nanotube functionalization on the structural and mechanical properties of polypropylene/MWCNT composites." *Macromolecules* 41, no. 20 (2008): 7536-7542.

[34] Du, JrH, Jinbo Bai, and HrM Cheng. "The present status and key problems of carbon nanotube based polymer composites." *Express Polymer Letters* 1, no. 5 (2007): 253-273.

[35] Ravindren, Revathy, Subhadip Mondal, Krishnendu Nath, and Narayan Ch Das. "Investigation of electrical conductivity and electromagnetic interference shielding effectiveness of preferentially distributed conductive filler in highly flexible polymer blends nanocomposites." *Composites Part A: Applied Science and Manufacturing* 118 (2019): 75-89.

[36] Park, Dong Hyup, Yun Kyun Lee, Sang Sun Park, Choon Soo Lee, Sung Hyun Kim, and Woo Nyon Kim. "Effects of hybrid fillers on the electrical conductivity and EMI shielding efficiency of polypropylene / conductive filler composites." *Macromolecular Research* 21, no. 8 (2013): 905-910.

[37] Lee, B. O., W. J. Woo, H. S. Park, H. S. Hahm, J. P. Wu, and M. S. Kim. "Influence of aspect ratio and skin effect on EMI shielding of coating materials fabricated with carbon nanofiber/PVDF." *Journal of Materials Science* 37, no. 9 (2002): 1839-1843.

[38] Chung, D. D. L. "Electromagnetic interference shielding effectiveness of carbon materials." *Carbon* 39, no. 2 (2001): 279-285.

[39] Wang, Baichen, Xia Zhou, Junshan Yin, and Li Wang. "Investigation on some matrix-dominated properties of hybrid multiscale composites based on carbon fiber/carbon nanotube modified epoxy." *Journal of Applied Polymer Science* 128, no. 2 (2013): 990-996.

[40] IEEE Standard Letter Designations for Radar-Frequency Bands, IEEE Std 521-2019 (Revision of IEEE Std 521-2002), 2020.

[41] National Frequency Allocation Plan-2018, Wireless Planning and Coordination Wing, Department of Telecommunications, Government of India, 2018.

[42] Feynman, R., 1959, December. There is plenty of room at the bottom: an invitation to enter a new field of physics. In Lecture at *American Physical Society Meeting* (Vol. 29).

[43] Salleo, A., S. T. Taylor, M. C. Martin, W. Panero, R. Jeanloz, T. Sands, and F. Y. Génin. "Laser driven phase transformations in amorphous silica." *Nature Materials 2*, no. 12 (2003): 796.

[44] Che, Shunai, Alfonso E. Garcia-Bennett, Toshiyuki Yokoi, Kazutami Sakamoto, Hironobu Kunieda, Osamu Terasaki, and Takashi Tatsumi. "A novel anionic surfactant templating route for synthesizing mesoporous silica with unique structure." *Nature Materials 2*, no. 12 (2003): 801-805.

[45] Suzuki, Keisei, Kenichi Ikari, and Hiroaki Imai. "Synthesis of silica nanoparticles having a well-ordered mesostructure using a double surfactant system." *Journal of the American Chemical Society* 126, no. 2 (2004): 462-463.

[46] Barik, T. K., B. Sahu, and V. Swain. "Nanosilica—from medicine to pest control." *Parasitology Research* 103, no. 2 (2008): 253-258.

[47] Rahman, Ismail Ab, and Vejayakumaran Padavettan. "Synthesis of silica nanoparticles by sol-gel: size-dependent properties, surface modification, and applications in silica-polymer nanocomposites—a review." *Journal of Nanomaterials* 2012 (2012).

[48] Veena, M. G., N. M. Renukappa, J. M. Raj, C. Ranganathaiah, and K. N. Shivakumar. "Characterization of nanosilica-filled epoxy composites for electrical and insulation applications." *Journal of Applied Polymer Science* 121, no. 5 (2011): 2752-2760.

[49] Reid, Alistair J., Martin D. Judd, Brian G. Stewart, and Richard A. Fouracre. "Partial discharge current pulses in SF6 and the effect of superposition of their radiometric measurement." *Journal of Physics D: Applied Physics* 39, no. 19 (2006): 4167.

[50] Lopes, Ivan JS, Shesha H. Jayaram, and Edward A. Cherney. "A study of partial discharges from water droplets on a silicone rubber insulating surface." *IEEE Transactions on Dielectrics and Electrical Insulation* 8, no. 2 (2001): 262-268.

[51] El-Kishky, H., and R. S. Gorur. "Electric field computation on an insulating surface with discrete water droplets." *IEEE Transactions on Dielectrics and Electrical Insulation* 3, no. 3 (1996): 450-456.

[52] Sarathi, R., V. Sri Harsha, Huw Griffiths, and Abderrahmane Haddad. "Understanding water droplet initiated discharges on epoxy nanocomposites under harmonic AC voltages adopting UHF technique." *IEEE Transactions on Dielectrics and Electrical Insulation* 21, no. 2 (2014): 918-925.

[53] Miao, Ying-Gang, Hong-Yuan Liu, Tao Suo, Yiu-Wing Mai, Fa-Qin Xie, and Yu-Long Li. "Effects of strain rate on mechanical properties of nanosilica/epoxy." *Composites Part B: Engineering* 96 (2016): 119-124.

[54] Guchhait, P. K., S. Bhandari, S. Singh, and M. Rahaman. "Study on the effect of nanosilica particles on morphology, thermo-mechanical and electrical properties of liquid polysulfide modified epoxy hybrid nanocomposites." *International Journal of Plastics Technology* 15, no. 2 (2011): 150-162.

[55] Iijima, Sumio. "Helical microtubules of graphitic carbon." *Nature* 354, no. 6348 (1991): 56-58.

[56] Dresselhaus, M. S., G. Dresselhaus, and R. Saito. "Physics of carbon nanotubes." *Carbon* 33, no. 7 (1995): 883-891.

[57] Popov, Valentin N. "Carbon nanotubes: properties and application." *Materials Science and Engineering*: R: Reports 43, no. 3 (2004): 61-102.

[58] Yuen, Siu-Ming, Chen-Chi M. Ma, Hsin-Ho Wu, Hsu-Chiang Kuan, Wei-Jen Chen, Shu-Hang Liao, Chia-Wen Hsu, and Han-Lang Wu. "Preparation and thermal, electrical, and morphological properties of multiwalled carbon nanotubeand epoxy composites." *Journal of Applied Polymer Science* 103, no. 2 (2007): 1272-1278.

[59] Lachman, Noa, and H. Daniel Wagner. "Correlation between interfacial molecular structure and mechanics in CNT/epoxy nano-composites." *Composites Part A: Applied Science and Manufacturing* 41, no. 9 (2010): 1093-1098.

[60] Cha, Jaemin, Gwang Hoon Jun, Jong Kyoo Park, Jung Cheol Kim, Ho Jin Ryu, and Soon H. Hong. "Improvement of modulus, strength and fracture toughness of CNT/Epoxy nanocomposites through the functionalization of carbon nanotubes." *Composites Part B: Engin*eering 129 (2017): 169-179.

[61] Nam, I. W., Haeng-Ki Lee, and J. H. Jang. "Electromagnetic interference shielding/absorbing characteristics of CNT-embedded epoxy composites." *Composites Part A: Applied Science and Manufacturing* 42, no. 9 (2011): 1110-1118.

[62] Singh, B. P., Veena Choudhary, Parveen Saini, and R. B. Mathur. "Designing of epoxy composites reinforced with carbon nanotubes grown carbon fiber fabric for improved electromagnetic interference shielding." *Aip Advances* 2, no. 2 (2012): 022151.

[63] Baranovskii, Sergei, and Oleg Rubel. "Charge transport in disordered materials." *Springer Handbook of Electronic and Photonic Materials* (2007): 161.

[64] Molinié, Philippe. "Measuring and modeling transient insulator response to charging: the contribution of surface potential studies." *IEEE Transactions on Dielectrics and Electrical Insulation* 12, no. 5 (2005): 939-950.

[65] Young, Thomas. "III. An essay on the cohesion of fluids." *Philosophical Transactions of the Royal Society of London* 95 (1805): 65-87.

[66] Kwok, Daniel Y., and August W. Neumann. "Contact angle measurement and contact angle interpretation." *Advances in Colloid and Interface Science* 81, no. 3 (1999): 167-249.

[67] Marmur, Abraham. "Thermodynamic aspects of contact angle hysteresis." *Advances in Colloid and Interface Science* 50 (1994): 121-141.

[68] Gao, Lichao, and Thomas J. McCarthy. "Contact angle hysteresis explained." *Langmuir* 22, no. 14 (2006): 6234-6237.

[69] Peddamallu, Nagachandrika, Krishnamurthy Sridharan, Tadachika Nakayama, and Ramanujam Sarathi. "Understanding the fundamental properties of epoxy molybdenum disulfide nanocomposites." *Polymer Composites* 40, no. 4 (2019): 1556-1563.

[70] Yehia E. Elmogahzy, “Finished fibrous assemblies.” *The Textile Institute Book Series, Engineering Textiles* (Second Edition), Woodhead Publishing, 2020, Pages 275-298

[71] Helmi, F.M.; Hefni, Y.A. A simple method for measuring the static water contact angle for evaluation the hydrophobicity of the consolidating and protective materials. In Proceedings of the *First International Conference of Egypt and Mediterranean Countries through* Ages, Cairo, Egypt, 2014; Volume 3, 327–341.

[72] Chillu, Naresh, R. Jayaganthan, R. Velmurugan, and R. Sarathi. "Investigation on the digital image correlation and charge trap characteristics of Al/epoxy nanocomposites." *Materials Research Express* 7, no. 2 (2020): 025035.

[73] Moreira, D. C., L. A. Sphaier, J. M. L. Reis, and L. C. S. Nunes. "Determination of Young's modulus in polyester-Al2O3 and epoxy-Al2O3 nanocomposites using the digital image correlation method." *Composites Part A: Applied Science and Manufacturing* 43, no. 2 (2012): 304-309.

[74] Einstein, A. "On the movement of small particles suspended in stationary liquids required by the molecular kinetic theory of heat." *Ann. d. Phys* 17, no. 549-560 (1905).

[75] Einstein, Albert. Investigations on the Theory of the Brownian Movement. *Courier Corporation*, 1956.

[76] Kerner, E. H. "The elastic and thermo-elastic properties of composite media." *Proceedings of the Physical Society*. Section B 69, no. 8 (1956): 808.

[77] Dittanet, Peerapan, and Raymond A. Pearson. "Effect of silica nanoparticle size on toughening mechanisms of filled epoxy." *Polymer* 53, no. 9 (2012): 1890-1905.

[78] Nielsen, Lawrence E. "Generalized equation for the elastic moduli of composite materials." *Journal of Applied Physics* 41, no. 11 (1970): 4626-4627.

[79] Islam, Md Saiful, Reza Masoodi, and Hossein Rostami. "The effect of nanoparticles percentage on mechanical behavior of silica-epoxy nanocomposites." *Journal of Nanoscience* 2013 (2013).

[80] Nicolais, L., and M. Narkis. "Stress-strain behavior of styrene-acrylonitrile/glass bead composites in the glassy region." *Polymer Engineering & Science* 11, no. 3 (1971): 194-199.

[81] Nicolais, L., and L. Nicodemo. "The effect of particles shape on tensile properties of glassy thermoplastic composites." *International Journal of Polymeric Materials* 3, no. 3 (1974): 229-243.

[82] Nicolais, L., and L. Nicodemo. "Strength of particulate composite." *Polymer Engineering & Science* 13, no. 6 (1973): 469.

[83] Rengaswamy, Kumaran, Dinesh Kumar Sakthivel, Alagar Muthukaruppan, Balasubramanian Natesan, Subramanian Venkatachalam, and Dinakaran Kannaiyan. "Electromagnetic interference (EMI) shielding performance of lightweight metal decorated carbon nanostructures dispersed in flexible polyvinylidene fluoride films." *New Journal of Chemistry* 42, no. 15 (2018): 12945-12953.

[84] Mondal, Subhadip, Sayan Ganguly, Mostafizur Rahaman, Ali Aldalbahi, Tapan K. Chaki, Dipak Khastgir, and Narayan Ch Das. "A strategy to achieve enhanced electromagnetic interference shielding at low concentration with a new generation of conductive carbon black in a chlorinated polyethylene elastomeric matrix." *Physical Chemistry Chemical Physics* 18, no. 35 (2016): 24591-24599.

[85] Al-Saleh, Mohammed H., and Uttandaraman Sundararaj. "X-band EMI shielding mechanisms and shielding effectiveness of high structure carbon black/polypropylene composites." *Journal of Physics D: Applied Physics* 46, no. 3 (2012): 035304.

[86] Katada, Koji, Yoshikazu Takada, Makoto Takano, Takeshi Nakanishi, Yoji Hayashi, and Ryosake Matsuoka. "Corona discharge characteristics of water droplets on hydrophobic polymer insulator surface." In Proceedings of the *6th International Conference on Properties and Applications of Dielectric Materials*, vol. 2, pp. 781-784. IEEE, 2000.

[87] Sarathi, R., V. Sri Harsha, N. J. Vasa, H. Griffiths, and Abderrahmane Haddad. "Water droplet initiated discharges on epoxy nanocomposites under DC voltages." *IEEE Transactions on Dielectrics and Electrical Insulation* 23, no. 3 (2016): 1743-1752.

[88] Nazemi, M. H., and V. Hinrichsen. "Experimental investigations on water droplet oscillation and partial discharge inception voltage on polymeric insulating surfaces under the influence of AC electric field stress." *IEEE Transactions on Dielectrics and Electrical Insulation* 20, no. 2 (2013): 443-453.

[89] Riba, Jordi-Roger, Andrea Morosini, and Francesca Capelli. "Comparative study of ac and positive and negative dc visual corona for sphere-plane gaps in atmospheric air." *Energies* 11, no. 10 (2018): 2671.

[90] Wenzel, Robert N. "Resistance of solid surfaces to wetting by water." *Industrial & Engineering Chemistry* 28, no. 8 (1936): 988-994

[91] Lewis, T. J. "Interfaces are the dominant feature of dielectrics at the nanometric level." *IEEE transactions on Dielectrics and Electrical Insulation* 11, no. 5 (2004): 739-753.

[92] Du, B. X., J. P. Jiang, J. G. Zhang, and D. S. Liu. "Dynamic behavior of surface charge on double-layer oil-paper insulation under pulse voltage." *IEEE Transactions on Dielectrics and Electrical Insulation* 23, no. 5 (2016): 2712-2719.

[93] Gao, Yu, Jilong Wang, Fang Liu, and Boxue Du. "Surface potential decay of negative corona charged epoxy/Al 2 O 3 nanocomposites degraded by 7.5-MeV electron beam." *IEEE Transactions on Plasma Science* 46, no. 7 (2018): 2721-2729.

[94] Kim, Young-Won. "Strength and ductility in TiAl alloys." *Intermetallics* 6, no. 7-8 (1998): 623-628.

[95] Naresh, K., K. Shankar, B. S. Rao, and R. Velmurugan. "Effect of high strain rate on glass/carbon/hybrid fiber reinforced epoxy laminated composites." *Composites Part B: Engineering* 100 (2016): 125-135.

[96] Phan, Chee Hong, Mariatti Jaafar, and Yin Hsian Koh. "Mild functionalization of carbon nanotubes filled epoxy composites: Effect on electromagnetic interferences shielding effectiveness." *Journal of Applied Polymer Science* 132, no. 38 (2015).

[97] Xu, Zhengbin, and Hai Hao. "Electromagnetic interference shielding effectiveness of aluminum foams with different porosity." *Journal of Alloys and Compounds* 617 (2014): 207-213.

[98] González, Marta, Guillermo Mokry, María de Nicolás, Juan Baselga, and Javier Pozuelo. "Carbon nanotube composites as electromagnetic shielding materials in GHz range." *Carbon Nanotubes-Current Progress of their Polymer Composites* 11 (2016): 297-321.

[99] Rohini, Rani, and Suryasarathi Bose. "Electrodeposited carbon fiber and epoxy based sandwich architectures suppress electromagnetic radiation by absorption." *Composites Part B: Engineering* 161 (2019): 578-585.

[100] Zhao, Qian, Kai Zhang, Shuang Zhu, Hanyang Xu, Dianguo Cao, Lina Zhao, Ronghua Zhang, and Wuliang Yin. "Review on the electrical resistance/conductivity of carbon fiber reinforced polymer." *Applied Sciences* 9, no. 11 (2019): 2390.

[101] Sankaran, Sowmya, Kalim Deshmukh, M. Basheer Ahamed, and SK Khadheer Pasha. "Recent advances in electromagnetic interference shielding properties of metal and carbon filler reinforced flexible polymer composites: a review." *Composites Part A: Applied Science and Manufacturing* 114 (2018): 49-71.

LIST OF PUBLICATIONS

- Abhishek Sharma, Myneni Sukesh Babu, Velmurugan, R., Imai, T. and Sarathi, R., "Impact of shear mixing time of epoxy-silica nanocomposites on its electrical and mechanical properties" *Nano Express*, *2*(1), p.010031, 2021